

**STUDIES ON CARBOHYDRATE DERIVED
SORBENTS FOR CARBON DIOXIDE
REMOVAL**

*A Thesis submitted
in partial fulfillment for the Degree of*

Doctor of Philosophy

by

DEEPTHI L. SIVADAS



**Department of Chemistry
INDIAN INSTITUTE OF SPACE SCIENCE AND
TECHNOLOGY**

Thiruvananthapuram – 695 547

October 2016

CERTIFICATE

This is to certify that the thesis entitled **Studies on Carbohydrate Derived Sorbents for Carbon Dioxide Removal** submitted by **Deepthi L. Sivadas**, to the Indian Institute of Space Science and Technology, Thiruvananthapuram, in partial fulfillment for the award of the degree of **Doctor of Philosophy** is a *bona fide* record of research work carried out by her under our supervision. The contents of this thesis, in full or in parts, have not been submitted to any other Institution or University for the award of any degree or diploma.

Prof. (Dr.) K. N. Ninan
Supervisor
Emeritus Professor
Department of Chemistry
IIST

Dr. K. Prabhakaran
Co-supervisor
Associate Professor
Department of Chemistry
IIST

Dr. R. Rajeev
Co-supervisor
Head, ASD
VSSC

Thiruvananthapuram

Counter signature of HOD with seal

October 2016

DECLARATION

I declare that this thesis entitled **Studies on Carbohydrate Derived sorbents for Carbon Dioxide Removal** submitted in partial fulfillment of the degree of **Doctor of Philosophy** is a record of original work carried out by me under the supervision of **Prof. (Dr.) K. N. Ninan, Dr. K. Prabhakaran and Dr. R. Rajeev**, and has not formed the basis for the award of any other degree or diploma, in this or any other Institution or University. In keeping with the ethical practice in reporting scientific information, due acknowledgements have been made wherever the findings of others have been cited.

Deepthi L. Sivadas

SC12D001

Thiruvananthapuram - 695 547

17/10/2016

ACKNOWLEDGMENTS

I would like to express my heartfelt gratitude towards my supervisors Professor (Dr.) K. N. Ninan, Dr. K. Prabhakaran and Dr. R. Rajeev for giving me the opportunity to work under their supervision and also for their academic guidance, continuous support and encouragement throughout this research work. I have been extremely lucky to have these supervisors who cared so much about my work, and who responded to my questions and queries so promptly by providing with their precious time.

I take this opportunity to thank Dr. Vinay Kumar Dadhwal, Director, IIST and Dr. K. S. Das Gupta, former Director, IIST for providing me with all the necessary facilities. It is my pleasure to extend my deep gratitude to Prof. Kuruvilla Joseph, the Dean (Student Activities) and the former Head of the Department of Chemistry, for his continuous support and encouragement during my work. I extend my sincere thanks to Dr. Nirmala Rachel, Head of the Department of Chemistry, for her constant support and valuable suggestions.

I thank Dr. K. Sivan, Director, Vikram Sarabhai Space Centre, Shri. P.S. Veeraraghavan, Shri. S. Ramakrishnan and Shri. M. C. Dathan, former Directors of VSSC for allowing me to initiate and continue my Ph. D work. Support and encouragements from Dr. B. Velayudham, Dr. S. Packirisamy and Dr. C. P. Reghunadhan Nair; former Deputy Directors (PCM) VSSC, Dr. C. S. Sharma, Deputy Director (PCM) VSSC and Dr. Benny K. George, Group Director ASCG is gratefully appreciated.

I have to extend my heartfelt thanks to doctoral committee members, Prof. C. P. Rao, Prof. S. Vasudevan, and Dr. P. Chakravarthy. I am very grateful to their guidance, constructive criticism and enthusiastic support during my research. I am indebted to the faculty members of Department of Chemistry for their whole hearted

support.

I am deeply indebted to all members of Analytical and Spectroscopy Division VSSC; Smt. Salu Jacob, Smt. R. Sadhana, Shri. R. Parameswar, Dr. K. P. Vijayalakshmi, Miss. Roopa Dimple, Smt. T. Jayalatha, Smt. R. Radhika, Smt. Rekha Krishnan, Shri. Appala Raju A. and my friends who has supported and shared lot of knowledge and also for the fruitful discussions during my thesis work.

I also offer my sincere appreciation my friends in IIST for their sincere help and support especially to Dr. R. Narasimman, Mr. Sujith Vijayan, Mr. Praveen, Dr. Raneesh Konnola, Shri. Dileep Kumar, Mrs. Rehna and Mrs. Jayashree.

Last but not least, I would like to thank my parents, sister, husband and kids for their constant love.

ABSTRACT

Global Warming is the increase in the average temperature of Earth due to increased emission of greenhouse gases, which absorb the heat that would otherwise escape from the Earth surface. CO₂ is the primary anthropogenic greenhouse gas. During the past few decades, much effort has been committed for the development of new CO₂ capture materials. Adsorbents for CO₂ employ one of the two possible adsorption mechanisms, either chemical adsorption or physical adsorption. In chemisorptions, CO₂ undergoes a covalent chemical reaction to bind CO₂ to certain sites on the sorbent with a much greater heat of adsorption. In physisorption, CO₂ is adsorbed to the solid support by either van der Waals force of attraction or pole-pole interaction.

Recently, much attention has been given to the use of biomass to produce functional materials in terms of economic, environmental and societal issues. Biomass, because of its low cost, huge amount, easy access and environmental friendship has increased demand as a raw material for CO₂ adsorbent. The focus of research work is on the development of different CO₂ adsorbents from biomass.

In the thesis work, regenerable CO₂ capture materials are prepared using different carbohydrates as the raw materials. Three types of CO₂ capture materials were developed viz., amine on solid support, microporous carbon and nitrogen-doped microporous carbon. These materials were evaluated for CO₂ adsorption capacity, recycle stability, selectivity etc.

Carbon dioxide adsorption on the supramolecular system of aniline encapsulated into β -cyclodextrin (β -CD) cavity is studied for the first time. Molecular level distribution of amine on solid support is achieved. Amine group of aniline oriented towards the wider rim of β -CD cavity is favourably exposed to the gas stream, which results in its maximum utilization for CO₂ capture. CO₂ adsorption capacity of 0.70 mmol/g (3.1 wt.%) and amine efficiency of 0.85 mol CO₂ adsorbed / mol of nitrogen in the adsorbent is observed for this system at ambient temperature and pressure. The mechanism of the chemisorption is through the formation of bicarbonate confirmed by NMR, Raman spectroscopy and molecular modelling studies. The heat of adsorption value from the DSC is - 94 kJ/mol, which compares well with that for chemisorption of CO₂. The pseudo-second order rate equation is used to describe the chemisorptions of β -CD – aniline complex.

Microporous carbon nanospheres are prepared from β -cyclodextrin by solvothermal carbonization in o-dichlorobenzene in presence of various

concentrations of p-toluene sulfonic acid (PTSA). The contribution of PTSA towards solvothermal char (STC) is established. The STC shows the highest surface area, porosity and CO₂ sorption capacity at a PTSA to β -CD weight ratio of 2.5. The surface area, pore volume and CO₂ sorption capacity are further increased by an in situ high temperature activation, due to the oxidation of carbon at high temperature by the oxygen present in the STC. The high temperature activation reduces the significance of PTSA concentration, as the activated STC showed surface area, micropore volume and CO₂ adsorption capacity in a close range at the PTSA to β -CD weight ratio in the range of 0.04 to 2.5. The highest CO₂ adsorption capacity increase from 2.4 to 3.5 mmol/g (10.6 to 15.4 wt. %) up on the high temperature activation. The activated STC adsorbs significant amount (0.35 mmol/g, i.e., 1.5 wt. %) of CO₂ from dry air containing 400 ppm CO₂.

More economical and accessible raw material cotton is selected for the preparation of porous carbon. Microporous carbonaceous materials were developed by the solvothermal carbonization of natural cotton for the first time. Morphology and surface area of solvothermal char (STC) depend on the p-toluene sulfonic acid (PTSA) catalyst concentration. STC shows maximum surface area of 477 m²/g, pore volume of 0.60 cm³/g and CO₂ sorption capacity (at 25 °C and 1 bar) of 1.3 mmol/g (5.7 wt %). STC shows the same adsorption capacity when tested with pure CO₂ gas at 25 °C for several adsorption-desorption cycles. High CO₂ uptake of 4.6 mmol/g (20.2 wt. %) at ambient temperature and 20 bars is exhibited by STC. STC-0.04 (prepared at PTSA to cotton weight ratio of 0.04) showed superhydrophobic character due to the nano projections on the fiber surface produced by heterogeneous nucleation of STC particles. STC-0.04 is an excellent sorbent for organic solvents from water.

Nitrogen enriched carbon with well-developed microporosity and superior CO₂ adsorption capacity are prepared by KOH activation of a nitrogen-containing polymer obtained by heating sucrose and urea. The nitrogen content, microporosity and surface area of the activated carbon depend on the concentration of urea and KOH. The maximum surface area, total pore volume and nitrogen content of the activated carbon achieved are 2366 m²/g, 1.16 cm³/g and 10.5 wt.%, respectively. A maximum CO₂ adsorption capacity of 7.0 mmol/g (30.8 wt. %) is achieved at 0°C and 1 bar pressure. The CO₂ adsorption capacity of 0.70 mmol/g (3.1 wt. %) from dry air containing 400 ppm CO₂ achieved is the highest reported in the category of carbonaceous materials. The CO₂ adsorption capacity of all prepared carbon materials is well correlated with the nitrogen content and microporosity. The CO₂ adsorption on activated carbon materials shows excellent selectivity over N₂, with one of the highest selectivity factor of 38, hence an ideal candidate for CO₂ removal.

TABLE OF CONTENTS

CERTIFICATE	v
DECLARATION	vii
ACKNOWLEDGEMENT	ix
ABSTRACT	xi
LIST OF FIGURES	xvii
LIST OF TABLES	xxiii
ABBREVIATIONS	xxv
NOTATIONS	xxvii
1. INTRODUCTION	1
1.1 Global warming	1
1.2 Sources of CO ₂	2
1.3 CO ₂ build up in closed crew cabins	3
1.4 Carbon dioxide removal technologies	5
1.4.1 Chemisorbents for CO ₂ removal	8
1.4.1.1 Lithium hydroxide based solid sorbents	8
1.4.1.2 Metal oxide based solid sorbents	10
1.4.1.3 Metal carbonate based solid sorbents	11
1.4.1.4 Amine based solid sorbents	13
1.4.2 Physisorbents for CO ₂ removal	20
1.4.2.1 Zeolite based solid sorbents	26
1.4.2.2 Metal Organic Framework based solid sorbents	31
1.4.2.3 Carbon based solid sorbents	34
1.5 Objective of the work	46
 2. SUPRAMOLECULAR SYSTEM OF ANILINE ENCAPSULATED β-CYCLODEXTRIN FOR CARBON DIOXIDE REMOVAL	
2.1 Introduction	48

2.2	Experimental	49
2.2.1	Synthesis of β -CD–aniline complex	49
2.2.2	Characterization of β -CD–aniline complex	50
2.3	Results and discussion	51
2.3.1	Confirmation of 1:1 complex of β -CD – aniline	52
2.3.2	CO ₂ adsorption of 1:1 complex of β -CD – aniline	54
2.3.3	Mechanism of CO ₂ adsorption by β -CD – aniline	55
2.3.4	Evaluation of heat of adsorption	60
2.3.5	Kinetics of CO ₂ adsorption	60
2.4	Conclusions	62
3.	CO₂ SORBENTS BY SOLVOTHERMAL CARBONIZATION AND IN SITU ACTIVATION OF β-CYCLODEXTRIN	
3.1	Introduction	66
3.2	Experimental	67
3.2.1	Synthesis of Solvothermal carbon from β -CD	68
3.2.2	Characterization of STC and activated STC	68
3.3	Results and discussion	70
3.3.1	Textural property evaluation of STC	71
3.3.2	CO ₂ adsorption evaluation of STC	73
3.3.3	Activation of STC – Effect of activation temperature	75
3.3.4	Textural property evaluation of activated STC	79
3.3.5	CO ₂ adsorption evaluation of activated STC	81
3.3.6	Reason behind optimum ratio of PTSA to β -CD as 2.5	84
3.3.7	CO ₂ adsorption mechanism	87
3.3.8	CO ₂ adsorption from air	88
3.3.9	Evaluation of heat of adsorption	90
3.3.10	Selectivity and recycle stability of STC	90
3.4	Conclusions	92

4. MICROPOROUS SUPERHYDROPHOBIC CARBON FROM NATURAL COTTON FOR CARBON DIOXIDE AND ORGANIC SOLVENT REMOVAL	
4.1 Introduction	96
4.2 Experimental	97
4.2.1 Preparation of solvothermal carbon from cotton	97
4.2.2 Characterization of solvothermal carbon materials	98
4.3 Results and discussion	100
4.3.1 Structure identification of STC	100
4.3.2 Morphology analysis of STC	103
4.3.3 Textural property evaluation of STC	105
4.3.4 CO ₂ adsorption evaluation of STC	108
4.3.5 Evaluation of heat of adsorption	111
4.3.6 Selectivity and recycle stability of STC	112
4.3.7 Removal of oil and toxic pollutants from water using carbon adsorbents	115
4.3.7.1 Organic solvent removal property of STC	116
4.4 Conclusions	122
5. NITROGEN ENRICHED MICROPOROUS CARBON FROM SUCROSE AND UREA FOR CO₂ REMOVAL	
5.1 Introduction	124
5.2 Experimental	126
5.2.1 Preparation of N-containing carbon	126
5.2.2 Characterization	128
5.3 Results and discussion	130
5.3.1 Proposed reaction between sucrose and urea	130
5.3.2 Phase structure and morphology	132
5.3.3 Textural property evaluation	138

5.3.4	CO ₂ adsorption evaluation	142
5.3.5	Correlation between CO ₂ adsorption capacity and micropore volume	145
5.3.6	Correlation between CO ₂ adsorption capacity and nitrogen content	146
5.3.7	Correlation between CO ₂ adsorption capacity and surface area	147
5.3.8	Comparison of CO ₂ adsorption capacity of all adsorbents developed	151
5.3.9	CO ₂ adsorption from air	154
5.3.10	Cyclic CO ₂ adsorption capacity from air	155
5.3.11	Isosteric heat of adsorption (Q _{st}) evaluation	156
5.3.12	CO ₂ /N ₂ selectivity	157
5.4	Conclusions	159

6. CONCLUSIONS AND FUTURE DIRECTIONS

6.1	Conclusions	161
6.2	Future Directions	165

References

List of Publications Based on the Thesis

LIST OF FIGURES

FIGURE	TITLE	PAGE UMBER
1.1	Atmospheric CO ₂ concentrations from 1958 to 2012	1
1.2	LiOH canisters used in Lunar Module and Command module of Apollo 15	9
1.3	Schematic of a typical Class 1 amine physically loaded on solid support	16
1.4	Schematic of a typical amine chemically linked with solid support	18
1.5	Schematic of a typical amine polymer supported on solid sorbent.	19
1.6	Types of adsorption isotherms	23
1.7	Schematic diagram of zeolites	27
1.8	A general structure of a MOF structure	32
1.9	Proposed mechanism for the conversion of cellulose to HTC	39
2.1	β - Cyclodextrin – Aniline complex	52
2.2	¹ H NMR spectra of β - Cyclodextrin and β - Cyclodextrin – Aniline inclusion complex	53
2.3	TG analysis of CO ₂ adsorption/desorption on β - CD-aniline complex	55
2.4	Effect of grinding on the crystallinity of aniline- β -CD complex- XRD data	56
2.5	¹ HNMR spectra of β -CD –aniline complex before and after CO ₂ purging	57
2.6	Raman spectra of β -CD –aniline complex before and after CO ₂ purging	58
2.7	Minimum energy structure of C ₆ H ₅ - NH ₃ ⁺ ...(HCO ₃ ⁻)...H ₂ O inside β -CD cavity	59

2.8	DSC curve of the activation of β -CD–aniline at 100 °C followed by CO ₂ adsorption at 30 °C	60
2.9	Kinetics of CO ₂ adsorption at different temperatures	61
2.10	Arrhenius plot for the evaluation of activation energy	62
3.1	(a) N ₂ adsorption-desorption isotherms, (b) DFT pore size distribution and (c) BJH pore size distribution of STC at various PTSA to β -CD weight ratios	72
3.2	CO ₂ adsorption of STC at various PTSA to STC weight ratios at (a) 25°C and (b) 0°C at 1 bar	74
3.3	TG-MS of STC at a PTSA to β -CD ratio of 0.04	77
3.4	SEM images of STC obtained at a PTSA to β -CD weight ratio of 0.04 (a) before activation (b) before activation-high resolution and (b) after activation-high resolution	78
3.5	N ₂ adsorption-desorption isotherm (a) and pore size distribution (b) of STC prepared at various PTSA to β -CD weight ratios after activation at 800 °C.	79
3.6	TEM images of (a) STC and (b) activated STC at a PTSA to β -CD weight ratio of 0.04	81
3.7	CO ₂ adsorption isotherm of activated STC prepared at various PTSA to β -CD weight ratios at (a) 25 °C and (b) 0 °C	82
3.8	Micropore size distribution of activated STC at various PTSA to β -CD weight ratios obtained from CO ₂ adsorption at 0 °C	84
3.9	SEM image of PTSA char	85
3.10	(a) TEM and (b) XRD spectrum of PTSA char carbonized at 800 °C.	85
3.11	TEM image of activated STC at PTSA to β -CD weight ratio of 10	86

3.12	Morphology of carbon obtained by direct carbonization of β -CD at 800 °C.	87
3.13	CO ₂ adsorption isotherm model of activated STC fit with D-R equation	88
3.14	TG graph showing direct adsorption of CO ₂ from air at 25 °C	89
3.15	DSC graph showing CO ₂ adsorption at 30 °C and desorption at 50 °C	90
3.16	CO ₂ adsorption isotherms at 25 °C showing the recyclability of activated STC.	91
3.17	Selectivity of CO ₂ adsorption over N ₂ adsorption of carbon nanospheres at 25 °C and 0 °C	91
3.18	Calculation of selectivity of CO ₂ adsorption over N ₂ adsorption at 25 °C	92
4.1	Photograph of a cotton tree with cotton fibres	97
4.2	FTIR spectra of STC at various PTSA to cotton weight ratios	102
4.3	XPS spectrum of STC 0.04	102
4.4	Raman spectra of STC at various PTSA to cotton weight ratios	103
4.5	FE-SEM images of STC at various PTSA to cotton weight ratios	104
4.6	Nitrogen adsorption–desorption isotherms of STC at various PTSA to cotton weight ratios	105
4.7	DFT pore size distribution of STC at various PTSA to cotton weight ratios	107
4.8	TEM images of STC-0 and STC-2.5	108
4.9	CO ₂ adsorption isotherms of STC prepared at various PTSA to cotton weight ratios at 25 and 0 °C at 1 bar	109
4.10	High pressure CO ₂ adsorption isotherms of STC-2.5 and STC-5 measured at 25 °C	110

4.11	DSC graph showing CO ₂ adsorption at 25 °C and desorption at 50°C	111
4.12	The CO ₂ adsorption isotherms at 25 °C showing the recyclability of STC	112
4.13	The adsorption isotherms showing selectivity of CO ₂ adsorption over N ₂ at 25 and 0 °C	112
4.14	Calculation of selectivity of CO ₂ adsorption over N ₂ adsorption. (a) 25 °C and (b) 0 °C	113
4.15	Static water contact angle of STC-0, STC-0.04, STC-1.0 and STC-2.5	115
4.16	AFM images of (a) STC-0 (b) STC-0.04, and (c) STC-2.5	117
4.17	Separation of chloroform (stained with Sudan red 5B) from water using STC-0.04	119
4.18	Removal of trace quantity of chloroform from water, and the physical separation of chloroform using a forceps	120
5.1	Structure of sucrose	126
5.2	Formation of cyanuric acid by the trimerization of urea	130
5.3	Trimerization of sucrose decomposition products	130
5.4	Proposed reaction and the structure of the polymeric product formed by heating sucrose and urea	131
5.5	XRD pattern of SU-x-250	132
5.6	FTIR spectra of SU-x-250	133
5.7	FESEM images of (a) SU-50-1-250 and (b) SU-50-1-650 at low magnification and (c) SU-50-1-650 at high magnification	134
5.8	Low-magnification (a) and high-magnification (b) HR-TEM images of SU-50-1-650	134
5.9	FTIR spectra of SU-x-1-650	136

5.10	XPS spectrum of SU-50-1-650	137
5.11	XRD pattern of SU-x-1-650	138
5.12	(a) N ₂ adsorption–desorption isotherms and (b) DFT pore size distribution of (1) SU-0-y-650, (2) SU-25-y-650, (3) SU-50-y-650, and (4) SU-75-y-650	141
5.13	CO ₂ adsorption capacity of SU-x-y-650 at 25 °C	144
5.14	CO ₂ adsorption capacity of SU-x-y-650 at 0 °C	144
5.15	Micropore size distribution obtained from CO ₂ adsorption at 0 °C of (1) SU-0-y-650, (2) SU-25-y-650, (3) SU-50-y-650, and (4) SU-75-y-650	145
5.16	Correlation between micropore volume and CO ₂ adsorption capacity.	146
5.17	Correlation between N content and CO ₂ adsorption capacity.	147
5.18	Correlation between CO ₂ adsorption capacity and the corresponding surface area.	148
5.19	Linear fit of SBET against CO ₂ adsorption capacity of SU-25-y-650	149
5.20	Linear fit of % N against CO ₂ adsorption capacity of SU-25-y-650	149
5.21	Linear fit of (a) CO ₂ adsorption vs. normalized N content (b) CO ₂ adsorption vs. normalized S _{BET}	151
5.22	Plots of textural properties against CO ₂ adsorption capacity	153
5.23	TG showing direct CO ₂ capture from air at 25 °C by SU-25-1-650	154
5.24	Cyclic capacity of SU-25-1-650 for direct CO ₂ capture from air at 25 °C	155
5.25	Isosteric heat of adsorption of SU-25-1-650	157
5.26	Adsorption isotherms showing the selectivity of	158

	CO ₂ adsorption over N ₂	
5.27	Calculation of selectivity of CO ₂ adsorption over N ₂ adsorption	158

LIST OF TABLES

TABLE	TITLE	PAGE NUMBER
1.1	CO ₂ adsorption capacities of amine physically loaded on to solid support	17
1.2	CO ₂ adsorption capacities of amine- covalently tethered to silica surfaces	18
1.3	CO ₂ adsorption capacity of zeolites	30
1.4	CO ₂ adsorption capacity of MOFs	33
1.5	CO ₂ adsorption capacity of activated carbon materials	37
1.6	CO ₂ adsorption capacity of biomass derived carbons	40
1.7	CO ₂ adsorption capacity of nitrogen doped carbon	42
2.1	Elemental analysis of β -CD and 1:1 β -CD-aniline complex	52
2.2	Chemical shift values of β - Cyclodextrin protons after complex formation	54
3.1	Yield and textural properties of STC prepared at various PTSA to β -CD weight ratios	73
3.2	CO ₂ adsorption properties of STC prepared at various PTSA to β -CD weight ratios	75
3.3	Variation of surface area, pore volume and oxygen concentration of STC with activation temperature	76
3.4	Textural properties of STC prepared at various PTSA to β -CD weight ratios after activation at 800 °C	80
3.5	Effect of activation on CO ₂ adsorption capacity of STC at various PTSA to β -CD weight ratios	83
4.1	Elemental composition of STC at various PTSA to cotton weight ratios	101
4.2	Textural properties of STC obtained at various PTSA to cotton weight ratios	106

4.3	CO ₂ adsorption capacities of STC STC prepared at various PTSA to cotton weight ratios	109
4.4	Comparison of the CO ₂ adsorption performance of the STC samples and other carbons with similar pore properties	110
4.5	Variation in chloroform removal efficiency of STC at various PTSA to cotton weight ratio	119
5.1	Composition of precursors and nomenclature of the resulting AC	128
5.2	Textural properties and N content of N-doped porous carbon	140
5.3	CO ₂ adsorption capacity and micropore volume of SU-x-y-650	142
5.4	CO ₂ adsorption capacity and % N normalized for a fixed surface area	150
5.5	CO ₂ adsorption capacity and S _{BET} normalized for a fixed surface area	150
5.6	Textural properties, % N and CO ₂ adsorption capacity of all the systems studied	152

ABBREVIATIONS

AC	Activated Carbon
AFM	Atomic Force Microscopy
BJH	Barrett-Joyner-Halenda
BET	Brunauer, Emmett and Teller
CD	Cyclodextrin
CNT	Carbon Nanotube
CO ₂	Carbon dioxide
CVD	Chemical Vapour Deposition
DFT	Density Functional Theory
DSC	Differential Scanning Calorimeter
DTG	Differential Thermogram
EDAX	Energy Dispersive Spectroscopy
FTIR	Fourier Transform Infrared Spectroscopy
HMT	Hydroxymethyl furfural
IUPAC	International Union of Pure and Applied Chemistry
MOF	Metal Organic Framework
MWNT	Multi-Walled Carbon Nanotube
PSD	Pore Size Distribution

PTSA	Para toluene sulfonic acid
SEM	Scanning Electron Microscopy
STC	Solvothermal Carbon
SWCNT	Single-Walled Carbon Nanotube
TGA	Thermogravimetric Analyzer
TEM	Transmission Electron Microscopy
XRD	X-Ray Diffractometer
XPS	X ray photoelectron spectroscopy

NOTATIONS

θ	Angle of diffraction
\AA	Angstrom
D	d-spacing
P	Equilibrium pressure
p_0	Saturation pressure
Q_{st}	Isosteric heat of adsorption
S_{BET}	BET surface area
T	Temperature
V_{p}	Total pore volume
V_{m}	Micropore volume
V_2	Ultramicropore volume

CHAPTER 1

INTRODUCTION

1.1 Global Warming

Global Warming is the increase of Earth temperature due to increased emission of greenhouse gases which absorb the heat that would otherwise escape from the Earth's surface. The gases that absorb the radiative heat (Infra red radiation) are water vapour, carbon dioxide (CO_2), nitrous oxide (N_2O), hydrofluorocarbons (CHF_3 , $\text{CF}_3\text{CH}_2\text{F}$), methane (CH_4) and sulphur hexafluoride (SF_6). Water vapour condenses above its saturated vapour pressure as rain or snow and hence it doesn't contribute to global warming. CO_2 is the primary anthropogenic greenhouse gas contributing more than $2/3^{\text{rd}}$ of the phenomenon of global warming (Yamasaki, 2003). From 1960 to 2010, CO_2 concentration in the atmosphere has increased from 310 to 390 ppm (Li et al., 2011). As shown in Figure 1, the CO_2 concentration has been increasing steadily since reliable measurements began in 1958.

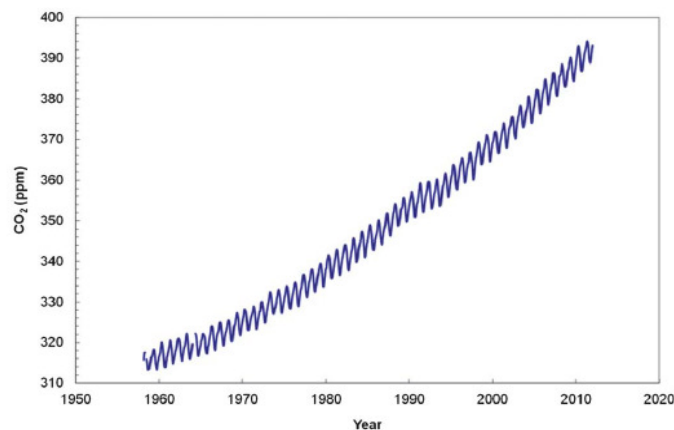


Figure 1.1 Atmospheric CO_2 concentrations from 1958 to 2012. (Source: CDIAC, Carbon Dioxide Information Analysis Centre)

According to the International Panel on Climate Change (IPCC), by the year 2100, the atmosphere may contain up to 421 - 936 ppm CO₂, causing a rise of average Earth temperature of around 2 to 4 °C (Parry, 2007). In the last hundred years, the average temperature of the world has increased by ~ 0.8 °C and is expected to increase again by 6.4% by the end of the 21st Century. The increase in the atmospheric temperature has led to a rise in the number of natural disasters; such as floods, droughts, widespread melting of ice, and an increase in average sea levels. These disasters directly or indirectly threaten human life and ecological systems on planet earth.

1.2 Source of Carbon Dioxide

Emission of CO₂ to Earth's atmosphere resulted from burning fossil fuels (i.e. Petroleum, coal and natural gas), from different industrial processes or from deforestation (Chou, 2013). Power plants contribute 25-30% share of global greenhouse gas emission. A 500 MW coal-fired power plant will generate almost 3 million tons of CO₂ per year (Liu et al, 2009). The spectacular growth of road transport has led to over 10% of CO₂ emissions. These emissions have increased by more than 50% since 1990 in spite of an improvement in vehicle fuel-efficiency. According to International Energy Agency, now road transport accounts for about three quarters of total transport emissions. Iron and steel industries make a 5% contribution in global greenhouse gas effect. The manufacturing process requires large amounts of energy to power high temperature processes, which contribute 4.5% of CO₂ emission to the atmosphere. Oil and gas production industries contribute 3% share of global greenhouse gas emissions. Deforestation, forest degradation and forest fires are responsible for over 10% of global emissions. Because of deforestation, the capacity of forests to absorb CO₂ is diminished. Also, large amounts CO₂ stored in trees and soils are released into the atmosphere. The International Energy Agency (IEA) anticipates that CO₂ capture and storage could take care of 15% of CO₂ emission to the

atmosphere from the above mentioned sources. According to Intergovernmental Panel of Climate Change (IPCC), it is possible to achieve a more than 50% reduction in CO₂ emissions from 2009 levels by 2050. It is estimated that over 30 billion tons of CO₂ can be captured and stored within the European Union by 2050. Globally, 240 billion tons of CO₂ could be captured by 2050. (Lee and Park, 2015). The 2015 United Nations Climate Change Conference, held in Paris, France, during 30 November to 12 December 2015 signed a new climate change agreement. It is called 'Paris Agreement', signed by 196 countries, aimed to reduce emissions of greenhouse gas. In the 12-page document, the members agreed to do their best for capping the global mean temperature well below 2 °C above pre-industrial levels and to pursue efforts to limit the temperature increase even further to 1.5 °C, by reducing their carbon output as soon as possible.

1.3 CO₂ Build up in Closed Crew Cabins

Yet another area where the CO₂ capture is of utmost importance is closed crew cabins in manned spacecraft and submarine. An important aspect of life support in manned spacecraft and submarines is the removal of carbon dioxide from the cabin air. CO₂ is expelled through respiration, and therefore its levels will naturally increase in a closed system, such as a spacecraft or submarine. As average person exhales about 1 kg of CO₂ and sheds about 2.3 kg of water as part of daily metabolic process, with higher emission rates during strenuous physical activity (Mulloth and Finn, 2005). CO₂ makes up approximately 0.04% of the terrestrial atmosphere and indoor air typically contains about 0.08% to 0.1% CO₂. An increase of the partial pressure of CO₂ (pCO₂) delivered to the lungs, i.e., hypercapnia, induces an increase of pCO₂ in the alveoli. Because CO₂ can freely diffuse through the alveolar membrane to the blood, it results in an increase of the CO₂ pressure in arterial blood (PaCO₂). Because CO₂ freely diffuses through tissue membranes, the toxicological effects of CO₂ appear very rapidly and are mainly

observed in the blood pH, lungs, heart and central nervous system. Studies in healthy individuals demonstrate no residual effects of breathing low to moderate CO₂ levels (<11 mmHg) for periods of 30-40 days. However, it is not uncommon for CO₂ levels to rise above the allowable concentrations in these enclosed environments (Guais, 2011). At CO₂ concentrations of about 3%, crew members will typically exhibit increased motor activity, euphoria, mental acuity and sleeplessness for about a day, followed by headache, mental depression and decreased memory, attentiveness, and appetite. Other effects of increased CO₂ concentration (in the range of 3-7%) have reduced body temperature, typically 0.5° - 1.5° C, increased urine production (up to three times of normal rate), reduced aerobic capacity (13% to 15% reduction). Acute CO₂ toxicity symptoms include fatigue, dizziness, flushing and sweating of face, visual disturbances, headache, etc. Exposure to more than 10% concentrations can cause nausea, vomiting, chills, visual and hearing illusions, burning of the eyes and loss of consciousness. Without medical support, respiratory depression, convulsion, shock, and death may result from CO₂ concentrations above 10%. United States Navy and NASA have set regulations on allowable CO₂ levels in submarines and spacecrafts respectively to ensure crew member safety. The Spacecraft Maximum Allowable Concentrations (SMACs) for carbon dioxide levels have been adjusted and depend on the duration of exposure (from one hour to 1,000 days). It is very difficult to set safe exposure limits, though, as the database regarding CO₂ and its effects suffer from a scarcity of robust data in-flight (James, J. T., 2008).

Unfortunately, “scrubbing” of spacecraft air is extremely power intensive. The microgravity environment poses an additional challenge in CO₂ removal in that a ventilation system is required to carry CO₂ away from the nose and mouth, as there are no gravitational driven convection forces in space. Thus, forced ventilation and air flow are crucial in microgravity to mix atmospheric components and to prevent pockets of CO₂. Crew members are frequently required to work behind racks and in tight spaces where air-flow can be

compromised and are consequently exposed to pockets of concentrated CO₂ (Roth, 1967).

1.4 Carbon Dioxide Removal Technologies

Since Earth's average temperature rises continually, Intergovernmental Panel on Climate Change (IPCC) suggested that global GHG emissions must be reduced by 80% by 2050 to avoid adverse effects of global warming (Pridmore et al, 2003). CO₂ Capture and Storage (CCS) is the capture of CO₂ without releasing them to the atmosphere. CCS consists of capturing CO₂, compressing, transportation, deposition in the ground or an ocean-bedrock sediment layer, and long-term monitoring (Li et al, 2013). CO₂ capture is a core technology and accounts for 70–80% of the total costs of CCS. It is classified as (i) post-combustion, (ii) pre-combustion and (iii) oxy-fuel combustion. Post-combustion capture technology involves collecting CO₂ from the emission gases of a power plant. Pre-combustion capture technology is a fuel conversion process (e.g., gasification of coal) prior to combustion; the density and pressure of CO₂ in the gases allow easy separation. Pre-combustion involves gasification of the primary fuel, coal or biomass. The fuel reacts with oxygen to give mainly CO and hydrogen. In Oxy-fuel combustion, or oxygen-fired combustion, high-purity oxygen is used instead of air. Thus, the density of CO₂ in the gas flow, i.e., the emission gas, becomes high, resulting in easy separation of CO₂. (Sistla, and Khanna, 2014). In comparison with two other processes, post-combustion CO₂ capture is quite competitive in cost.

During the past few decades, much effort has been committed to the development of new CO₂ capture technologies, which includes chemical absorption using liquids, physical adsorption using solid etc. (Aaron and Tsouris, 2005). Absorption with liquid amine is the most widely applied technology for

CO₂ capture. CO₂ removal from flue gas by sorption with aqueous amines viz., monoethanolamine (MEA), diethanolamine (DEA) has been established since 1930 and is still believed to be a reasonable technology. But liquid amines face some drawbacks such as high volatility leading to high amine consumption, high alkalinity causing vessel erosion, and high energy consumption for regeneration because of the presence of large amounts of water (Chaffee et al., 2007). In contrast, adsorption using solid adsorbents could overcome these disadvantages and exhibit promising application for carbon capture. Solid adsorbents such as activated carbons (AC), carbon nanotubes (CNT), zeolite, metal organic frameworks (MOFs), alkali-metal carbonate, metal oxide and amine-modified materials (AMMs) are often used to capture CO₂ (Choi et al, 2009).

Adsorption processes using solid sorbents have many advantages, such as low regeneration energy, greater CO₂ adsorption capacity, selectivity, ease of handling, etc. The regeneration energy requirement for CO₂ capture for solid amine is less compared to liquid amines. Moreover, the heat capacity of solid sorbent is comparatively lower than that of an aqueous amine solution (Samanta et al, 2012).

Efficient and economic CO₂ capture has several characteristics: large CO₂ adsorption capacity, fast adsorption and desorption kinetics, favourable adsorption and desorption temperature, and excellent cycling stability. These criteria are described in detail below (Samanta et al, 2012).

CO₂ adsorption capacity: CO₂ adsorption capacity can be expressed by two terms viz., equilibrium capacity and working capacity. Equilibrium adsorption capacity indicates the maximum CO₂ adsorption capacity of the material. Working adsorption capacity is defined for a short adsorption time. The equilibrium adsorption capacity of a sorbent material is important because it dictates the amount of adsorbent required, which fixes the volume of the adsorber vessels and

thus to the capital cost of the system. In practice, working capacity is preferred to be used in place of equilibrium capacity. The adsorption equilibrium can be measured either gravimetrically (generally using Thermo Gravimetric Analysis) or volumetrically (using surface area analyser). The gravimetric CO₂ adsorption refers to the quantity of CO₂ adsorbed per unit of mass of the material, which provides the mass of the adsorbent required to form the adsorbent bed. On the other hand, the volumetric CO₂ uptake measures how densely CO₂ can be stored within the material providing information on the volume of the adsorbent bed.

Selectivity for CO₂: The adsorbent should preferentially adsorb CO₂ in the presence of other molecules (for example, N₂). Closed crew cabin atmosphere and flue gas streams contain N₂ and O₂. It is also important that solid sorbents also show high capacity for CO₂ in the presence of significant amounts of water vapor.

Adsorption/desorption kinetics: It is essential for a good adsorbent to have fast adsorption/desorption kinetics for CO₂. The adsorption/desorption kinetics control the cycle time, thus the material with fast kinetics is preferred. The overall CO₂ adsorption kinetics of functionalized solid adsorbent is influenced by reaction kinetics of CO₂ with the functional group present and the resistance of the gas phase through the pores of sorbent.

Chemical stability: CO₂ capture sorbents especially base-functionalized sorbents should be stable in an environment of oxidizing gas viz. SO_x, NO_x and other contaminants such as heavy metals.

Regeneration of sorbents: The heat of adsorption of a regenerable adsorbent, a measure of the energy required for regeneration, should be considerably low. The lower the heat of adsorption, the lower the regeneration cost. Heats of adsorption are in the ranges of 25 to 50 kJ/ mol and 60 to 90 kJ/mol for physisorbents and chemisorbents, respectively.

Sorbent costs: Practically useful adsorbents will be those that effectively and economically capture CO₂ from flue gas streams.

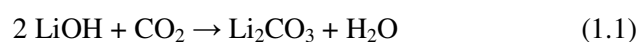
Sorbent development for CO₂ capture is an active field with new materials being developed with high adsorption capacity. Each of the sorbents employs one of the two possible adsorption mechanisms, either chemical adsorption or physical adsorption. The following sections (1.4.1 and 1.4.2) summarize important chemisorbents and physisorbents developed for CO₂ capture applications.

1.4.1 Chemisorbents for CO₂ removal

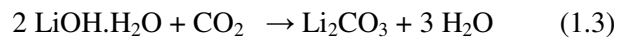
An emerging area of research and development is the realization of new materials which can selectively chemisorb CO₂ from a gas mixture with good selectivity, adsorption capacity and relatively fast kinetics of sorption. Chemisorption is driven by chemical reaction occurring at the exposed surface. In chemisorption, CO₂ undergoes a covalent chemical reaction to bind to certain sites on the sorbent with a much greater heat of adsorption. Metal oxide, metal hydroxide and amine based chemisorbents are widely used material under this category.

1.4.1.1 Lithium hydroxide based solid sorbents

Lithium hydroxide is a non-regenerable system for CO₂ removal, widely used in short duration manned space missions. Two types of LiOH canister used in Lunar Module and Command module of Apollo 15 are shown in Figure 1.2. These materials react with CO₂ to form carbonate; the net reaction is given as Equation 1.1:



One gram of LiOH can theoretically absorb 0.92 gram of CO₂. The reaction between LiOH and CO₂ can only take place in the presence of water vapor. The net reaction is actually the combination of the following two reactions (Equation 1.2 and 1.3)



If there is no sufficient water present, the hydrate, LiOH·H₂O, cannot be formed, resulting in incomplete carbon dioxide reaction. However, an excess of water vapor can also be a problem, causing a water film to form around the LiOH granules which acts as a barrier, again resulting in incomplete reaction between LiOH and CO₂. Insufficient water vapor is not a concern in scrubber design due to the saturated moisture content of the exhaled human breath; however, excess water is a different case. From the reactions, it can be seen that one mole of water is produced for every mole of CO₂ absorbed. It is apparent that as the reaction occurs and water is produced, a film barrier can build up to the point where reaction can no longer continue in a complete manner. The water film could cause premature breakthrough and reduce canister efficiency [Jaunsen, 1989].



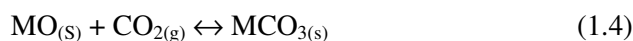
Figure 1.2 LiOH canisters used in the Lunar Module and Command module of Apollo 15

The kinetic factors which drive the removal of CO₂ by LiOH include higher partial pressure of CO₂, high vapor pressure of water and removal of heat. Bed dynamics, including absorbent bed length and linear gas velocity, also have significant effects on rates of LiOH consumption. Particle characteristics such as granule porosity alter the surface area and subsequently affect the reaction rate significantly. Optimal reaction bed temperatures and water vapor pressure ranges for absorption of CO₂ have already been examined for LiOH.

1.4.1.2 Metal oxides based solid sorbents

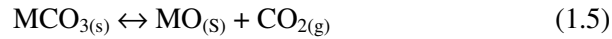
Alkali and alkaline earth metal oxides have been reported as regenerable chemisorbents for CO₂. Alkali metal oxides (e.g., Li₂O and Na₂O) have a stronger basicity than alkaline earth metal oxides. However, bare Li₂O is expensive, unstable, and difficult to store, which limits its use for CO₂ capture. MgO and CaO are widely used for CO₂ capture due to their wide availability in natural minerals, low cost, and easy bulk production. CaO-based materials have higher CO₂ adsorption capacities compared to MgO, thus used more intensively (Wang et al, 2011). In large-scale CO₂ capture applications, calcium oxide based adsorbents materials are thought to be advantageous compared to other adsorbents on account of the low cost and wide availability of precursors (limestones or dolomites). The maximum theoretical CO₂ adsorption capacity of CaO is 17.8 mmol/g. (Lu, 2014).

One mole of metal oxide can chemically adsorb a stoichiometric equivalent of CO₂ to form an alkaline earth metal carbonate through the following reaction:



Where M can be, Mg, Ca, Sr or Ba. The reaction is exothermic.

While regenerating, the carbonate decomposes to form oxides, liberating CO₂, as shown in Equation (1.5).



The problem associated with CaO adsorbents is that they suffer from a rapid degradation of CO₂ capture capability during the repetition of carbonation/calcination cycles. This reduction is due to two reasons viz., pore blocking and adsorbent sintering (Lu et al, 2012). To stabilize the CO₂ capture performance of CaO based system, the widely adopted methods are introduction of dopants or high sintering temperature. (Valverde, 2013). Supports SiO₂, Al₂O₃ (Lan et al, 2014; Yu and Chen, 2014), TiO₂, calcium titanate (Lide, 2014) etc were incorporated into the system for high cycle stability.

Magnesium oxide has also been investigated as adsorbent for CO₂ (Feng et al, 2007). Beruto et al (1987) have reported that the CO₂ adsorption by MgO is essentially on its surface, whereas upto 20% of CO₂ taken up by CaO is not on the surface, but in the lattice or at grain boundaries.

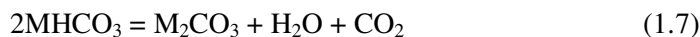
1.4.1.3 Metal carbonate based solid sorbents

Alkali metal carbonates are regenerable chemisorbents for CO₂, which is being considered for long time for CO₂ capture. Since the operating temperatures of metal carbonates are in the range 60-200 °C, these are suitable for flue gas CO₂ capture applications. In the CO₂ adsorption process, metal carbonates react with CO₂ in the presence of moisture at 60 - 110 °C and form alkali-metal bicarbonate. Desorption is done by heat treatment of the bicarbonate at 100-200 °C, releasing the CO₂. The adsorption and desorption equations are shown below.

Carbonation (Equation 1.6)



Decarbonation (Equation 1.7)



The maximum theoretical capacity of Na_2CO_3 is 9.43 mmol/g (41.5%) and that of K_2CO_3 is 7.23 mmol/g (32%) (Hayashi et al., 1998). These dry regenerable adsorbents have the additional advantage of low cost.

The problems associated with metal carbonates are the slow carbonation rate, temperature limitation, low long-term stability and non-repeatable performance of these sorbents under flue gas conditions. Many attempts have been made to resolve these problems. The best method is dispersing metal carbonate on supports such as Al_2O_3 , active carbon, TiO_2 , SiO_2 , etc., so as to enhance the adsorption rate and to prevent the pressure drop. Wu et al (2008) reported a CO_2 adsorption capacity of 6 mmol/g for $CaCO_3$ nanoparticles coated on Al_2O_3 at 923 K. Okunev et al.(2003) investigated the influence of type of porous support on the CO_2 sorption of K_2CO_3 . A completely reversible regeneration was observed in case of an activated carbon supported sorbent system. The study concluded that the dynamic CO_2 adsorption capacity decreases in the following sequence: alumina > activated carbon > vermiculite > silica gel. In 2009, Lee et al developed a new dry sorbent system, “KZrI30” (30 wt% K_2CO_3/ZrO_2). The material showed CO_2 capture capacity of 2.1 mmol/g and the capacity was almost same in repeated cycle operation in presence of 9% water in the air stream. The enhanced CO_2 capture capacity is due to the conversion of the entire K_2CO_3 to $KHCO_3$ in presence of ZrO_2 support. On the other hand, supports such as MgO and Al_2O_3 showed decrease in CO_2 adsorption capacity after each regeneration, due to the partial conversion of K_2CO_3 to $KAl(CO_3)_2(OH)_2$, $K_2Mg(CO_3)_2$ etc.

Metal oxides and carbonates are used for moderately high temperature CO₂ adsorption, especially flue gas CO₂ capture. However, amine based solid sorbents are widely used and the best CO₂ chemisorbent at room temperature applications.

1.4.1.4 Amine based solid sorbents

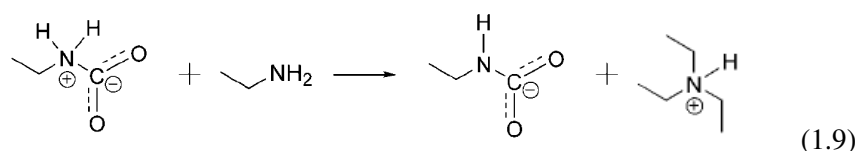
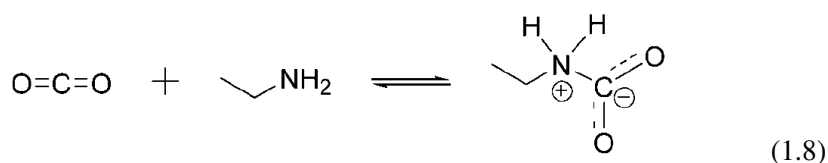
For CO₂ capture applications, the immobilization of amines onto a solid support (e.g., porous silica) has several advantages. For liquid amines, a large energy cost is paid to heat H₂O in the amine solution during the regeneration. A portion of this cost can be avoided by replacing H₂O with a solid support having lower heat capacity. Amine supported solid sorbents are cost-effective regenerable sorbents, with low heat of adsorption. Unlike amine solutions, degradation due to evaporation is less for supported amines. Also, the contact between silica particles and other solid surfaces is lower, causing less problem of vessel corrosion than an aqueous amine system.

From 2000 onwards, many research groups are trying to improve the CO₂ sorption capacity of solid amine based sorbent systems via., (1) immobilization of amines on different porous solid materials, (2) selection of proper amine and (3) enhancing CO₂ diffusion. A variety of microporous/mesoporous materials (metal organic frame works, zeolites, porous polymers, silica, CNT, graphite etc) loaded with organic amines have been investigated for CO₂ adsorption (Qi et al (2012), Gadipelli et al (2016), Loganathan et al, 2016). Supported amine sorbents have been classified into three classes:

Class 1: This class of solid amine sorbents is prepared by physically loading monomeric or polymeric amine onto the porous support

- Class 2: This class of adsorbents, in which the amine, mainly amine-containing silane group, is covalently linked to a solid support, such as porous silica.
- Class 3: These supported adsorbents, amine containing monomers are polymerized, thus the resulting solid polymer is rich in amine functional groups.

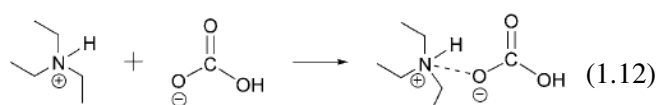
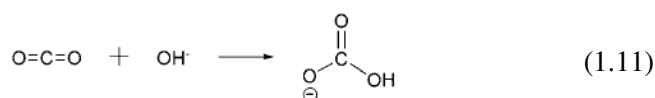
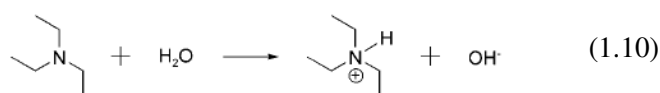
Adsorption of CO₂ using amines involves chemical reaction, and the interaction is controlled by several factors. Primary and secondary amines directly react with CO₂ forming intermediate zwitterion first. This happens by the attack of lone pair of nitrogen to the carbon of CO₂. De-protonation of zwitterion is done using free amine, resulting in carbamate. In the presence of moisture, deprotonation may be done by water, instead of amine. This zwitterionic mechanism was first proposed by Caplow (1968), as shown in Equations 1.8 and 1.9.



Under dry condition, two moles of amines are required to remove one mole of CO₂, whereas in wet condition, where H₂O or OH⁻ is present, one mole of amine removes one mole of CO₂. Amine efficiency is defined as the number of moles of CO₂ captured per unit mass divided by the number moles of nitrogen per unit mass. Amine efficiency gives the reflection of the efficiency of adsorbent for maximum utilization of available amines for CO₂ removal. Under dry condition, since two amines are utilized for removing one CO₂ molecule, the amine efficiency of adsorbent is 0.5 mol CO₂ per mol N, whereas, under humid

condition, water can also act as a base, the maximum amine efficiency is 1.0 mol CO₂ per mol N.

Tertiary amines do not directly react with CO₂. Instead, it initiates the formation of bicarbonate. In the first step, the tertiary amine reacts with H₂O to form a quaternary cationic species and OH⁻. Hydroxide ion then attacks CO₂ to form bicarbonate. The final step is the ionic association of bicarbonate and protonated amine (Equations 1.10, 1.11 and 1.12). This mechanism was first proposed by Donaldson (1980).



Amine physically loading onto porous support

The simplest method of supporting amine on porous support is to physically mix the amine with the support. This method is called wet impregnation. In this method, porous support (eg: silica, activated carbon) is suspended in a solution of amine diluted with volatile organic solvent. Amine diffuses into the pore of support by concentration driving force or in some cases chemical affinity, after which the solvent is removed by evaporation. Schematic of a typical amine loaded into the pores of solid support is shown in Figure 1.3. All the amine loaded into the porous material may not be accessible to the CO₂.

This may be due to the fact that amines may sandwich in between solid support, and sterically screened to capture CO₂.

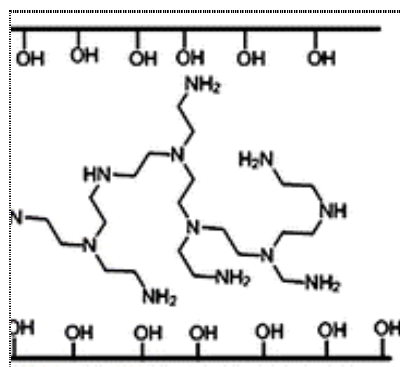


Figure 1.3 Schematic of a typical Class 1 amine physically loaded on solid support

The first amine impregnated CO₂ adsorbent (PEI/MCM-41) was developed by Xu et al. (2002). The adsorbent had a CO₂ capacity of 3.0 mmol g⁻¹ at 75 °C under a dry 100% CO₂. For the impregnated systems, supports having a larger pore volume give a better adsorption performance. Son et al. (2008) impregnated PEI onto different mesoporous silica materials (i.e. MCM-41, SBA-15, SBA-16, KIT-6) and discovered that the adsorption capacity increased with an increase of the pore diameter. There have been a number of amines investigated for impregnation into silica supports, viz., polyethylenimine (PEI), Tetraethylene pentamine (TEPA) etc. The selection of amine depends on the concentration of amine group per unit weight, thermal stability of amine etc. The physical loading of amine on porous support is simple compared to the chemical linking of amines on solid support as discussed in the subsequent section on amine chemically linked to porous support. Moreover, the modification of pore size and pore volume of the support can enhance the amine loading and CO₂ adsorption capacity. However, leaching of the amines during regeneration is a drawback for amine impregnated solid sorbents (Samanta et al., 2011). Therefore, the stability and regeneration of the amine-impregnated solid sorbents have not been tested effectively under real flue gas conditions. CO₂ adsorption capacities

of amine physically loaded on to porous support reported in the literature are summarized in Table 1.1.

Table 1.1 CO₂ adsorption capacities of amine physically loaded on to solid support

Amine	Support	CO₂ adsorption capacity, mmol/g	Reference
TEPA	MCM-41	5.02	Yue et al, (2008)
PEI	Silica foam	5.8	Qi et al (2012)
PEI	KIT-6	3.07	Son et al (2008)
PEI	Carbon	3.0	Wang et al (2012)
TEPA	carbon derived from MOF	6.0	Gadipelli et al (2016)
TEPA	Fibrous nano silica	4.5	Sing et al, 2016
Triamine	Pore expanded MCM-41	2.1	Loganathan et al, (2016)

Amine chemically linked to porous support

The second main class of solid supported amines is those in which the amine is covalently bound to the silica support, generally, through alkyl-silyl linkages. The advantage of these adsorbents over amine-impregnated silica is that the amine cannot leach even under elevated temperature. This strong covalent linkage of amine to the silica surface makes it a suitable candidate for repeated adsorption and desorption cycles with a consistent adsorption capacity. Silane chemistry is the most commonly used method for synthesizing covalently tethered amines. Here, amino alkoxy silane reacts with silica surface in an organic solvent. The alkoxy silyl groups condense with silanol groups on the surface of the support to form new Si-O-Si linkages with the liberation of alcohol. Since trialkoxysilanes contain three reactive alkoxy groups, they are

typically used to create as many new linkages to the silica surface as possible. Also, the alkoxy silane with maximum density of amine group is preferred for condensation, since the nitrogen density of solid sorbent is also a critical factor affecting CO₂ adsorption capacity. Figure 1.4 represents the schematic of a typical amine chemically linked with solid support.

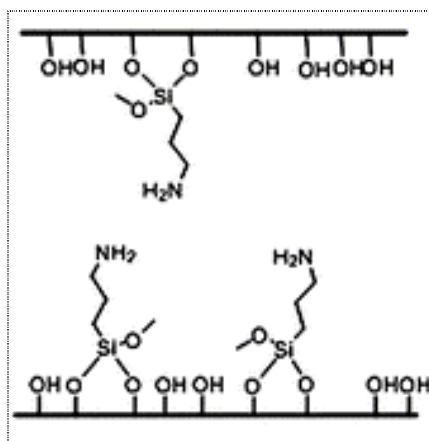


Figure 1.4 Schematic of a typical amine chemically linked with solid support

CO₂ adsorption capacities of amine chemically linked to solid support reported in the literature are summarized in Table 1.2.

Table 1.2 CO₂ adsorption capacities of amine- covalently tethered to silica surfaces

Silane	Support	CO ₂ ads. capacity, mmol/g	Reference
Disilane	SBA-15	1.95	Zheng, 2005
Aminopropyltrimethoxysilane	MCM-22	1.5	Yang et al (2012)
Tri amine-containing silane	MCM-41	2.0	Serna (2010)
Aminopropyltrimethoxysilane	ITQ-6	1.2	Zukal et al. (2009)
Amine and vinyl silane	POSS	2.5	Abhilash et al (2015)
Triethylene tetramine	Fe-Zr	4.1	Yang et al, 2015

Amine functionalized polymers

Porous polymeric amine sorbents can be prepared by the polymerization of amine containing monomers or covalent functionalization of polymers/oligomers with high amine content into polymer support. Figure 1.5 shows the schematic of a typical amine polymer supported on solid sorbent.

A novel covalently bound hyperbranched aminosilica (HAS) sorbent with high amine content was developed by Jones et al.(2008) HAS was synthesized via a one-step surface polymerization reaction of aziridine monomer inside SBA-15 pores. The material showed a superior CO₂ adsorption capacity of 3.08 mmol/g, using 10% CO₂ in the air stream. They found that the material is having higher amine loadings of 7 mmol N/g and, therefore contributed to a better adsorption capacity. Liang et al (2008) investigated the step-wise polymerization of melamine dendrons from monoamine and SBA-15. The material showed a CO₂ adsorption capacity of 1 mmol/g at room temperature.

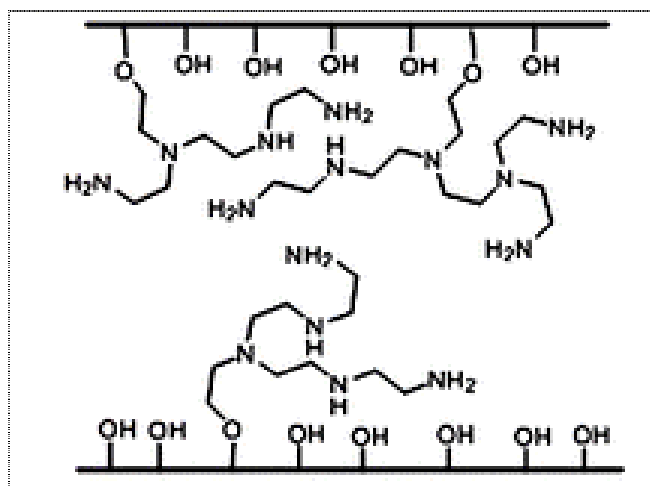


Figure 1.5 Schematic of a typical amine polymer supported on solid sorbent.

Regeneration of amine sorbent

The general desorption conditions used for amine systems are temperature swing accompanied by inert gas purging. Increase in temperature provide energy for the desorption process since desorption is an activation process. There were reports where PEI-impregnated silicas can be regenerated by inert gas flow alone, provided that the adsorption temperature is sufficiently high to provide the activation energy required for desorption. Xu et al [2005] measured fully regenerable capacity over 10 cycles of PEI supported amines with just an inert gas purge for desorption. For chemically linked amines on support, the desorption temperature depends on the type of amine used and the structure formed with CO₂. The CO₂ desorption of silane functionalized SBA-15 was studied by Hiyoshi (2005). They concluded that the desorption temperature increase in the order mono < di functionalized SBA-15. There are possibilities of different structures (including bidentate species) when multiple amines react with CO₂. The number of bidentate species formed during CO₂ adsorption may change after repeated adsorption-desorption cycles. Hence, there may be some shift in desorption temperatures of chemically linked amines on solid support.

There are some problems associated with chemisorbents viz., a) the low thermal stability (< 150 °C) of amines, which restricts their regeneration temperatures, b) poisoning of binding site, leading to decrease in the capacity of the sorbent, c) limited recycle stability, d) high regeneration energy requirement. These limitations are solved to large extent by using physisorbents.

1.4.2 Physisorbents for CO₂ removal

Physical adsorption relies on the affinity of CO₂ to the surface of a material without forming a chemical bond. Adsorbents separate CO₂ from a stream by preferentially attracting it to the material surface through weak van der Waals forces as well as by quadrupole-ion and quadrupole - quadrupole

interactions between the quadrupole of CO₂ and the ionic/polar sites of the solid adsorbent surface. During capture, the chemical potential of the adsorbed CO₂ is lower than that of CO₂ in the gas mixture. In spite of a decrease in entropy during adsorption ($\Delta S < 0$), the high exothermic nature of the adsorption ($-\Delta H$) results in a decrease in chemical potential ($\Delta G = \Delta H - T\Delta S$).

CO₂ from flue gas and closed crew cabin atmosphere may be removed using solid physisorbent materials, viz., porous carbonaceous materials, zeolites, metal-organic frameworks (MOFs) etc. Since adsorption is a surface phenomenon, a successful adsorbent is usually highly porous material with a high surface area. By definition, a porous material is a solid matrix composed of an interconnected network of pores (voids). The International Union of Pure and Applied Chemistry (IUPAC) has defined three classes of porous materials, viz., microporous (pore size < 2 nm), mesoporous (pore size 2-50 nm). (Sing, et al, 1985). In microporous materials, gas adsorption take place by three-dimensional condensation of the adsorbate inside a strong electromagnetic field induced by the narrow pore dimensions. The system properties are close to a single-phase, where interphase adsorbate–adsorbent interactions do not exist. Due to strong van-der-Waals interactions, micropores are suitable for gas-phase adsorption. In mesoporous materials, adsorption proceeds via consecutive formation of adsorbate layers on pore wall which is completed by the phenomenon of capillary condensation. Macropores cannot be filled by capillary condensation, since its porous properties are similar in character to conventional flat surfaces (Greg and Sing 1982).

A large number of studies have been carried out on parameters which control the gas adsorption, viz.,(i) Nature of adsorbent and adsorbate (ii) Surface area and porosity of the adsorbent (iii) Pressure and (iv) Temperature. In case of adsorbents, material with large specific surface area is preferable for providing large adsorption capacity. But, the size of the micropores determines the accessibility of adsorbate molecules to the internal adsorption surface. Therefore, the pore size distribution of adsorbents is another important property for evaluating adsorption efficiency of adsorbents. Porous materials such as zeolite,

mesoporous polymers and carbon molecular sieves can be specifically synthesised with precise pore size distribution and hence can be tailored for a particular separation. Adsorption process also depends on the pressure of the adsorbate gas. Adsorption of gas follows Le Chatelier's principle which states that with the increase of pressure, the magnitude of adsorption also increases and vice versa. The increase of pressure increases the chemical potential of the gas ($d\mu = RTd\ln p$ whereas μ is the chemical potential, R is the Universal gas constant, T is the absolute temperature and p is the partial pressure of the adsorbate). Therefore, more molecules get adsorbed on the surface to decrease the chemical potential of the system (Brunauer, S., 1943). Physisorption also depends on the temperature of adsorbate gas or the adsorption environment. Physisorption is very effective particularly at a temperature close to the critical temperature of a given gas. Meanwhile, chemisorption occurs at temperatures much higher than the critical temperature (Sing, 1998).

Easily liquefiable gases such as SO_2 , NH_3 and CO_2 adsorb more readily than gases like H_2 , N_2 and O_2 which do not liquefy easily. This is due to the Van der Waals or molecular forces existing in easily liquefiable gases are much greater than permanent gases. Depending on the nature of the adsorbates such as molecular weight, polarity, size and other physical and chemical properties, the type of adsorbents also varies. (Dabrowski, 2001).

Physisorption is based on the van der Waals force of attraction between gas and the sorbent, which do not lead to a significant change in the electronic orbital patterns of the gas and the sorbent. The adsorbed quantity of gas on an adsorbent depends on the temperature (T) and the pressure (p) of the gas. Therefore, the number of moles of the adsorbed gas per gram of adsorbent (n) at a particular temperature can be described by the Equation

$$n=f(p,gas,solid) \quad (1.13)$$

Clapeyron (1834) stated the ideal gas law, the volume of an ideal gas at the standard temperature (T_{STP} : 273 K) and pressure (P_{STP} : 1 atm) is 22414 cm^3/mol and the number of moles n can be calculated as Equation (1.14).

$$n = V_{STP} / 22414 \text{ (mol)} \quad (1.14)$$

The gas adsorption isotherm based on the gas law theory $PV = nRT$, is used for extracting the information of surface area, pore size, pore size distribution and so on. The quantity (volume) of adsorbed material - pressure relationship at a constant temperature is represented by adsorption isotherm. Adsorption isotherm can be divided into six types (Figure 1.6) (Brunauer, 1943).

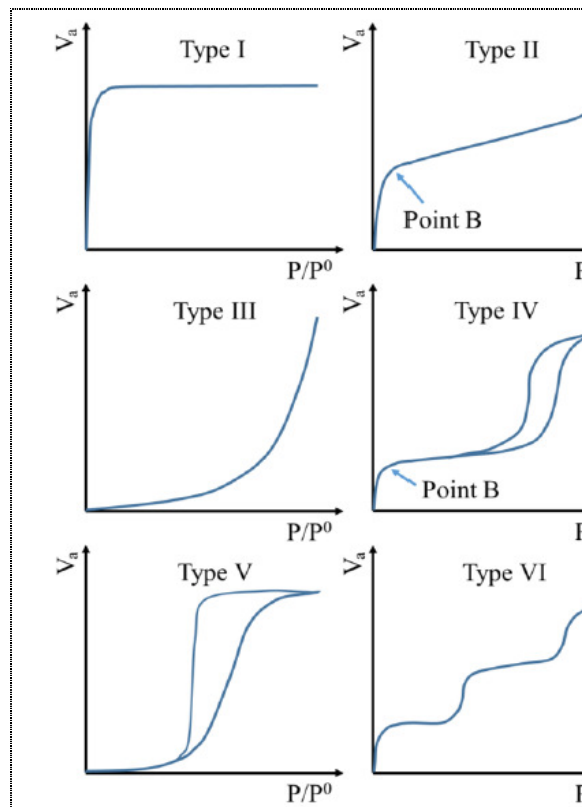


Figure 1.6 Types of adsorption isotherms

Type I isotherm represents a fast initial uptake at low pressures with a limiting quantity at high pressures and a reversible isotherm in some cases. This isotherm normally appears in microporous materials, which have pore sizes of a few diameters of the adsorbate molecule. Therefore, the limit of the adsorbed quantity is governed by the accessible micropore volume. The Type I isotherm is also named Langmuir isotherm due to the formation of monolayer.

Type II isotherm is exhibited by macroporous powders (pore size larger than 50 nm). Here, monolayer and multilayer adsorptions occur during the whole adsorption process and the point B (inflection point or knee of the isotherm) is often taken to indicate the completion of the monolayer coverage and the beginning of the multilayer.

Type III isotherm is exhibited by materials where adsorbate - adsorbate affinity dominates over adsorbate / adsorbent affinity and increasing adsorption occurs after the completion of an interfacial monolayer. The isotherm is convex to the pressure axis during the whole adsorption procedure. Type I, II and III are more or less reversible.

Type IV isotherm exists by mesoporous materials. The desorption branch of **Type IV** isotherm shows the hysteresis loop, which is different from the adsorption branch. The hysteresis is associated with a capillary condensation in mesopores. At the low pressure range, the Type IV isotherm is similar to the Type II isotherm with point B.

Type V isotherm corresponding to the Type III isotherm arises, when the interaction between an adsorbate and an adsorbent is very small. Due to the existing pores a hysteresis loop occurs.

Type VI isotherm results from a uniform non-porous substrate adsorbing stepwise multilayers. The step height demonstrates the monolayer capacity for each adsorbed layer and the step sharpness depends on the system and the temperature.

Langmuir [1916] described the Type I isotherm appropriately to chemisorption. There are several Langmuir assumptions: i) only one molecular single layer formed on the adsorbent surface (monolayer adsorption), ii) homogeneous adsorbent surface and iii) no interactions among adsorbed gas molecules. The Langmuir Equation is

$$V_a = V_m b p / (1 + b p) \quad (1.15)$$

V_a and V_m are the volumes of the adsorbed gas molecules and the completely covered monolayer, respectively at pressure p and b is an empirical constant.

Later, Stephen Brunauer, P.H. Emmett and Edward Teller (1938) studied the gas adsorption in multi-molecular layers and generated a universal Equation of multilayer adsorption based on the Langmuir concept which is known as BET theory. BET concepts are i) equal energy for each adsorbed layer ii) infinite number of adsorption layers iii) no interaction among each adsorption layer iv) equal rate of gas molecular condensation on an already adsorbed layer compared to the rate of evaporation from this adsorbed layer. The linear form of BET Equation is :

$$\frac{p}{V_a(p_0 - p)} = \frac{1}{V_m C} + \frac{C - 1}{V_m C} \left(\frac{p}{p_0} \right) \quad (1.16)$$

Here p_0 is the saturation gas pressure and C is the BET constant and related to the heat of adsorption (E_1) of the first layer and the heat of liquefaction

(EL) of the adsorbate, V_a and V_m are the volumes of the adsorbed gas molecules at pressure p and the completely covered monolayer respectively.

In physisorption, a gas molecule attaches on any sites of the surface. Gas molecule has a very high selectivity on adsorbent surface in chemisorption. The energy of chemisorption is normally higher than the necessary energy of physisorption. Generally, further adsorption happens after the completion of the first layer with physisorption and the adsorbate spreads out on the condensed gas monolayer to form a multilayer. Thus, BET theory is adapted for physisorption. However, for chemisorption the adsorbate reacts with adsorbent and forms a monolayer, thus Langmiur theory is adapted for chemisorption.

The main advantage of physical adsorption methods is the possibility for low energy requirement to regenerate the sorbent material and quick regeneration time associated with changing pressure. (Hermann et al, 2005). Next section summarizes the recent progress in CO₂ capture using solid chemisorbents and physisorbents for CO₂ capture.

1.4.2.1 Zeolite based solid sorbents

Zeolites are microporous crystalline framework materials, which are widely used for gas separation and purification. Zeolites are crystalline alumina silicate that possesses a framework formed by a 3D assembly of tetrahedra $[\text{SiO}_4]$ and $[\text{AlO}_4]^-$ (Figure 1.7). This three dimensional arrangement gives rise to diverse framework structures. The structural formula of zeolite is $\text{M}_{x/n}[(\text{AlO}_2)_x(\text{SiO}_2)_y] \cdot w\text{H}_2\text{O}$. In this, M is an alkali or alkaline earth cation, n is the valence of the cation and w is the number of water molecules / unit cell. The x and y are the total number of alumina and silicate tetrahedra respectively per unit cell. The ratio y/x usually has values in the range of 1 to 5, for the silica Zeolite. The primary building unit for zeolites is the tetrahedron and the

secondary building units are the geometric arrangements of tetrahedra. The building units may be simple polyhedra such as cubes, hexagonal prisms or octahedra. The structures can be formed by repeating Secondary Building Units.

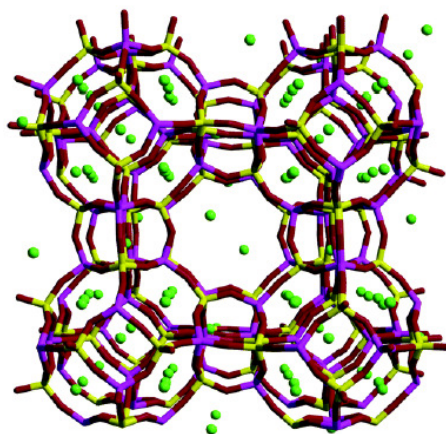


Figure 1.7 Schematic diagram of zeolite (silicon, aluminum, oxygen and sodium in zeolite 4A are indicated in yellow, purple, red and green, respectively (Source: Jaramillo and Chandross, 2004)

The packing of zeolites structure allows the formation of regular cavities joined by the channels, where the molecules with an appropriate size such as CO₂, water etc. can accommodate. (Bonenfant, 2008). Conventional zeolites are based on silicate frameworks in which substitution of some of the Si with Al leads to a negative charge on the framework. This negative charge is compensated by certain cations (Li⁺, Na⁺, K⁺, Ca²⁺, Ba²⁺ etc.) by penetrating to the pore network. These cations can be exchanged to tune the pore size or the adsorption characteristics. Because of their well defined crystalline structures, the sorbents have uniform pore sizes in the range of 0.5 nm to 1.2 nm. This property allows them to separate CO₂ molecules by means of the molecular sieving effect. Separation of gases in zeolites can also occur through the mechanism of selective adsorption of molecules that have a relatively large energetic dipole and quadrupole.

Basicity of zeolites caused by cations allows strong accommodation of acidic CO₂ molecules. The most of known zeolites have a CO₂ adsorption capacity from 0.15 to 5.5 mmol /g (Ko et al, 2003). The adsorption capacity of zeolites depends on several factors including the size, distribution and the number of cations, Si/Al ratio, the polarity and size of adsorbed molecules, the presence of water etc (Xu et al, 2002). An extensive screening study of a dozen synthetic zeolites, including 5A, 13X, NaY, ZSM-5 etc was conducted by Harlick and Tezel (1998) for the removal of CO₂ from flue gas. The CO₂ adsorption capacity of zeolite depends on pore size and loading pressure. At low pressures, the density of the adsorbate is highest in the smaller pores because the adsorbed molecules have the tendency to occupy the positions where the adsorbate-adsorbate interactions are less than the adsorbate-pore interactions. At high pressures CO₂ might occupy the central region of the pores. (Samios, 2000).

Zeolite system has been used in long duration space missions, on Skylab, Shuttles and the Space Station. There are generally two types of Zeolite based CO₂ removal systems, two bed system and a four bed system. The difference between the two systems is that the first contains both water and CO₂ adsorption beds within a single canister whereas the second has each bed in a separate canister. Because the two-bed system contains both water and CO₂ sorbents within the same canister, desorption of CO₂ to space vacuum also requires the dumping of water. Hence two bed system is commonly used when water recovery is not necessary. In case of four bed system, each of the four beds is contained in separate canisters, which permits the conservation of water or CO₂ or both.

Factors affecting CO₂ adsorption by zeolites

Basicity of zeolite: Basicity of zeolite is mainly created by the accommodation of cations into the zeolite structure; which increases the electron density of oxygen framework. Basic strength of zeolites containing the cations of

Group 1A increases as following: $\text{Li}^+ < \text{Na}^+ < \text{K}^+ < \text{Rb}^+ < \text{Cs}^+$. It has also been reported that the basicity of oxygen atoms of zeolites NaX and NaY is strongly decreased by the replacement of Na^+ cations by the Ba^{2+} cations. This is due to the decrease of partial negative charge of oxygen atoms adjacent to Ba^{2+} cations (Ko et al, 2003).

Number of exchangeable cations: The adsorption of gas by the zeolites is also determined by the number of cations which are able to interact with adsorbates. The higher CO_2 adsorption of zeolite CaX than the zeolite CaY is due to greater number of Ca^{2+} in the zeolite CaX which are able to interact directly with the adsorbed CO_2 molecules, than in zeolite CaY (Harlick and Tezer, 1998).

Influence of Si/Al ratio: It has been shown (Xu et al, 2002) that the CO_2 adsorption capacity and selectivity of zeolites increases when the Si/Al ratio decreases. This phenomenon is due to an increase of electric field in the zeolites pores induced by increasing number of aluminium present at the surface of zeolites. Additionally, when the Al^{3+} content increases, the number of counter ions also increases, which in turn increase the basicity of zeolite.

Influence of the size of pores: The pores size of zeolites is a factor that influences the capacity and rate of CO_2 adsorption. The pore size must be appropriate to allow the adsorbed molecules to penetrate within it. The correlation between the CO_2 adsorption capacity of zeolites and the size of their pores again depend on the pressure of gas. The affinity of the zeolite NaA for CO_2 is higher than that of zeolites NaX and at low pressures due in part to small pore diameter of zeolite A. This high affinity of zeolite NaA allows a better selectivity for CO_2 in the presence of N_2 and O_2 than NaX and NaY (Bonenfant, 2008).

Presence of water: The presence of water can decrease the CO₂ adsorption capacity of zeolites by decreasing the strength and the heterogeneity of the electric field. Moreover, the presence of water supports the bicarbonates formation on the zeolites surface (Xu et al, 2002). This will generate strongly bound CO₂ (bicarbonate species), which requires a higher temperature for desorption. CO₂ adsorption capacity of different zeolites is tabulated below. (Table 1.3)

Table 1.3 CO₂ adsorption capacity of zeolites.

Type of zeolites	CO ₂ adsorption capacity, mmol/g (at 25 °C, 1 bar)	Reference
Natural	0.8	Siriwardane et al, 2003
Na-X	2.7	Diaz, 2008
Zeolite 13X	4.61	Harlick et al, 2004
Erionite	2.8	Huesca et al, 1999
ZSM-5 with ethylene diamine	6.1	Amine et al, 2015
Nano zeolites	4.8	Pham et al, 2016

Regeneration of zeolites

The regeneration of zeolites can be performed either by pressure swing adsorption or by temperature swing adsorption. Most of the zeolites recover the fresh adsorption capacities without much degradation even after several adsorption - desorption cycles. But, there are some exceptions. For zeolites 13X, a small decrease in CO₂ adsorption capacity is observed from second cycle onwards. This is due to the chemisorptions of small amount of CO₂ to the zeolite surface, in the form of carbonate generated by the interaction of CO₂ with metal

ion adjacent to the exchangeable cation. The formation of carbonate ion is accelerated under humid condition due to the fact that water catalyse the chemisorptions and stabilization of carbonate species on the surface by hydrogen bonding (Xu et al, 2002).

The selectivity of zeolite for CO₂ over methane and water is still low, and the adsorption capacities rapidly decline when the temperature increases above room temperature. The CO₂ capture performance of the zeolite-based CO₂ sorbents can be improved by either changing the composition and structure of framework, cationic exchange, or zeolite purity.

1.4.2.2 Metal Organic Framework (MOF) based solid sorbents

Metal organic frameworks are new class of crystalline porous materials, which have attracted attention in the past two decades due to their structural and chemical diversity viz., high surface area (up to 5000 cm²/g), high thermal and chemical stabilities, high void volume (55-90%), low densities etc. MOF materials generally consist of three dimensional organic-inorganic hybrid structure formed by metal based nodes (e.g. Al³⁺, Cr³⁺, Cu²⁺, Zn²⁺ etc.) bridged by organic groups (e.g. carboxylate, pyridyl) through co-ordination bonds. A general structure of MOF is shown in Figure 1.8. Due to the strong co-ordination bonds, MOFs have geometrically and crystallographically well defined framework structures. These crystalline structures are robust enough to allow the removal of the included guest species, retaining the porosity. The crystallinity of MOFs also allows precise structural characterization by X-ray diffraction methods, thus facilitating their rational design and the formulation of structure–function relationships.

Great progress in MOFs-based CO₂ adsorbents has been achieved during the past several years. Compared to other porous materials viz., zeolites, activated carbon etc., most MOFs have a higher surface area and micro pore volume, leading to the highest CO₂ uptakes. The adsorption measured at ambient

temperature and low pressure is mainly controlled by chemical feature of the pore surface. High CO₂ adsorbing materials generally possess high functionalities on the surfaces. The adsorption isotherms at high pressure are influenced by the surface area of MOFs.

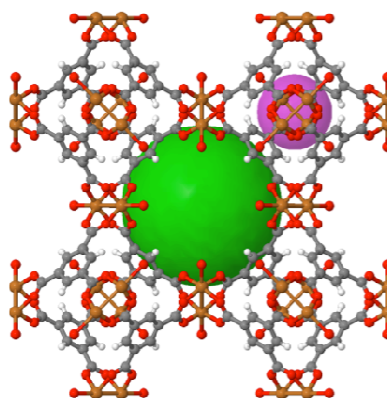


Figure 1.8 A general structure of MOF

By varying the organic linker, MOFs can be tuned and designed systematically. The general method of MOF synthesis involves the reaction of metal precursors and the ligands in organic solvent in mild condition, followed by the removal of solvent by vacuum drying. The experimental parameters viz., temperature, solvent compositions, reaction times, reagent ratios, reagent concentrations etc. are to be optimized for the realization of highly porous ordered crystalline structure. Other synthetic approaches viz., solvothermal synthesis, solid state synthesis and microwave synthesis are also executed for the realization of MOF. Due to the easily controllable synthesis and modification, MOFs have great advantages compared to zeolites and carbon in controlling pore size and shape for required gas separation.

The framework $[\text{Zn}_4\text{O}(\text{btb})_2]$ (MOF-177, $\text{btb}^{3-} = 1,3,5$ -benzenetribenzoate), which has a surface area of 4500 m²/g exhibits the highest capacity for CO₂, taking up 33.5 mmol/g at 32 bar and 298 K. (Manson et al,

2011). By comparison, zeolite 13X adsorbs 7.4 mmol/g at the same conditions. High surface area frameworks such as $[\text{Cu}_2(\text{BPnDC})_2(\text{bpy})]$ (SNU-6, bpy=4,4'-bipyridine, BPnDC^{2-} =benzophenone-4,4'-dicarboxylate, SA_{BET} = 2590 m^2/g) also possesses a high CO_2 uptake capacity and preferential CO_2 adsorption over CH_4 . Major drawback of MOF based CO_2 adsorbent is its high affinity for water (Babarao and Jiang, 2009). It is reported that even with the presence of 0.1 wt. % water in CO_2/CH_4 mixture, the selectivity of MOF towards CO_2 decreases by 1 order of magnitude. Yu and Balbuena (2013) made a detailed study on the effect of water on CO_2 adsorption of Mg-MOF-74. They concluded that the CO_2 adsorption capacity decreases by the presence of water molecule linked to coordinatively unsaturated metal site. CO_2 adsorption capacity of some of the recently reported MOFs is given in Table 1.4.

Table 1.4 CO_2 adsorption capacity of MOFs

Type of MOF	CO_2 adsorption capacity, mmol/g (at 25 °C, 1 bar)	Reference
Mg-MOF-74	6.3	Bao et al, 2011
Zn-MOF-74	5.5	Yazaydin et al, 2009
bio-MOF-11	3.5	An et al, 2010
$\text{Cu}_3(\text{BTC})_2$	2.75	Wade Dinca, 2012
Mg/DOBDC	4.95	Mishra et al, 2014
diamine-appended MOF	4.2	McDonald et al, 2015
H6CPB MOF	6.5	Nguyen et al, 2015

Regeneration of MOF

The heats of adsorption of CO₂ with MOFs are generally low and comparable to those of physical adsorbents such as zeolites. Heats of adsorption of MOFs were reported in the range of -30 to -45 kJ/mol (Bourrelly et al, 2005). This indicates low energy requirement for regeneration of the adsorbent.

The solid physisorbents viz., zeolites and MOFs have certain disadvantages. Zeolite is an attractive CO₂ adsorbent in terms of high adsorption capacity and low cost, but presence of water is seriously unfavourable due to the competitive adsorption of water with CO₂. Also the regeneration energy required for zeolites are high. MOFs are expensive for CO₂ capture from a practical point of view, and the uncertainty of structure stability under oxidation atmosphere and decrease in CO₂ adsorption capacity in presence of moisture confines the MOFs research in bench scale. In contrast, porous carbons are considered as good adsorbent for CO₂ in terms of high stability, chemical inertness, low cost etc. The following section summarizes different types of carbon adsorbents for CO₂ capture applications.

1.4.2.3 Carbon based solid sorbents

Carbon-based materials are considered as one of the most promising physical adsorbents for CO₂, because of their low cost, excellent thermal and chemical stability, low energy requirements for regeneration, hydrophobic surface, and CO₂-friendly adsorption sites on the pore surface and other physical properties. They are particularly good for gas adsorption applications because they are lightweight, and have very high specific surface areas and large pore volumes. Also, the adsorption/ desorption temperatures are below 373 K and can be used at atmospheric pressure (Seema et al, 2014). The carbon materials prepared from various precursors show CO₂ adsorption capacity in the range of 0.6-6 mmol/g at ambient temperature and 1 atm. (Deanna et al., 2010, Wei et al,

2013). These materials have an advantage over other adsorbents viz. zeolites, MOF, amine on solid support, etc., in terms of the low cost and wide availability of raw materials. The lower heat of adsorption on activated carbons indicates that CO₂ is weakly adsorbed on the carbons, requiring less energy for desorption (Balsamo et al, 2013). Carbon is less affected by the presence of moisture in the gas compared to the zeolites due to the hydrophobic nature of most of the microporous carbons (Bezerra, 2011). Also, they show excellent reversibility even after several regeneration cycles compared to the zeolite.

Earlier studies give emphasis on the synthesis of carbon material with very high surface area for achieving maximum CO₂ capture efficiency. Recent studies show that carbon with micropores of pore size less than 1 nm are required to maximize the CO₂ adsorption capacity (Zhang et al, 2013, Wickramaratnea and Jaroniec, 2013). Jiménez et al (2012) studied the CO₂ sorption behaviours of several types of carbon (platelet, fishbone, and ribbon) and amorphous carbon at room temperature. The results explained that the lower the graphitic constituent content (or the higher the amorphous carbon content) in the carbon materials is, the higher will be the CO₂-sorption capacity. Numerous carbon materials, including activated carbons, biomass derived carbons and nitrogen-doped carbons have been thoroughly investigated for CO₂ adsorption. The adsorption kinetics of CO₂ on activated carbons is fast; approaching their equilibrium capacity on the time scale of minutes. Pore structures of the activated carbons are represented by bi-disperse pore models including micropores and macropores. In this sense, the CO₂ adsorption kinetics of activated carbons has been explained in terms of the diffusional mass transport through these pores between which the adsorbate molecules can be exchanged.

Activated carbon

Activated carbons are well-known adsorbent materials, studied widely in CO₂ separation applications. Activated carbon materials have meso- or

microporous structures which favor easy diffusion of gas through the material without much resistance. The commonly used precursors are fossil fuels (coal, petroleum coke pitch) biomass (wood, nut shell and bamboo), or organic polymers (Plaza et al., 2009, Plaza et al., 2012, Hu et al, 2008). The synthesis of activated carbon usually consists of carbonization followed by activation processes. Carbonization process is the heating and pyrolysis of precursor material in inert atmosphere, by removing non-carbon elements such as hydrogen, oxygen, and nitrogen, leaving behind char. This carbonaceous material is in the form of a rigid carbon skeleton showing poor surface area. Textural properties of char is improved by the second step, high temperature activation process, during which more micro/ meso porosity and active sites are created, which increases the surface area. There are two types of activation process viz., physical activation and chemical activation. Physical activation is carried out using steam, CO₂ or air at high temperature. In chemical activation processes, KOH, H₃PO₄, or ZnCl₂ react with carbon skeleton leading to a well-developed carbon structure with large meso / micro pores. Chemical activation requires lower temperatures than physical activation.

Carbon precursors, activating agents, activating temperature and heating rate in the preparation of activated carbon (AC) significantly affect the textural property and adsorption behavior of CO₂. Activation can also be done by template method. Template method has advantage of developing ordered pores, especially mesopores with narrow pore size distribution (Chen et al., 2012).

Activated carbons are one of the best CO₂ adsorbent materials in terms of adsorbent regeneration stability and sustainability. i. e., the adsorption isotherms of carbons generally do not show noticeable changes even after large number of adsorption/desorption cycles. This excellent reversibility of adsorption capacities is attributed to the chemical inertness of carbon with CO₂ and moderate adsorption strength of these materials for CO₂. This advantage often

makes this material a competitive adsorbent with zeolites, especially for the applications in which the energy requirement for regeneration is a critical factor. Also, compared to zeolites, the affinity of carbon materials towards water is less. But, although the hydrophobic nature of most activated carbons reduces the affinity towards water, the storage under humid conditions still results in a decrease of adsorption capacity, due to slow condensation of water molecules into the pores. CO₂ adsorption capacity of some of the activated carbon materials are listed in Table 1.5.

Table 1.5 CO₂ adsorption capacity of activated carbon materials

Precursor	Preparation method	CO ₂ adsorption capacity, mmol/g (at 25 °C, 1 bar)	Reference
Petroleum coke	carbonization-activation(KOH)	3.5	Hu et al (2011)
graphene and polypyrrole	carbonization-activation (KOH)	4.3	Chandra et al (2012)
Acetonitrile	carbonization (Hard Templating method)	4.4	Xia et al 2011
phloroglucin and formaldehyde	carbonization (Soft Templating Method)	1.5	Saha and Deng (2010)
MOF-5	Carbonization (1100 °C)	6.1	Srinivas et al (2014)
spent coffee grounds	carbonization-activation (KOH)	3.0	Travis et al (2015)

Biomass derived carbon

Nowadays, the foremost interest among the carbon researchers is the production of carbonaceous materials from biomass. Biomass, because of its low

cost, abundance, easy access and environmental friendly nature, is accepted as a potential starting material for the synthesis of functional porous carbonaceous materials.

Hydrothermal or solvothermal carbonization (HTC or STC) of biomass is a commonly employed technique for the preparation carbon adsorbent from biomass (Titirici et al, 2007). The hydrothermal and solvothermal carbonization processes involve heating the biomass materials in sealed vessels in aqueous and non-aqueous medium, respectively (Hu et al, 2008). During this process, the organic matter in the biomass is thermo-chemically decomposed in a sealed reaction container under a controlled temperature between 100 and 200 °C. Usually, the biomass includes plant materials (agricultural residues, wood and herbaceous energy crops) and carbohydrates (sugars, starch, hemicelluloses, cellulose, lignin etc). The advantage of HTC is that it can convert precursor into carbonaceous solids with high yields at relatively low temperature (Libra et al, 2011). “Soft” plant tissues without an extended crystalline cellulose scaffold yield globular carbonaceous nanoparticles with very small sizes and less porosity. (eg: pine needles). “Hard” plant tissues with crystalline cellulose scaffold, can preserve shape and large-scale structural features on the macro- and microscale. Due to considerable mass loss, there arises the significant structural change on the nanometer scale, resulting in a sponge-like, continuous carbonaceous network with a well-defined mesoporous structure (Hu et al, 2008). The HTC of carbohydrates involves much complex chemistry. It involves hydrolysis of the biomass to glucose. The dehydration followed by fragmentation of glucose can give rise to different soluble products, such as furfural derivatives (5-hydroxymethylfurfural, furfural, 5-methylfurfural etc.), organic acids and aldehydes (lactic, propenoic, levulinic, formic acid etc.), and phenols. Then, polymerization or condensation reactions occur, forming the final carbonaceous material. The condensations have been identified to occur at least along aldol-condensation, cycloaddition reactions, and a hydroxymethyl-mediated furan resin condensation. Among the HTC process of different

biomass, hexose-based carbon sources mainly produce 5-hydroxymethylfurfural as the reaction-driving dehydration product, while pentose mainly works via the (more reactive) furfural (Figure 1.9). (Titirici et al, 2008). Chemical activation of solvothermal / hydrothermal carbons materials improves the microporosity, surface area etc.

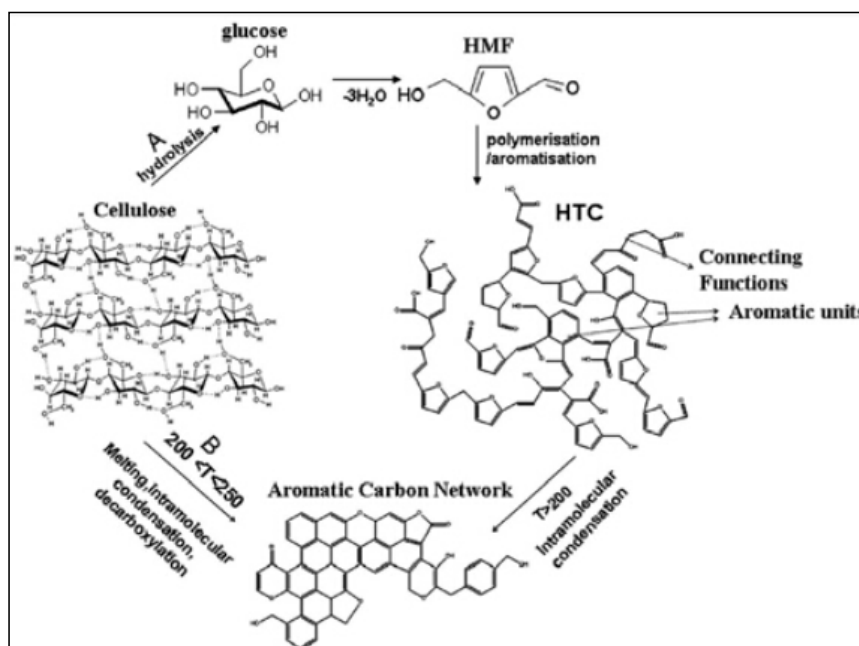


Figure 1.9 Proposed mechanism for the conversion of cellulose to HTC (Ref: Sevilla and Fuertes, 2009)

Direct pyrolysis with activation of renewable biomass is a well accepted technology for the development of highly porous carbon materials. Waste leaves were used to prepare porous carbon by pyrolysis, followed by KOH activation. The material showed very high specific surface area of $3400 \text{ m}^2/\text{g}$ and total pore volume of $1.8 \text{ cm}^3/\text{g}$. It showed CO_2 adsorption capacity of 6.0 and 4.36 mmol/g at 1 atmosphere pressure and 0°C and 25°C , respectively. Sevilla and Fuertes (2011) used the eucalyptus sawdust as precursor and KOH as the activating agent to prepare a series of activated carbons at different KOH/C ratios and activating temperature. The highest CO_2 adsorbed amount reached 6.6 mmol/g , much higher than the AC prepared from other biomass. Plaza et al. (2010) employed

olive stone as precursor and CO₂ as activating agent to prepare a series of AC with different porosity, and the AC had the adsorbed amount of 2.4 mmol/g for CO₂ at 25 °C and 1 bar. CO₂ adsorption capacity of some biomass derived carbon materials are listed in Table 1.6.

Table 1.6 CO₂ adsorption capacity of biomass derived carbons

Precursor	Preparation method	CO ₂ adsorption capacity, mmol/g (at 25 °C, 1 bar)	Reference
eucalyptus sawdust	activation(KOH)	4.8	Sevilla and Fuertes, 2011
almond shell	carbonization-activation(CO ₂)	2.6	Plaza et al, 2010
olive stone	carbonization - activation (CO ₂)	2.4	Plaza et al, 2009
soybean	carbonization-activation(ZnCl ₂)	0.93	Thote et al. 2010
Peanut shell	carbonization – activation (KOH)	4.4	Li et al, 2015
Jujun grass	Hydrothermal carbonization – activation (KOH)	5.0	Coromina et al, 2016

Nitrogen doped carbon

Many works have proven that the CO₂ capture capacity of activated carbons can be significantly increased by introducing nitrogen functional groups into their structures. Electronegativity of nitrogen is 3.5, which is higher than that of carbon (3.0). Nitrogen-containing functionalities are responsible for an increase in the surface polarity of carbon and basicity, which is beneficial for the adsorption of CO₂ (Wang et al, 2011). Nitrogen-doped porous carbon is usually

prepared by treating porous carbon or precursor with ammonia, amines, or urea or using various nitrogen-containing carbon precursors including synthetic polymers, biomass or biomass derivatives, ionic liquids and so on (Zhou et al, 2014). Pevida et al (2008) reported the fabrication of N-doped carbon materials by the carbonization of melamine–formaldehyde resins, which show a CO₂ adsorption uptake of up to 2.25 mmol/ g at room temperature and 1 atm. Ammoxidation (oxidation in presence of ammonia and oxygen) is one of the most effective methods of nitrogen-enrichment to carbon materials, which includes a simultaneous oxidation and nitrogenation of the precursor. Highly nanoporous N-doped carbons were synthesized by Yang et al (2015) with coconut shell by combining ammoxidation with KOH activation. The resultant carbons have highly developed porosity and large nitrogen loadings. The prepared carbons exhibit high CO₂ adsorption capacities of 3.5–4.3 and 4.8–6.5 mmol/g at 25 and 0 °C under atmospheric pressure, respectively. Ello et al (2013) prepared highly porous nitrogen doped carbon aerogel by sol-gel method using resorcinol-formaldehyde as carbon precursor and urea as the nitrogen source. The carbon aerogel thus prepared has highly porous interconnected sphere-like nodules. The CO₂ adsorption capacity showed an increase in trend with an increase in urea concentration. The maximum CO₂ adsorption capacities up to 3.6 mmol/g (298K) and 4.5 mmol/g (273K) were achieved.

Liu et al (2015) prepared a series of highly porous nitrogen doped carbon using furfural and urea as the carbon and nitrogen source respectively. The nitrogen content of this material is modulated in the range of 10.13 to 13.19 wt% by controlling the urea content of the initial polymer. Thus prepared N-doped porous carbon materials showed a high CO₂ adsorption capacity of 4.6 mmol/ g at ambient temperature and pressure.

X -ray photoelectron spectroscopy (XPS) is the major tool to identify the type of N atoms in the N-doped carbon. Four types of nitrogen configurations

as pyridine-like nitrogen (N-6, 398.4±0.1 eV), pyrrole-like nitrogen (N-5, 400±0.1 eV), graphite-like nitrogen (N-Q, 401.3±0.2 eV) and pyridine-N-oxide (N-X, 403.1±0.2) are present in N-doped carbons. The enhanced basicity can be related to the lone pair of electrons in pyridinic-N as well as to the increased electron density in the delocalized p-orbitals in case of graphene with graphitic-N. CO₂ adsorption capacity of various nitrogen doped carbons are summarized in Table 1.7.

Table 1.7 CO₂ adsorption capacity of nitrogen doped carbon

Precursor	CO ₂ adsorption capacity, mmol/g (at 25 °C, 1 bar)	N content, %	Reference
Imine polymer	1.95	5.58-8.74	Wang l, 2013
polyindole nanofibers	3.2	4.1	Saleh et al, 2013
N-doped mesoporous carbon from urea-formaldehyde resin	2.3	3.1	Yu et al, 2014
Polypyrrole	3.9	10	Sevilla, 2011
Hexamethylenetetramine and resorcinol	2.7–4.0		Liu et al, 2012
Urea-formaldehyde - furfuralcohol co-polymer	2.9–13.9	3.7	Liu et al, 2015
petroleum coke - urea	4.4		Hu et al, 2015
gelatin and starch	3.84	3.0	Alabadi, 2015
Melamine microspheres	2.9	14.4	Li et al, 2016

Carbon molecular sieves and Carbon nanotubes

Carbon molecular sieves (CMS) are commonly developed from petroleum coke, which is widely used as gas adsorbent. CMS represent a class of microporous carbon materials, whose unique textural characteristics permit the kinetic separation of gas mixtures, and thus studied for CO₂ capture. For a CMS to be useful for gas separation, it must possess a narrow pore size distribution (PSD), with high micropore volume; result in good selectivity and high adsorption capacity, respectively (Foley, 1995). The pore size of CMS is narrower than that of AC, so CMSs are widely used in gas separation processes.

The CMS preparation involves three steps, viz., carbonization of the raw materials, and chemical and/or physical activation of the chars to produce AC and pore modification of the AC to convert it to CMS. In the pore modification step there are two techniques, the first one is on controlled thermal treatment of a carbon precursor and the second method is based on the modification of the pores by chemical vapor deposition (CVD) technique. In the CVD method, deposition of cracked hydrocarbon occurs at the pore opening to reduce the size of the pore entrance. Commonly used hydrocarbons are methane, benzene, toluene, hexane, etc. The CVD conditions (temperature, time of deposition and gas composition) should be defined perfectly since the extra vapor deposition leads to pore mouth blockage and reduction in adsorption capacity (Banisheykholeslami, 2015). Carbon molecular sieve membranes were prepared on α -alumina supports by carbonization of a resorcinol–formaldehyde resin loaded with boehmite by Rodrigues et al (2014).

A porous monolithic carbon fiber composite molecular sieve was developed by Burchell et al. (1997). The material showed a CO₂ adsorption capacity of 2.27 mmol/g at room temperature and 1 bar. Carbon molecular sieve (CMS) was prepared from broom corn stalk precursor by carbon vapor

deposition of methane by Banisheykholeslami (2015). The material exhibited a CO₂ adsorption capacity of 2.2 mmol/g and CO₂/CH₄ selectivity of 26.

The use of new generation materials, such as carbon nanotubes (CNT) and graphene, has become an active area of research for adsorption of CO₂ over the last several years. By choosing the appropriate pore size and shape, CNT can act as a suitable candidate for CO₂ separation and sequestration (Razavi et al, 2011). CNTs have been proven as a potential candidate for CO₂ capture from flue gas due to their unique physicochemical properties as well as high thermal and chemical stability. The adsorption of CO₂ on MWCNT takes place near the carbon surface only due to the Van der Waals interactions between carbon atom of CNT and CO₂ molecule.

Cinke et al. (2003) reported adsorption of CO₂ on high pure single-walled carbon nanotubes (SWCNT) of surface area of 1587 m²/g and a total pore volume of 1.55 cm³/g. The CO₂ adsorption capacity of SWCNTs was 4.5 mmol/g at 35 °C. Based on Monte Carlo simulations, Huang et al. (2007) showed that the CO₂ adsorption in the range of 4-9 mmol/g is an increasing function of the diameter of the CNT. CNTs demonstrated a higher selectivity toward CO₂ than other sorbents, such as ACs, zeolite 13X, and MOFs that have reported in the literature. Razavi et al. (2011) also reported a higher selectivity of CO₂ over nitrogen adsorption on CNT. Lu et al. (2012) compared the adsorption capacity of MWCNTs with activated carbon and zeolite. Under the same adsorption condition, MWCNTs recorded a CO₂ adsorption capacity of 1.57 mmol / g while activated carbon and zeolites adsorbed 1.65 mmol /g and 1.44 mmol / g, respectively. Recently Adeniran and Mokaya (2015) synthesized CNT from CCl₄, reported a CO₂ adsorption capacity of 4.8 mmol/g (at 25 °C, 1 bar). Khalili et al (2013) reported that the amount of CO₂ adsorbed on MWCNT was almost two times higher than that on activated carbon, though the specific surface area of activated carbon was about two times higher than that of MWCNT. This can

be attributed to the high pore volume, hollowness and lower mass density of MWCNT adsorbent which had stronger impacts on the level of CO₂ loading. Acid treatment of MWCNT also increased the amount of CO₂ capture over entire range of pressure without any destruction and real damage on the morphology of MWCNT. Grand-canonical Monte Carlo simulations and adsorption experiments were conducted by Rahimi et al (2013) to understand the adsorption of CO₂ onto bundles of double-walled carbon-nanotubes. They observed that the adsorption sequence changes with the inter tube distance (d). At $d \leq 0.5$ nm, adsorption proceeds with increasing loading in the order- grooves and inner surface adsorption \rightarrow fill interstitial region \rightarrow fill inner region. At higher distances, $d > 0.5$ nm, the sequence changes in the order- inner surface adsorption + partial outer surface adsorption \rightarrow complete outer surface adsorption \rightarrow fill interstitial, groove, inner adsorption. The CO₂ adsorption capacity changes from 1.9 mmol/g to 3 mmol/g when the inter-tube distance changes from $d \leq 0.5$ nm to $d > 0.5$ nm.

Regeneration of carbon

Since the adsorption of CO₂ by porous carbon materials involves only weak force of interactions viz., van der Waal's force and dipole-quadrupole interaction, less energy is required for desorption of adsorbed CO₂. Especially, the mild adsorption strength in low-pressure regime is beneficial, considering that adsorbents must be regenerated in practice. Compared to zeolites, carbon adsorbents have a weaker physical interaction with CO₂, having lower heats of adsorption, allowing desorption process more energy easier (Kikkinides et al, 1993). Recyclability is an important factor for an acceptable adsorbent material. A good adsorbent should retain its adsorption capacity without any change after several adsorption-desorption cycle. Siriwardane et al (2001) studied the adsorption isotherms of activated carbons over multiple adsorption/ desorption cycles. The authors concluded that activated carbon isotherms showed extremely reproducible operating cycles without any noticeable changes in the curves,

demonstrating the excellent reversibility of adsorption on the activated carbon adsorbents.

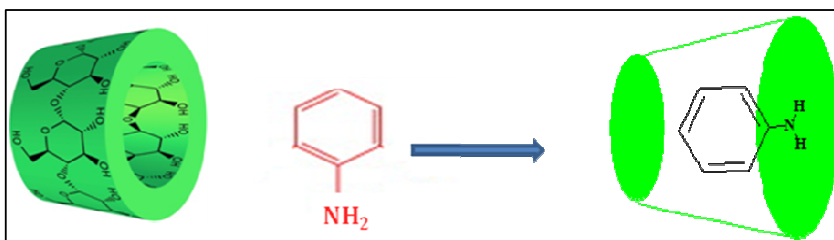
1.5 Objectives of the Work

Recently, much attention has been attracted to the use of biomass to produce functional materials due to economic, environmental and societal issues. Because of its low cost, easy availability and environmental friendly nature, there has been an increased demand of biomass as the raw material for carbon based adsorbents for CO₂ and other toxic contaminants. Carbohydrates are a class of easily available biomass. The focus of the research work is the development of different CO₂ adsorbents from carbohydrate based biomass. The objectives of the research work are:

- Development of a carbohydrate based solid amine sorbent to minimize the utilization of organic or toxic chemicals.
- Study on the CO₂ adsorption capacity, thermal stability, recycle stability etc. of the developed amine system
- Development of porous carbon for CO₂ capture from different carbohydrate based biomass
- Development of nitrogen doped porous carbon for CO₂ capture from carbohydrate
- Study on the factors viz., surface area, porosity and nitrogen content affecting the CO₂ adsorption capacity.
- Feasibility study of porous carbon for the separation of organic solvent and other toxic materials from water.

CHAPTER 2

SUPRAMOLECULAR SYSTEM OF ANILINE ENCAPSULATED β -CYCLODEXTRIN FOR CARBON DIOXIDE REMOVAL



Deepthi, L. S., Vijayalakshmi, K. P., Rajeev, R., Prabhakaran, K. and Ninan, K. N. (2013). Supramolecular β -cyclodextrin–aniline system: a new class of amine on solid support for carbon dioxide capture with high amine efficiency. *RSC Advances*, 3: 24041–24045.

2.1 Introduction

Several studies on the development of solid sorbents for the removal of carbon dioxide from combustion streams, in a closed crew cabin or with other emission sources have been reported recently (Samanta et al, 2009; MacDowell et al, 2010; Rutherford and Do, 2011; Monge et al, 2011; Kamiuto and Abe, 1988; Furukawa et al, 2010; Das et al, 2012; Babarao and Jiang, 2008). Liquid amines are widely used for CO₂ removal for flue gas. Introduction of amine functionalities on solid sorbents improves their CO₂ adsorption efficiency and selectivity (Sayari et al, 2012; Ma et al, 2009, Cui et al, 2011). Amine functionalities are introduced on solid sorbents either by physical impregnation of the amines on a porous support or through alkyl-silyl linkages (Xu et al, 2002; Hicks et al, 2008; Tsuda and Fujiwara, 1992). In addition, co-polymerization with monomers containing amine functionalities is employed for the preparation of porous polymer sorbents with amines for CO₂ adsorption (Satyapal et al, 2001; Lu et al, 2012; Rabbani and El-Kaderi, 2012; Pacheco et al, 2012; Ochiaiv et al, 2008, Liu et al, 2008). The amine group on the solid sorbents aids the CO₂ adsorption through the formation of carbamate or bicarbonate as given in Equation (2.1) and Equation (2.2) respectively. (Caplow et al, 1968; Mahajani and Joshi, 1988; Shimizu et al, 2011; Vaidya and Kenig, 2007; Cyril and Alper, 2012).



The adsorption capacity of solid amine based chemisorbents varies from 0.5–6.0 mmol/g for amine-impregnated silica sorbents, 0.5–5.5 mmol/g for amine grafted solid sorbents, 0.3–4.0 mmol/g for amine-impregnated carbon and 4.0–7.5 mmol/g for porous amine polymers (Sevilla et al, 2012). But most

of these systems suffer from the toxicity associated with amine leaching and limited stability of the regeneration process.

Cyclodextrins (CD) are cyclic oligosaccharides consisting of six to eight α -(1,4)-linked D-glucopyranose units with a torus shaped structure having a hydrophobic cavity. β -CD contains seven glucose units and has a hydrophobic cavity of a 0.7 nm diameter (Grigoras and Conduruta, 2006). β -CD forms inclusion complexes with a large variety of guests by supramolecular hydrophobic interactions. The 1:1 complex of aniline with β -CD is well known (Prasannan et al, 2011). The inclusion complex formation enables the molecular level distribution of the aniline in β -CD. As β -CD is an easily available, non-toxic and green material, it is interesting to study the β -CD–aniline complex for CO₂ capture. The present chapter reports the CO₂ adsorption characteristics of a β -CD–aniline complex. Though similar guest–host systems have been widely studied for drug delivery applications, this is the first study using an amine encapsulated into a cyclodextrin cavity for CO₂ removal.

2.2 Experimental

β -cyclodextrin ($\geq 97\%$) and aniline were purchased from Aldrich, India and used as received.

2.2.1 Synthesis of β -CD–aniline complex

A 1:1 complex of aniline in β -cyclodextrin was prepared from β -cyclodextrin and aniline. 7.2 mmol of freshly distilled aniline was added to 100 ml of an aqueous solution containing 7.2 mmol of β -cyclodextrin. The mixture was stirred for 4 hours at room temperature and then refrigerated at 4 °C for 12 hours. The crystallized inclusion complex was filtered off and washed with a minimum amount of cold water and dried at room temperature. The white

powder of β -CD–aniline complex obtained was characterized by ^1H NMR and elemental analysis.

2.2.2 Characterization of β -CD–aniline complex

Elemental analysis: The carbon, hydrogen and nitrogen content of the complex were determined using Perkin Elmer PE 2400 model CHNS elemental analyser. An exactly known weight (0.2 mg) of the sample was combusted in an atmosphere of pure and dry oxygen and the concentrations of individual components were measured as a function of their thermal conductivity.

XRD analysis: XRD analysis was carried out using Bruker D8 Discover small angle X-ray Scattering Spectrometer, Germany with copper $K\alpha$ radiation. Data were digitally recorded in continuous scan in the range of angle from 10° to 90° .

^1H NMR analysis: ^1H -NMR spectral analyses were performed on a Bruker 500 MHz FT-NMR Spectrometer by dissolving sample in DMSO- d_6 .

Raman analysis: Raman spectra were recorded using WITec alpha 300R Confocal Raman microscope (WITec GmbH, Germany) using the 532 nm line of an Nd:YAG laser as the excitation wavelength. An average of five spectra was collected with an integration time of 2 seconds/spectra to obtain a single spectrum. The spectrometer was calibrated using the 520 cm^{-1} line of Silicon prior to analysis.

Moisture content analysis: The moisture content analysis of the β -CD–aniline complex was carried out using a Karl Fischer titrator model Vergo/Matic-D. One gram of the sample was dissolved in 1:1 methanol-toluene mixture and titrated directly with Karl-Fischer reagent, with a blank correction for the same quantity of the solvent.

CO₂ adsorption evaluation: The CO₂ adsorption capacity of the complex was measured using a thermogravimetric analyzer (Q 50, TA instruments, USA). The initial activation of the sorbent was carried out by heating approximately 15 mg of sample loaded in the platinum pan of the thermal analyzer, heated to 100 °C in pure nitrogen (99.99% purity) at a flow rate of 50 ml/ min. The temperature was then decreased to 30 °C and pure CO₂ (99.99% purity) was then introduced at the same flow rate. The equilibrium CO₂ adsorption capacity of the sample was calculated from the mass gain after holding it at 30 °C in CO₂ for 60 minutes. Subsequently, the desorption of CO₂ was carried out by increasing the temperature to 50 °C and holding it at the same temperature for 10 minutes in pure N₂ flowing at the rate of 50 ml/ min.

Measurement of heat of adsorption: The heat of adsorption of CO₂ on the complex was determined using differential scanning calorimetry (Q 50, TA instruments, USA). The samples were heated at 100°C in nitrogen atmosphere to remove pre-adsorbed moisture.

2.3 Results and Discussion

It is well known that the cavity in β -CD is hydrophobic. The inclusion complex formation involves the interaction of phenyl group of aniline with the hydrophobic cavity of β -CD. A schematic representation of the aniline- β -CD inclusion complex is shown in Figure 2. 1. The amino moiety of aniline orients towards the wider rim of the β -CD. (Prasannan et al, 2011).

Since the cyclodextrin cavity is highly hydrophobic, the transfer of the hydrophobic part of the aniline molecule from water into the cyclodextrin cavity may be compared with typical hydrophobic interaction processes, i.e. the transfer of an organic molecule from an aqueous to organic phase. Aniline molecule has a small volume with cross sectional diameter of about 4.0 Å and only one aniline

can fit into the cavity of β -CD with internal diameter of 7 Å (Rekharsky and Inoue, 1998).

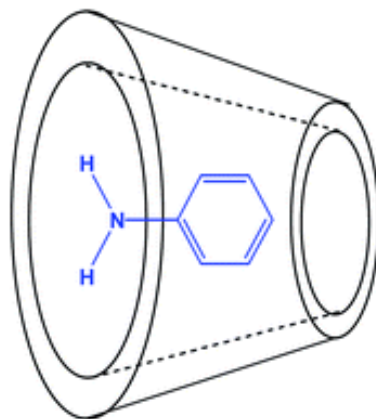


Figure 2.1 β - Cyclodextrin – Aniline complex ($C_{48}H_{77}O_{35}N$)

2.3.1 Confirmation of 1:1 complex of β -CD – aniline complex

Elemental analysis (Table 2.1) also confirmed 1:1 complex of β -CD with aniline based on the fact that percentage of nitrogen atom in the complex matches well with theoretical value of nitrogen in 1:1 complex (given in bracket).

Table 2.1 Elemental analysis of β -CD and 1:1 β -CD-aniline complex

Compound	Carbon, (wt. %)	Hydrogen, (wt. %)	Nitrogen, (wt. %)
β -Cyclodextrin	44.4	6.22	-
β -Cyclodextrin-aniline	46.8 (46.9)	7.1 (6.3)	1.1 (1.1)

^1H NMR spectroscopy is the most reliable technique available to characterize inclusion complex of cyclodextrin. The ^1H -NMR spectrum of β -CD-aniline complex (Figure 2.2) showed aromatic protons from ortho position of aniline as a doublet at 6.55 ppm, meta and para protons as triplets at 7.00 and

6.49 ppm, respectively.

Demarco and Thakkar (1970) observed that if the guest is incorporated inside of the host molecule, the protons located in the interior of the cavity (C3-H, C5-H and C6-H) would be shielded by the guest. As can be seen in Table 2.2, these protons are shielded at high magnetic fields while the other ones are not highly affected (they are situated on the outer surface of β -CD). The ratio of number of aromatic protons of aniline (five) and protons of β -CD (forty-nine) confirmed that one molecule of aniline is encapsulated in the cavity of one molecule of β -CD.

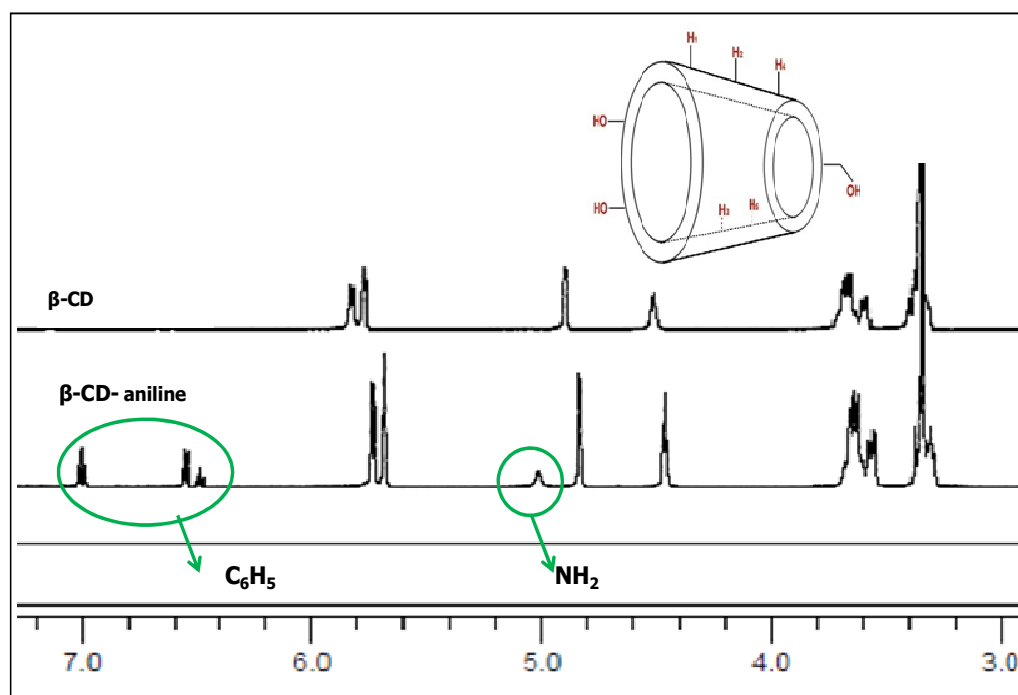


Figure 2.2 ^1H NMR spectra of β -Cyclodextrin and β -Cyclodextrin – Aniline inclusion complex in DMSO-d_6

Table 2.2 Chemical shift values of β - Cyclodextrin protons after complex formation

	H1	H2	H3	H4	H5	H6
β -CD	4.89	3.38	3.82	3.45	3.74	3.79
β -CD-aniline complex	4.83	3.31	3.67	3.37	3.57	3.62
$\Delta\delta$	0.06	0.07	0.15	0.08	0.17	0.17

2.3.2 CO₂ adsorption of β -CD–aniline complex

Figure 2.3 shows the CO₂ adsorption of the β -CD–aniline complex at 30 °C and at 1 bar pressure measured using a thermogravimetric analyzer. The β -CD–aniline complex shows a slow, but significant CO₂ uptake of 3.1 wt % CO₂, which corresponds to an amine efficiency of 0.85 mol of CO₂ per mol of nitrogen. Amine efficiency is defined as the number of moles of CO₂ adsorbed per mol of nitrogen (Chaikittisilp, 2011; Fauth, 2012) and the maximum reported amine efficiency is 0.88 mol of CO₂ per mol of nitrogen by Guerrero et al (2008). The relatively low gravimetric efficiency is due to the low nitrogen content (1.1 wt%) of the β -CD–aniline complex. A high amine efficiency reveals the maximum accessibility of CO₂ to the amine in the adsorbent. On the other hand, amines supported on solid sorbents show low amine efficiencies since the amines are sandwiched in between particles forming agglomerates and not all of the amines are accessible to CO₂. The high amine efficiency obtained in the present case is due to the molecular level distribution of aniline in the β -CD cavity. Under identical experimental conditions, the β -CD–aniline complex adsorbed 0.3 wt% of N₂ when exposed to pure nitrogen gas for 60 minutes, showing selectivity towards CO₂ adsorption over nitrogen. The desorption of CO₂ from the complex takes place at temperatures as low as 50 °C indicating the easy regeneration of the sorbent for further CO₂ adsorption. The β -CD–aniline complex has a high stability constant (Liu and You, 2001) and remains stable even after several CO₂ adsorption–desorption cycles.

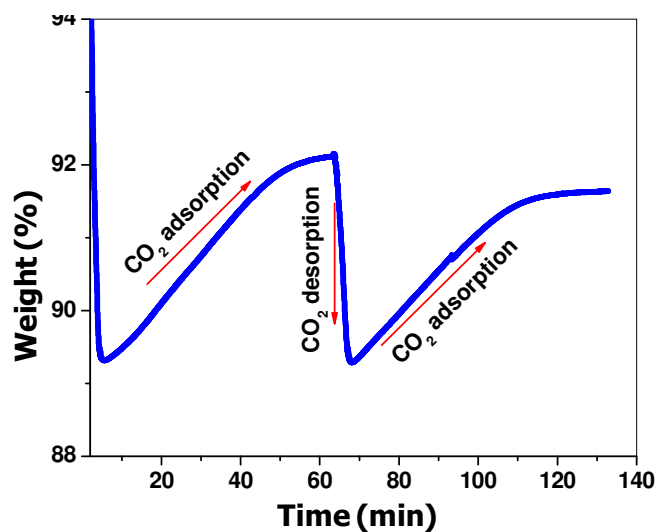


Figure 2.3 TG analysis of CO₂ adsorption/desorption on β-CD-aniline complex

2.3.3 Mechanism of CO₂ adsorption by β-CD – aniline complex

The β-CD–aniline complex shows many peaks in the XRD spectrum, which correspond to the crystalline channel-type inclusion complex (Prasannan, 2011). Upon grinding using a mortar and pestle, the number of diffraction peaks drastically reduced, due to the β-CD–aniline complex changing to an amorphous state. Figure 2.4 shows the effect of grinding on the crystallinity of the β-CD–aniline complex.

A transformation from crystalline to amorphous state by grinding was also observed in a metal organic framework (MOF) of γ-cyclodextrin by Stoddart, Yaghi and coworkers (2011). The MOF of γ-CD adsorbs CO₂ only in its crystalline form is due to the presence of micropores in the crystalline framework. On the other hand, the β-CD–aniline complex adsorbs more or less the same amount of CO₂ in its crystalline as well as its amorphous forms. This confirms that the adsorption of CO₂ in the β-CD– aniline complex is only due to the amine group of aniline in the complex.

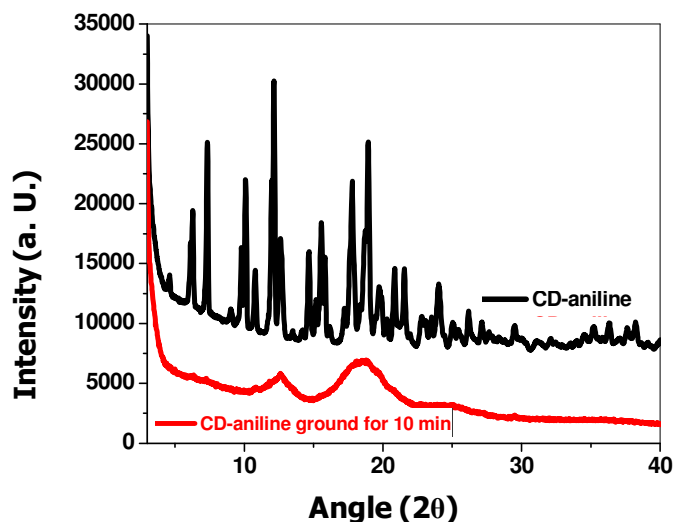


Figure 2.4 Effect of grinding on the crystallinity of aniline- β -CD complex- XRD data

Generally, the chemisorption of CO_2 on an amine functionalized solid sorbent under dry conditions is through the carbamate formation between two amine groups and one CO_2 molecule. This results in an amine efficiency of less than 0.5 mol CO_2 per mol N. On the other hand, an amine efficiency as high as 0.88 is reported under moist conditions (Gassensmith et al, 2011), in which the chemisorption is through bicarbonate formation involving one amine group, one water molecule and one CO_2 molecule. As the β -CD-aniline complex forms a channel type crystal structure, the chance that the amine groups of two of the β -CD-aniline complex molecules come into close enough proximity to favor the formation of a carbamate with CO_2 is less likely. This, coupled with the high amine efficiency of 0.85 mol CO_2 per mol N obtained in the present work indicates that the chemisorption is through the formation of bicarbonate.

The bicarbonate formation is also evidenced from the NMR spectrum of the β -CD-aniline complex before and after the CO_2 adsorption. The NMR spectra of the β -CD-aniline complex before and after exposure to CO_2 gas are shown in Figure 2.5. A singlet corresponding to the two $-\text{NH}_2$

protons observed at 5.01 ppm in the ^1H NMR spectrum of the β -CD–aniline disappeared after exposure to CO_2 gas. However, a new NMR signal at 5.71 ppm corresponding to the three protons of $-\text{NH}_3^+$ appeared after exposure to CO_2 . The new signal merges with the nearest NMR signal of cyclodextrin protons. It is clear from the NMR spectra that the β -CD protons are unaltered during CO_2 adsorption, indicating that the CO_2 adsorption is not due to carbonate ester formation with the hydroxyl groups of β -CD as in the MOF of γ -CD (Stoddart, Yaghi and coworkers, 2011).

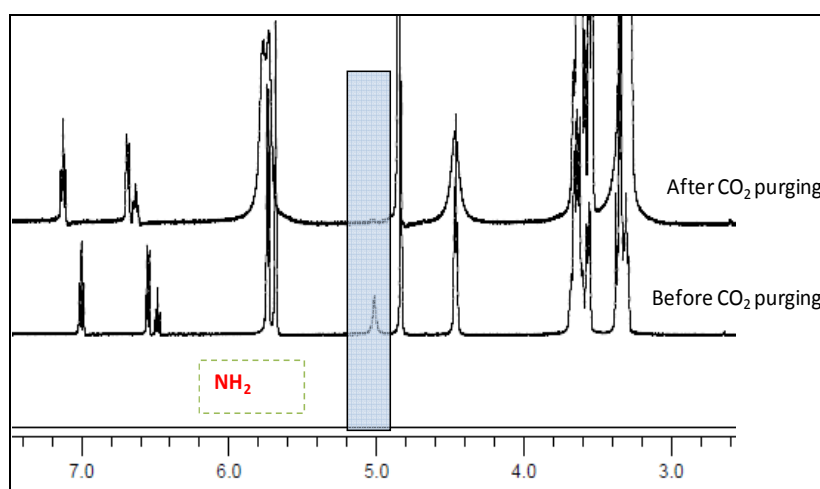


Figure 2.5 ^1H NMR spectra of β -CD –aniline complex before and after CO_2 purging

The chemisorption of CO_2 through bicarbonate formation is further evidenced from the Raman spectra of β -CD–aniline complex before and after exposure to CO_2 gas, measured using a Confocal Raman Microscope. Raman spectra of the β -CD–aniline complex before and after exposure to CO_2 gas are shown in Figure 2.6. The low intensity peaks appeared at 1610 cm^{-1} and 1000 cm^{-1} in the Raman spectrum of the β -CD–aniline complex before exposure to CO_2 gas are intensified after exposure. These peaks correspond to the C–O antisymmetric stretching and C–OH stretching, respectively, of the bicarbonate (Davis and Oliver, 1972). The low intensity peaks observed at 1610 cm^{-1} and 1000 cm^{-1} before exposure to CO_2 gas are due to the bicarbonate formation

with atmospheric CO₂.

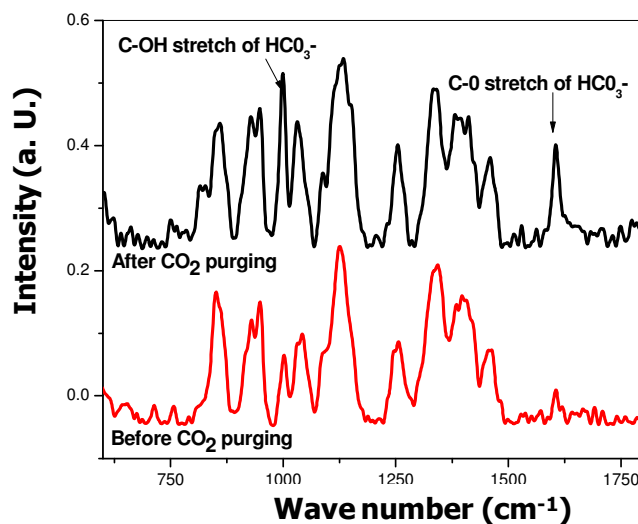


Figure 2.6 Raman spectra of β -CD –aniline complex before and after CO₂ purging

Generally, CO₂ adsorption through the bicarbonate formation requires strict control of humidity, and the water required for the bicarbonate formation is supplied along with the carbon dioxide gas. It is well known that the β -CD contains 6 to 7 molecules of water within the cavity (Bender and Komiyama, 1978; Rekharsky and Inoue, 1998). The water molecules present within the β -CD cavity are expelled only partially during the formation of the inclusion complex with aniline. The moisture content analysis of the β -CD–aniline complex using a Karl Fischer titrator showed the presence of 3.4 wt% water (Hadaruga et al, 2012). The water molecules present outside the cavity of the β -CD–aniline complex were removed before the analysis, by heating at 100 °C. The result shows the presence of an average of 2.4 moles of water inside the cavity of one mole of the β -CD–aniline complex. The presence of water molecules inside the cavity of the β -CD–aniline complex is also confirmed by molecular modeling. These residual water molecules present within the cavity of the β -CD–aniline complex participate in the formation of the bicarbonate. The participation of water present inside the β -CD cavity in the bicarbonate

formation is confirmed by the fact that the β -CD–aniline complex showed a decrease in amine efficiency from 0.85 to 0.31 mol of CO_2 per mol of N, when activated at 100 °C under 10^{-3} millibar pressure for 4 hours. This is due to the removal of the majority of the water present in the β -CD cavity by heating under vacuum. The CO_2 adsorption capacity of aniline– β -CD complex shows only a slight decrease after the first cycle. This indicates that majority of the water regenerated during desorption of CO_2 is retained within the β -CD cavity. However, there could be further decrease in CO_2 adsorption after a number of cycles in dry air if the entire regenerated water is not retained within the cavity.

Molecular modeling studies using the semi-empirical PM6 method as implemented in the Gaussian09 suite of programs showed that the orientation of the amine group of aniline was towards the wider rim of the β -CD and two water molecules were accommodated inside the cavity. The amine group oriented towards the wider rim of the β -CD is easily accessible to the CO_2 stream and one of the H_2O molecules inside the cavity is able to react to form the β -CD – aniline- bicarbonate complex. Figure 2.7 shows the minimum energy structure of the zwitterionic complex, $\text{C}_6\text{H}_5\text{-NH}_3^+(\text{HCO}_3^-)/\text{H}_2\text{O}$, which is stabilized by a network of hydrogen bonding interactions among the hydroxyl groups of the β -CD, NH_3^+ moiety, bicarbonate and water.

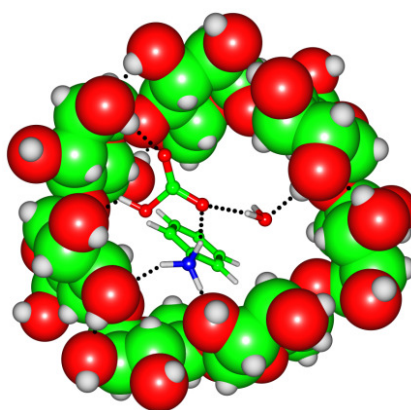


Figure 2.7: Minimum energy structure of $\text{C}_6\text{H}_5\text{-NH}_3^+ \dots (\text{HCO}_3^-) \dots \text{H}_2\text{O}$ inside β -CD cavity. Red, blue, green and gray spheres are O, N, C and H atoms, respectively.

2.3.4 Evaluation of heat of adsorption

The DSC curve of the β -CD–aniline complex in a moisture-free CO_2 atmosphere at 30 °C is shown in Figure 2.8. The sample was initially activated at 100 °C in a nitrogen atmosphere. The strong endothermic peak observed during activation is due to the removal of water molecules bound to the outer surface of the β -CD. The exothermic peak observed corresponds to the adsorption of CO_2 at 30 °C. The heat of adsorption value calculated from the DSC is -94 kJ/mol , which compares well with that reported for the chemisorption of CO_2 .

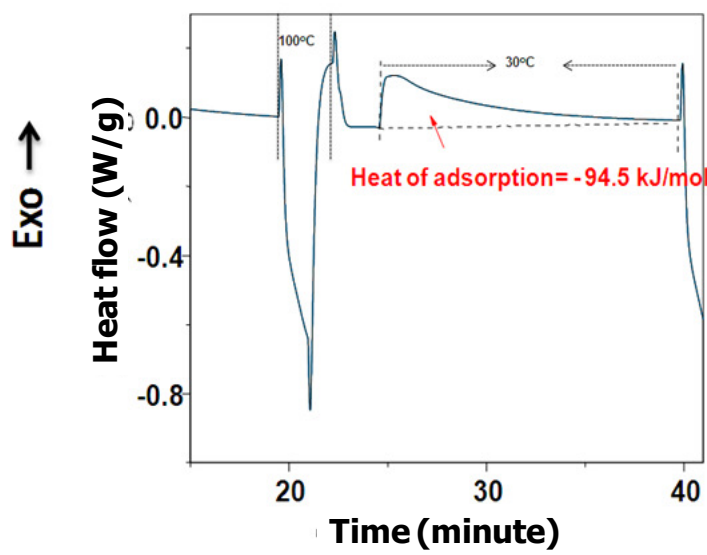


Figure 2.8 DSC curve of the activation of β -CD–aniline at 100 °C followed by CO_2 adsorption at 30 °C.

2.3.5 Kinetics of CO_2 adsorption

The kinetics of CO_2 adsorption and desorption are extremely important from a practical perspective. The activation energy for the reaction of CO_2 and the β -CD–aniline complex was evaluated by studying the adsorption behavior

of the complex at 30, 35, 40 and 50 °C. Figure 2.9 shows the CO₂ adsorption by the β-CD– aniline complex at various temperatures.

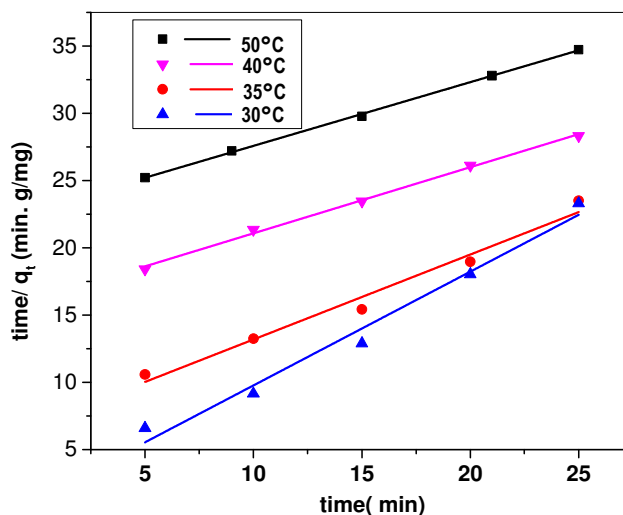


Figure 2.9 Kinetics of CO₂ adsorption at different temperatures

A pseudo-second order rate expression was used to describe the chemisorption of the β-CD–aniline complex by plotting the inverse of the quantity of gas adsorbed at a particular time against the corresponding time (Ho, 2006). The pseudo second order rate equation is given in Equation (2.3), where q is the quantity of gas adsorbed at temperature t , q_e is the equilibrium quantity of CO₂ adsorbed and k_2 is the pseudo second order rate constant.

$$t/q = 1/k_2 q_e^2 + t/q_e \quad (2.3)$$

The plot of the logarithm of the rate constant against the reciprocal of absolute temperature gave a straight line graph (Figure 2.10). The activation energy calculated from the slope of the straight line is 32.6 kJ/ mol, which agrees with the published activation energy data of CO₂ adsorption by other amines (Samanta et al, 2009).

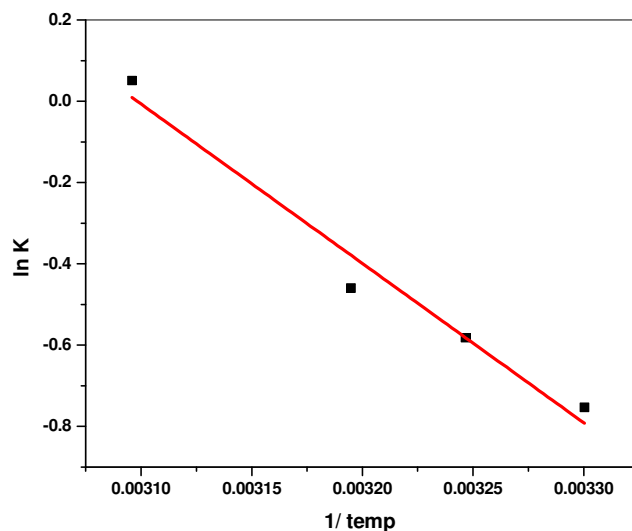


Figure 2.10 Arrhenius plot for the evaluation of activation energy

Though the β -CD–aniline complex sorbent has a low gravimetric efficiency and slow adsorption kinetics, it has a number of advantages. The complex is prepared through a simple green route using environmentally friendly non-toxic chemicals. In addition, the β -CD–aniline complex remains stable for months, whereas an amine supported on solid sorbents has a tendency to be oxidized. Moreover, no humidification of the adsorbate gas stream is required in β -CD–aniline sorbent system, whereas stringent control of humidity is essential for efficient CO_2 adsorption on the amine functionalized porous silica sorbent.

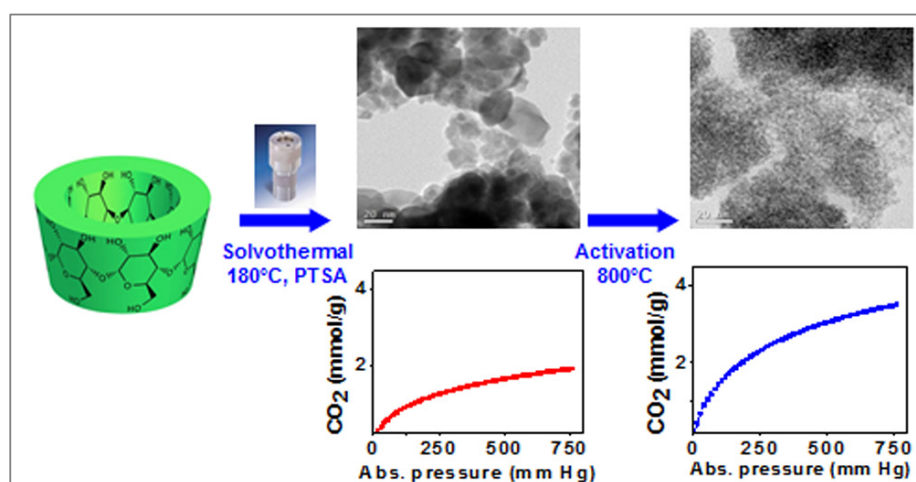
2.4 Conclusions

The β -CD–aniline complex with the amine group oriented towards the wider rim of the β -CD showed a high amine efficiency for CO_2 adsorption. The chemisorption of CO_2 is through the formation of a bicarbonate, as evidenced from NMR, Raman spectroscopy and molecular modeling. The system requires no humidification of the adsorbate gas stream, as water present within the β -CD

cavity participates in the bicarbonate formation. Molecular level control of amine on support was achieved, resulted in maximum utilization of amine for CO₂ removal. Since –NH₂ group of aniline is pointed towards the outer rim of cyclodextrin, it is exposed to the gas stream resulting in maximum efficiency of CO₂ absorption. Effect of activation temperature, adsorption temperature and crystallinity on CO₂ adsorption capacity was studied. The green nature and low temperature regeneration would make this an attractive sorbent for CO₂ capture, especially in space capsules of manned space mission.

CHAPTER 3

CO₂ SORBENTS BY SOLVOTHERMAL CARBONIZATION AND *IN SITU* ACTIVATION OF β -CYCLODEXTRIN



Deepthi, L. S., Narasimman, R., Rajeev, R., Prabhakaran, K. and Ninan, K. N. (2015). Effect of catalyst concentration and high temperature activation on the CO₂ adsorption of carbon nanospheres prepared by solvothermal carbonization of β -cyclodextrin. *Journal of Materials Research*, 30 (11): 1761-1771.

3.1 Introduction

Porous carbonaceous structures are well-known adsorbent materials, studied in CO₂ separation applications due to their high surface area, excellent thermal and chemical stability, low-energy requirements for regeneration, hydrophobic surface properties, and viable CO₂-friendly adsorption sites on the pore surface and other physical properties. The carbonaceous materials prepared from various precursors show CO₂ adsorption capacity in the range of 0.6–5 mmol/g at ambient temperature and pressure (Deanna et al, 2010; Wei et al, 2013). These materials also have an advantage over other adsorbents, namely zeolites, MOF, amine on solid support, etc., in terms of the low cost and wide availability of raw materials. The lower heat of adsorption on activated carbons indicates that CO₂ is weakly adsorbed on the carbons, requiring less energy for desorption (Balsamo et al, 2013). Carbon based adsorbent materials are less affected by the presence of moisture in the feed gas compared to the zeolites due to their hydrophobic nature (Bezerra et al, 2011). Also, they show excellent reversibility even after several regeneration cycles compared to the zeolites. Earlier studies emphasized on the synthesis of high surface area carbon material for maximum CO₂ capture efficiency. Recent studies revealed that carbon with micropores, especially pore size less than 1 nm are required to maximize the CO₂ adsorption capacity (Zhang et al, 2013). Numerous carbon materials, including activated carbons, biomass derived carbons (Hu et al, 2008; Plaza et al, 2012), and nitrogen-doped carbons (Xing et al, 2012; Xiaoyu, 2013) have been thoroughly investigated for CO₂ adsorption. Nowadays, the leading interest among the carbon researchers is the production of carbonaceous materials from biomass. Biomass, because of its low cost, abundance, easy access, and environmental friendly nature, is accepted as a promising starting material for the synthesis of functional carbonaceous materials (Titirici et al, 2007).

Novel CD-based carbon materials had been prepared by Shin et al. in 2008 from β -CD solutions under the hydrothermal conditions at 160 °C. Shin et al. described the mechanism of carbon formation from CD under hydrothermal conditions as the hydrolysis of CD to glucose, and an intramolecular dehydration reaction resulting in the formation of 5-hydroxymethyl-2-furaldehyde followed by continued dehydration/polymerization and aromatization reactions. Recently, Zhao et al. (2013) reported a novel approach to prepare CD-based carbon materials with high specific surface area through a solvothermal carbonization process using o-dichlorobenzene as the solvent and p-toluene sulfonic acid (PTSA) as the catalyst. The amount of PTSA used in the study was mentioned as catalytic amount. Our preliminary investigations with the system showed that the amount of PTSA is very critical in developing micro/mesoporosity in the solvothermal char (STC). Moreover, a detailed study on the CO₂ adsorption using the STC is lacking. In this contest, we have prepared a series of solvothermal carbon materials from β -CD with varying amount of PTSA and optimized the PTSA concentration for maximum CO₂ absorption capacity. We have also studied the contribution of PTSA toward the STC yield. The effect of high-temperature activation on further improvement in microporosity and CO₂ adsorption capacity was evaluated. The role of two step carbonization, namely solvothermal carbonization followed by high-temperature activation toward the formation of microporous carbon with better CO₂ adsorption capacity was confirmed by comparing with carbon material prepared by direct carbonization of β -CD.

3.2 Experimental

β -CD (> 97%), p-toluene sulfonic acid monohydrate (PTSA), and o-dichlorobenzene from Aldrich, India was used as received.

3.2.1 Synthesis of solvothermal carbon (STC) from β -cyclodextrin

All solvothermal carbonizations were done using a Teflon-lined stainless steel autoclave of 25 mL capacity. Mixtures of β -CD (250 mg) and PTSA with PTSA to β -CD weight ratios in the range of 0–10 suspended in o-dichlorobenzene (10 mL) were ultrasonicated for 30 min. The reaction mixture was then transferred to the autoclave, sealed and kept in an air oven at 180 °C for 24 h. After the reaction, the autoclave was cooled down to room temperature. The black solid residue, denoted as STC, was filtrated and washed successively with acetone, distilled water, and ethanol. The product was dried in vacuum at 120 °C for 24 h.

High-temperature activation of the STC was conducted in an ultra-high pure argon atmosphere in tubular furnace at different temperatures, namely 400, 500, 700, 800, 900, and 1000 °C for 2 h. The heating rate used for carbonization was 2 °C/min. The same atmosphere was maintained during the cooling of the furnace.

3.2.2 Characterization of STC and activated STC

Thermogravimetric analysis: Thermogravimetric analysis of the STC (approximately 20 mg) was carried out using TG-MS model Perkin Elmer Pyris 1 thermogravimetric analyzer. The evolved gas analysis was carried out using a Clarus SQ 8T mass spectrometer connected to the thermogravimetric analyzer.

Elemental analysis: The carbon, hydrogen and sulfur contents of the samples were determined using Perkin Elmer PE 2400 model CHNS elemental

analyser. An exactly known weight (0.2 mg) of the sample was combusted in an atmosphere of pure and dry oxygen and the concentrations of individual components were measured from that of their thermal conductivity.

FE-SEM analysis: The morphology of the STC before and after high-temperature activation was obtained through field emission scanning electron microscopy (JEOL microscope JSM 6060, Tokyo, Japan). Au film was deposited on the surface of the carbons to improve conductivity.

HR-TEM analysis: Microstructure of the carbon samples was evaluated using transmission electron microscope model FEI (TEM, Tecnai G2 30 S-TWIN, Hillsboro, OR) with an accelerating voltage of 300 kV. For TEM measurements, the sample dispersed in acetone was drop-casted on the carbon-coated copper grid and dried in vacuum at room temperature before observation.

Textural properties evaluation: The porous textural properties of the STC before and after high-temperature activation were analyzed using the volumetric N₂ adsorption–desorption at -196 °C using a surface area analyzer (Micromeritics Tristar II, Norcross, GA). The STC before and after high-temperature activation were degassed at 120 and 300 °C, respectively, for 16 h prior to the analysis. The lower degassing temperature chosen for the former was to avoid the decomposition of the sample. The specific surface area was measured from the isotherm in the relative pressure range between 0.05 and 0.2 according to the Brunauer–Emmett–Teller (BET) method. The pore size distribution was obtained from density functional theory (DFT). The Barrett-Joyner- Halenda (BJH) method was used to find out the mesopores from the adsorption curve of the isotherm. The micropore volume was calculated from the t-plot. The total pore volume was estimated from the amount of N₂ adsorbed at a relative pressure of 0.99.

CO₂ adsorption measurements: The CO₂ adsorption capacity of the STC

before and after the activation was evaluated at 0 and 25 °C by volumetric gas adsorption studies using the surface area analyzer. The samples were degassed overnight. The degassing temperature was 120 and 300 °C for STC before and after the activation, respectively. The volumetric CO₂ absorption measurements were carried out using 200 mg of STC and the sample is equilibrated at each pressure for 20s before collecting the data.

The heat of adsorption of CO₂ on the STC before and after activation was determined using differential scanning calorimetry (DSC). The samples were heated at 100 °C in nitrogen atmosphere to remove pre-adsorbed moisture and CO₂ molecules.

The adsorption of CO₂ from air was studied by gravimetric method using a Perkin Elmer Pyris 1 thermogravimetric analyzer with the following temperature protocol. About 5 mg of the adsorbent was loaded in a platinum pan of the thermogravimetric analyzer and heated at 110 °C for 10 min under argon flow at a rate of 100 mL/min for desorption of adsorbed molecules. The gas flow was shifted from argon to dry air (air dried over silica trap) containing 400 ppm CO₂ once the sample temperature reached 25 °C. The weight gain of the sample for a period of 12 h was taken as direct CO₂ adsorption capacity.

3.3 Results and Discussion

It has been reported by Zhao et al. (2013) that the solvothermal carbonization of β -CD in o-dichlorobenzene using catalytic amount of PTSA produces microporous carbon with surface area of 699 m²/g and total pore volume of 0.40 cm³/g. Our investigations with the system for CO₂ capture showed that the surface area and microporosity of STC increased with an increase in the PTSA concentration and the surface area values close to that

reported by Zhao et al. could be achieved at a PTSA to β -CD weight ratio of 2.50. Moreover, elemental analysis showed the presence of 30–40 wt% oxygen in STC. We have also observed that the STC yield increased with an increase in the PTSA concentration indicating that PTSA contributes to the char yield.

3.3.1 Textural property evaluation of STC

The N_2 adsorption–desorption isotherm and pore size distribution, obtained from the adsorption data using DFT and BJH, of the STC at various PTSA concentrations are shown in Figure 3.1. Contrary to Zhao et al., we observed a strong hysteresis between adsorption and desorption branches, indicating major mesoporosity. The yield, oxygen content, and textural properties of STC obtained at various PTSA to β -CD weight ratios are given in Table 3.1. The BET surface area (S_{BET}) of STC increased from 27 to 620 m^2/g with an increase in PTSA to β -CD ratio up to 2.5. With further increase in PTSA to β -CD ratio, S_{BET} showed a decrease in trend. Micropore surface area also showed the same trend. The maximum micropore surface area, micropore volume and % microporosity were exhibited by the STC with PTSA to β -CD ratio of 2.5. Peaks at pore size nearly 100 Å are observed in the pore size distribution obtained from BJH calculations in addition to the micropores revealed by the DFT calculations.

Char yield was found to increase with an increase in PTSA to β -CD ratio. The decrease in the oxygen content in the STC (from 40.1 to 30.0) with an increase in the PTSA concentration indicates an increase in the condensation of oxygen containing functional groups at higher concentrations of PTSA.

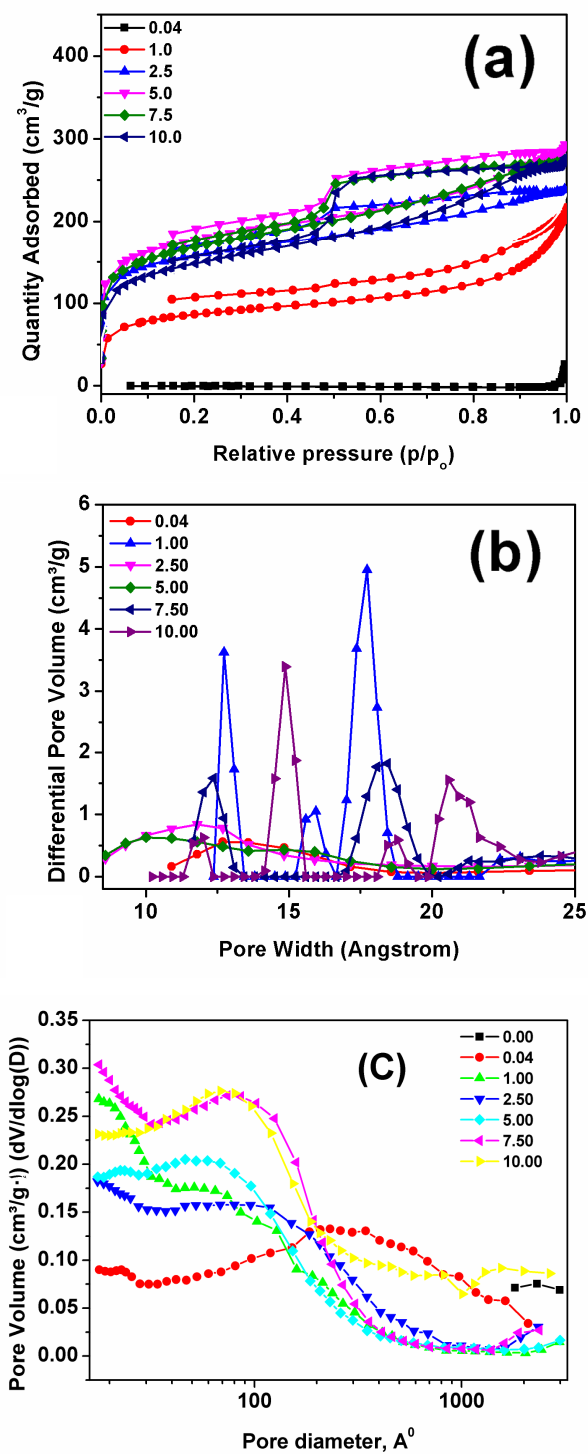


Figure 3.1 (a) N_2 adsorption-desorption isotherms, (b) DFT pore size distribution and (c) BJH pore size distribution of STC at various PTSA to β -CD weight ratios

Table 3.1 Yield and textural properties of STC prepared at various PTSA to β -CD weight ratios

PTSA to CD ratio	Char yield (wt.%)	Oxygen (wt.%)	S_{BET} (m^2/g)	S_{tm} (m^2/g)	V_{p} (cm^3/g)	V_{m} (cm^3/g)	Micro porosity (%)
0.00	37.2	40.1	< 1	-	-	-	-
0.04	37.2	38.1	27	-	0.23	0.06	23.9
1.00	40.0	37.3	552	296	0.37	0.08	24.0
2.50	44.4	36.1	620	326	0.44	0.11	24.6
5.00	50.0	35.1	550	248	0.43	0.09	21.2
7.50	55.0	34.5	514	235	0.43	0.07	15.9
10.00	58.1	30.0	437	170	0.36	0.05	12.8

V_{p} is the single point pore volume calculated from adsorption isotherm at $P/P_0 = 0.99$; S_{BET} is the BET specific surface area obtained from the adsorption data in the P/P_0 range from 0.05 to 0.2, S_{tm} is the micro pore surface area and V_{m} is the total micro pore volume.

3.3.2 CO₂ adsorption evaluation of STC

Figure 3.2 shows the CO₂ adsorption on the STC prepared at various PTSA to β -CD weight ratios. The CO₂ adsorption capacity of the STC increased with an increase in the PTSA concentration and reached a maximum at a PTSA to β -CD weight ratio of 2.5 and then showed decreasing trend with further increase in the PTSA concentration. The variation of CO₂ adsorption capacity with the PTSA concentration is in accordance with the variation of surface area and pore volume. In addition,

the polar hydroxyl functional groups present in the STC have a positive impact on the CO₂ adsorption as reported by Zhao et al (2013). That is, the CO₂ quadrupole likely to interact with the polar hydroxyl groups on the walls of the micropores. The maximum CO₂ adsorption capacity obtained at 1 bar pressure was 1.64 and 2.44 mmol/g at 25 and 0 °C, respectively. The CO₂ adsorption capacity of STC at different PTSA to β -CD ratio is summarized in Table 3.2.

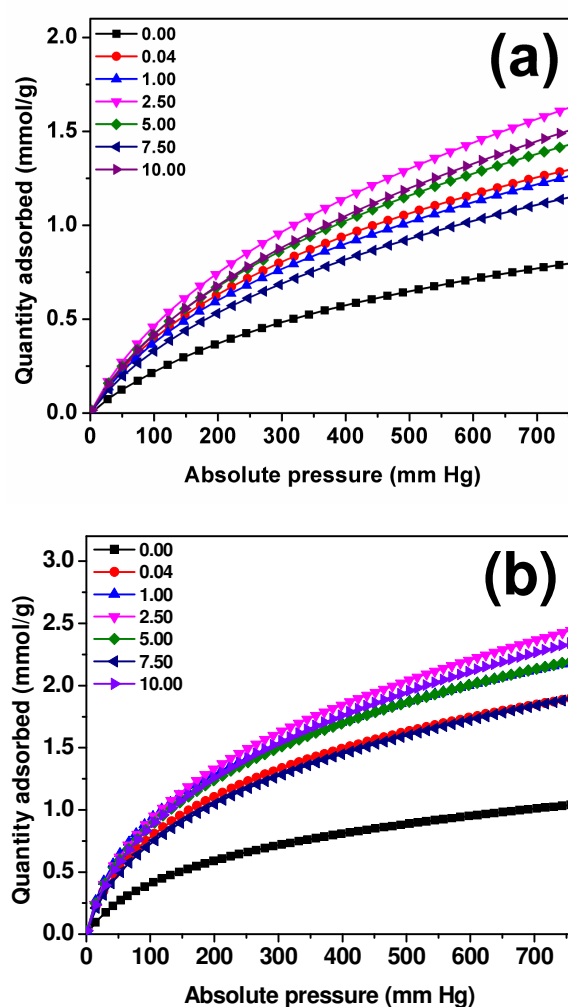


Figure 3.2 CO₂ adsorption of STC at various PTSA to STC weight ratios at (a) 25°C and (b) 0°C at 1 bar

Table 3.2 CO₂ adsorption properties of STC prepared at various PTSA to β -CD weight ratios

PTSA to β -CD weight ratio	CO ₂ adsorption properties of STC	
	0 °C (mmol/g)	25 °C (mmol/g)
0.0	1.0	0.80
0.04	1.9	1.3
1.0	2.2	1.3
2.5	2.5	1.6
5.0	2.2	1.4
7.5	1.9	1.1
10.0	1.7	1.1

The requirement of exorbitantly high concentration of PTSA makes this route a costlier one for the preparation of microporous carbon for CO₂ adsorption. Moreover, the CO₂ adsorption capacity of the STC is relatively low in spite of the high surface area. It is well known that the CO₂ adsorption capacity depends more on the microporosity in the adsorbent than the total surface area (Zhang et al, 2013). These factors prompted us to study the effect of high-temperature activation of STC prepared at various PTSA concentrations to increase their microporosity and CO₂ adsorption capacity.

3.3.3 Activation of STC – Effect of activation temperature

The effect of activation temperature on the surface area, pore volume, and oxygen concentration of STC prepared at a PTSA to β -CD weight ratio of 0.04 is shown in Table 3.3. Oxygen content decreased from 34.9 to 16.2 wt % when the activation temperature increased from 400 to 900 °C. S_{BET} also

increased with activation temperature and the maximum S_{BET} (535 m^2/g) and total pore volume (0.40 cm^3/g) were observed at an activation temperature as high as 800 °C for PTSA to β -CD weight ratio of 0.04. Further increase in activation temperature decreased the surface area and porosity due to the sintering of pores at temperature of 800 °C for STC at a PTSA to β -CD weight ratio of 0.04.

It is clear that the increase in surface area and microporosity during heat treatment is due to an in situ activation by the removal of carbon by the reaction with oxygen present in the STC. Thus, STC prepared with PTSA to β -CD weight ratios in the range of 0 to 10 were subjected to in situ activation at 800 °C before CO_2 adsorption studies.

Table 3.3 Variation of surface area, pore volume and oxygen concentration of STC with activation temperature (PTSA to β -CD weight ratio- 0.04)

Activation temperature (°C)	Oxygen content (wt. %)	S_{BET} (m^2/g)	V_p (cm^3/g)	V_m (cm^3/g)
180	38.1	27	0.23	0.06
400	34.9	342	0.29	0.13
500	28.7	419	0.34	0.18
700	16.4	441	0.34	0.18
800	16.2	650	0.45	0.23
900	16.2	400	0.32	0.14

TG-MS (Thermogravimetric – mass spectroscopy) analysis of the STC is shown in Figure 3.3. The gases evolved at each weight loss were

evaluated using quadrupole mass spectrometer attached to TG analyzer. Mass spectra were recorded in the electron impact mode at 70 eV, scanning the m/z 10–250 range. The initial weight loss of nearly 17% observed at temperature below 150 °C, detected by mass spectrometer as m/z 18, corresponds to the loss of adsorbed moisture. Nearly 2.5% weight loss observed at temperature in the range of 150–300 °C is attributed to the evolution of SO_2 , detected by mass spectrometer as m/z 64. The weight loss of 30% observed in the temperature range of 300–800 °C is due to the removal of carbon as CO (m/z 28) by the reaction with oxygen present in the STC. This removal of carbon as CO would create additional micropores in the STC. The char residue obtained at 800 °C is approximately 50%.

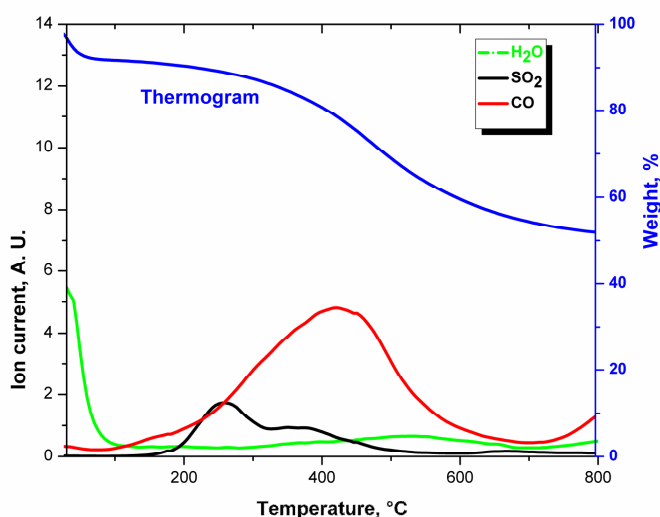


Figure 3.3 TG-MS of STC at a PTSA to β -CD ratio of 0.04

Figure 3.4 shows the SEM photomicrographs of STC and activated STC prepared at a PTSA to β -CD weight ratio of 0.04. The STC produced from β -CD at all the studied PTSA concentrations contains spheres of size less than 500 nm as seen in Figure 3.4 (a). These spheres are agglomerates of smaller particles as shown in Figure 3.4 (b). The majority of the agglomerates lose their spherical morphology during high-temperature activation as evidenced from the Figure 3.4 (c).

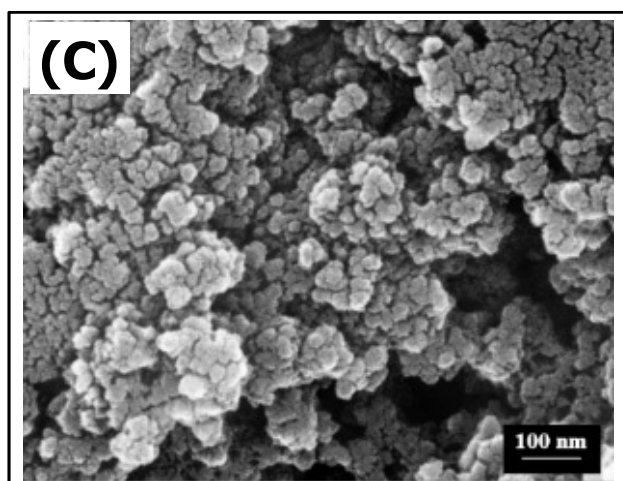
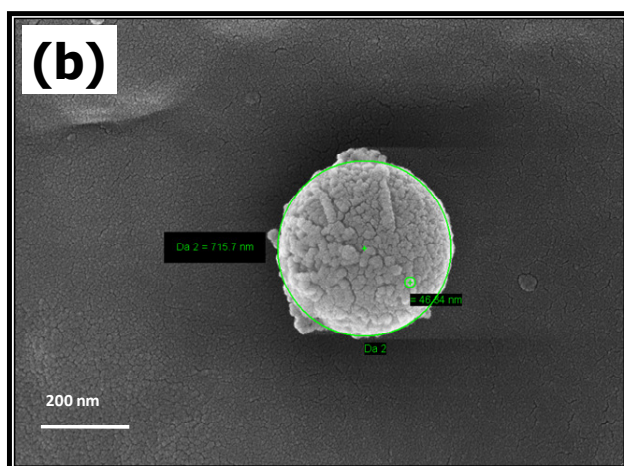
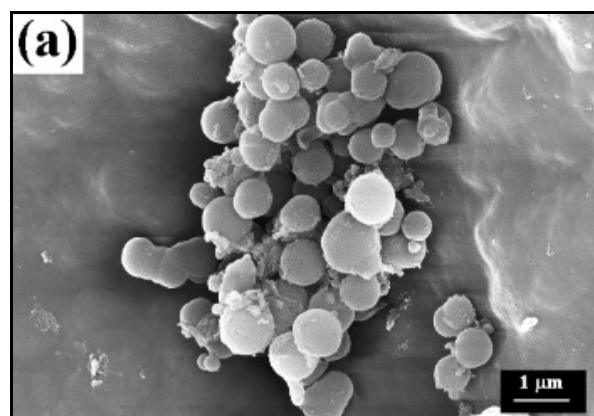


Figure 3.4 SEM images of STC obtained at a PTSA to β -CD weight ratio of 0.04 (a) before activation (b) before activation-high resolution and (c) after activation-high resolution

3.3.4 Textural property evaluation of activated STC

Figure 3.5 shows the N₂ adsorption–desorption isotherm and pore size distribution, calculated from the adsorption data of STC activated at 800 °C. The textural properties of the activated STC are given in Table 3.4. The surface area and total pore volume of the activated STC also showed increasing trend with the PTSA concentration up to a PTSA to β -CD weight ratio of 2.5 and then showed decreasing trend with further increase in the PTSA concentration.

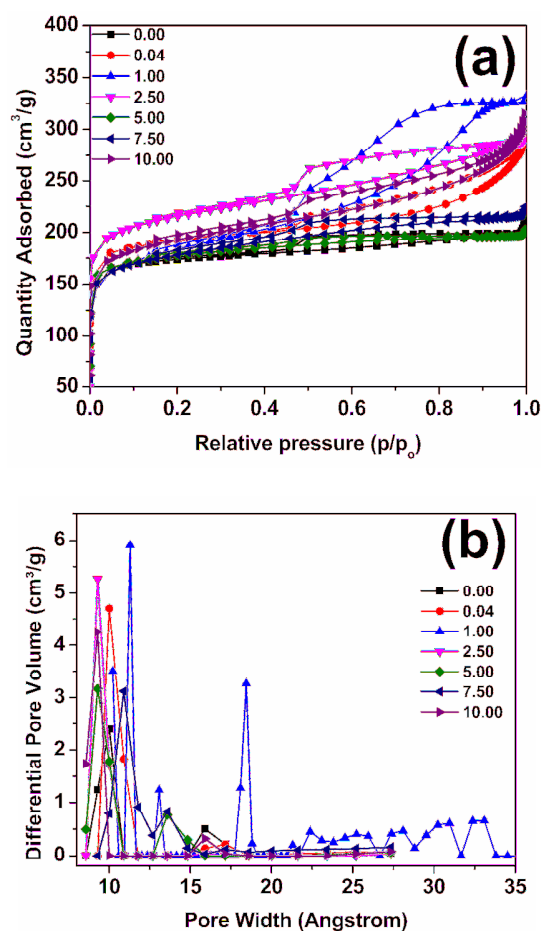


Figure 3.5 N₂ adsorption-desorption isotherm (a) and pore size distribution (b) of STC prepared at various PTSA to β -CD weight ratios after activation at 800 °C.

Moreover, the contribution of micropore to the total pore volume increased due to the activation. This shows that majority of the pores created due to the removal of carbon by the in situ activation at higher temperature is micropores.

Table 3.4 Textural properties of STC prepared at various PTSA to β -CD weight ratios after activation at 800 °C.

PTSA to β-CD weight ratio	S_{BET} (m^2/g)	S_{tm} (m^2/g)	V_{p} (cm^3/g)	V_{m} (cm^3/g)	Micropor osity (%)
0	590	495	0.32	0.22	66.8
0.04	650	527	0.45	0.23	50.7
1.0	674	530	0.47	0.24	50.2
2.5	736	536	0.50	0.25	50.0
5	603	477	0.31	0.20	65.8
7.5	609	435	0.34	0.18	51.9
10	667	471	0.49	0.19	38.5

However, the increase in surface area and pore volume with the PTSA concentration in the activated STC was not as significant as before the activation. STC prepared without PTSA increased the surface area from $< 1 \text{ m}^2/\text{g}$ to $590 \text{ m}^2/\text{g}$ after activation. At the same time, STC prepared at a PTSA to β -CD weight ratio of 0.04 showed surface area increase from 27 to $650 \text{ m}^2/\text{g}$. Whereas, at higher PTSA to β -CD weight ratio, viz., 10, surface area increased from 437 to $471 \text{ m}^2/\text{g}$. That is, the STC prepared at low PTSA concentration showed a considerable increase in surface area and pore volume upon high-temperature activation. This is further evidenced from the TEM study as the dense particles in the STC prepared at a PTSA to β -CD weight

ratio of 0.04 showed worm-like microporous structure after activation at 800 °C. The TEM micrograph of STC and activated STC at a PTSA to β -CD weight ratio of 0.04 is shown in Figure 3.6. The STC prepared at PTSA to β -CD weight ratios in the range of 0.04–2.5 showed more or less the same microstructure after the activation.

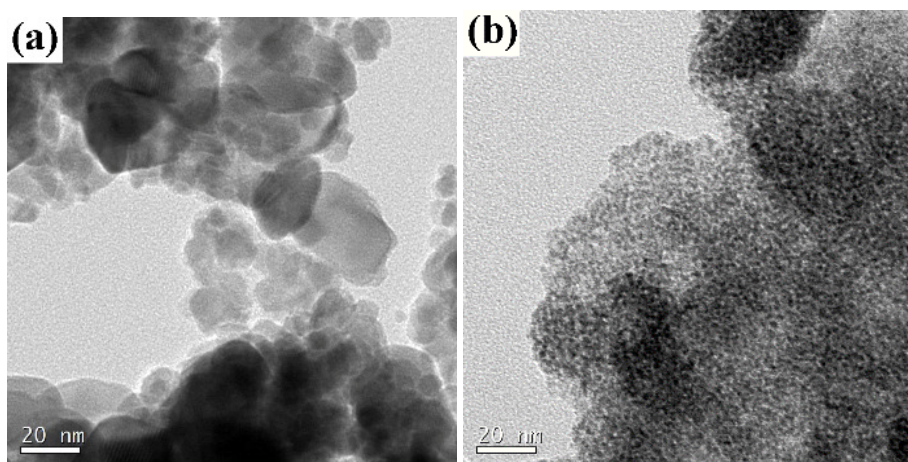


Figure 3.6 TEM images of (a) STC and (b) activated STC at a PTSA to β -CD weight ratio of 0.04.

3.3.5 CO₂ adsorption evaluation of activated STC

The CO₂ adsorption on the activated STC prepared at various PTSA concentrations is shown in Figure 3.7. The activated STC showed higher CO₂ adsorption capacity compared to the corresponding one before activation (Table 3.2). The maximum CO₂ adsorption capacity of the obtained activated STC is 3.58 and 2.56 mmol/g at 0 and 25 °C, respectively. Unlike the STC, the activated STC showed an increase in CO₂ adsorption capacity at 25 °C from 2.44 to 2.56 mmol/g when the PTSA to β -CD weight ratio increased from 0 to 2.5. Further increase in the PTSA concentration showed a decrease in CO₂ adsorption capacity. The activated STC prepared at PTSA to β -CD weight ratios in the range of 0–2.5 showed CO₂ adsorption capacity of 3.39–3.58 mmol/g at 0 °C. The percentage increase in CO₂ adsorption capacity of STC

prepared at PTSA to β -CD weight ratio of 0, 0.04, 2.5 and 10 are 225, 82, 47 and 80% respectively at 25 °C. These results shows that large requirement of PTSA for creating high surface area of STC can be avoided if an additional step of high temperature activation is performed. The effect of activation on CO₂ adsorption capacity of STC prepared at various PTSA concentrations is summarized in Table 3.5.

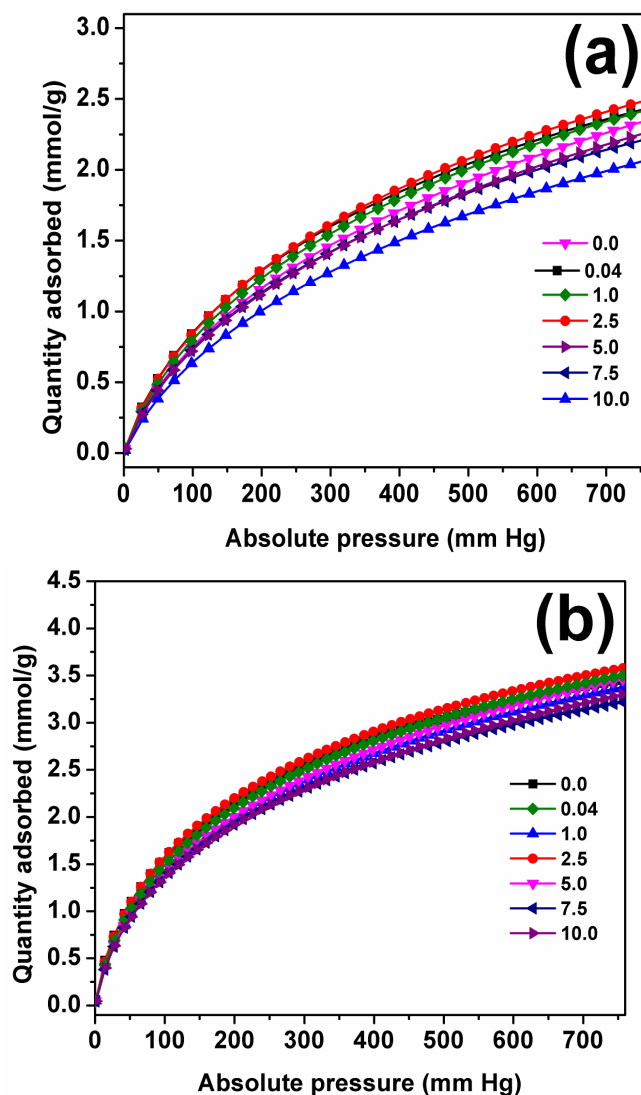


Figure 3.7 CO₂ adsorption isotherm of activated STC prepared at various PTSA to β -CD weight ratios at (a) 25 °C and (b) 0 °C.

Table 3.5 Effect of activation on CO₂ adsorption capacity of STC at various PTSA to β -CD weight ratios

<i>PTSA to β-CD weight ratio</i>	<i>Before activation</i>		<i>After activation</i>		<i>% increase in ads. capacity at 0 °C</i>	<i>% increase in ads. capacity at 25 °C</i>
	<i>0 °C</i>	<i>25 °C</i>	<i>0 °C</i>	<i>25 °C</i>		
0.00	1.04	0.80	3.39	2.44	225	205
0.04	1.90	1.27	3.45	2.49	82	96
1.00	2.20	1.30	3.50	2.50	59	92
2.50	2.44	1.64	3.58	2.56	47	57
5.00	2.20	1.44	3.46	2.42	57	68
7.50	1.89	1.16	3.22	2.22	70	91
10.00	1.72	1.06	3.10	2.13	80	101

The volume and size distribution of ultramicropores in porous materials are estimated from CO₂ adsorption isotherms (Zhang et al, 2013). The DFT calculation on CO₂ adsorption at 0 °C showed the presence of ultramicropores in the activated STC. The pore size distribution obtained by DFT calculation on CO₂ adsorption at 0 °C is shown in Figure 3.8. Ultra micropores with diameter of ~ 0.6 nm and ~ 0.9 nm contribute a differential pore volume of ~0.7 cm³/g and ~0.5 cm³/g, respectively. The increase in CO₂ adsorption capacity observed is mainly due to ultramicropores, as the ultramicropores highly favor the adsorption of CO₂ molecules.

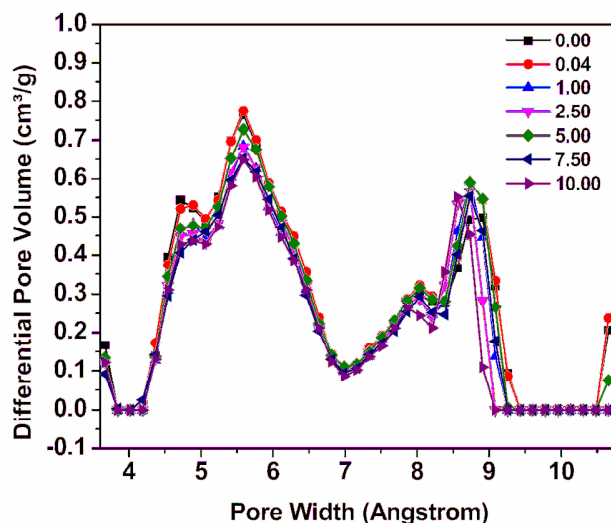


Figure 3.8 Micropore size distribution of activated STC at various PTSA to β -CD weight ratios obtained from CO₂ adsorption at 0 °C

3.3.6 Reason behind optimum concentration of PTSA to β -CD as 2.5

It has been reported that the formation of a rigid prepolymer with a high degree of polymerization is required to pre-organize the molecules to produce the microporosity and to preserve the microporosity during subsequent carbonization (Feinle et al, 2016). The increase in surface area, pore volume, and CO₂ adsorption capacity of STC with an increase in the PTSA concentration up to 2.5 times the weight of β -CD indicates that a high concentration of catalyst is required to form the prepolymer with the high degree of polymerization. On the other hand, a decrease in surface area, pore volume, and CO₂ adsorption capacity at PTSA to β -CD weight ratio above 2.5 is due to the contribution of PTSA to the STC yield.

The contribution of PTSA to STC yield was confirmed by the fact that the solvothermal experiment conducted with PTSA in o-dichlorobenzene without the β -CD produced a brown char having the elemental composition 59.5 wt% carbon, 2.2 wt% hydrogen, 4.8 wt% sulfur, and 33.5 wt% oxygen.

The STC obtained from the PTSA has flakes like morphology as evidenced from the SEM image as shown in Figure 3.9. This STC is amorphous and gave 50 wt% residue when carbonized at 800 °C in argon atmosphere for 2 h. The residue obtained contains graphite-like carbon as evidenced from the TEM image and x-ray diffraction spectra (Figure (3.10)). Selected area diffraction of the activated STC from PTSA also showed pattern of ordered crystalline nature of the residue (Inserted image of Figure 3.10 (a)).

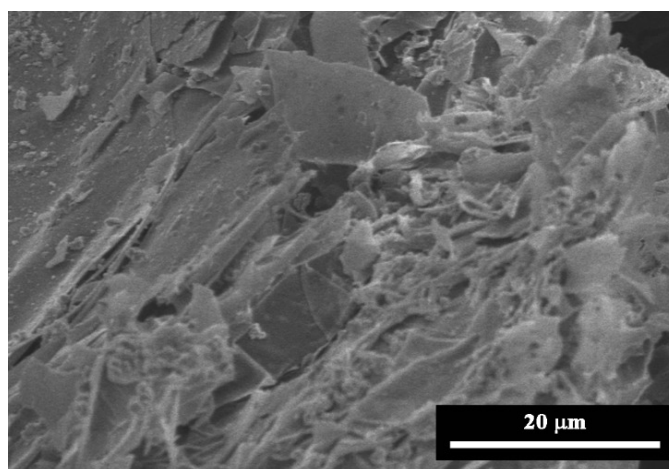


Figure 3.9 SEM image of PTSA char

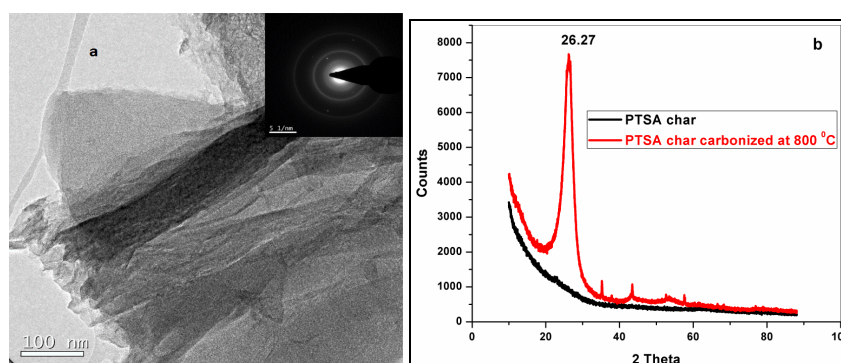


Figure 3.10 (a) TEM and (b) XRD spectrum of PTSA char carbonized at 800 °C.

The STC produced from PTSA and the carbon produced by pyrolysis of the same at 800 °C have the surface area of 0.8 and 1.8 m²/g and the total pore volume of 0.008 and 0.12 cm³/g, respectively. These observations indicate that the PTSA in o-dichlorobenzene produces some polymeric structure which produces graphite-like carbon on pyrolysis at 800 °C. This is confirmed by the fact that the high-temperature activation of STC produced at higher PTSA to β -CD ratios showed microporous amorphous region due to the carbon from β -CD and dense graphite-like regions due to the carbon from PTSA in the TEM image. Figure 3.11 shows the TEM image of the activated STC at a PTSA to β -CD weight ratio of 10 showing the amorphous and graphite-like region.

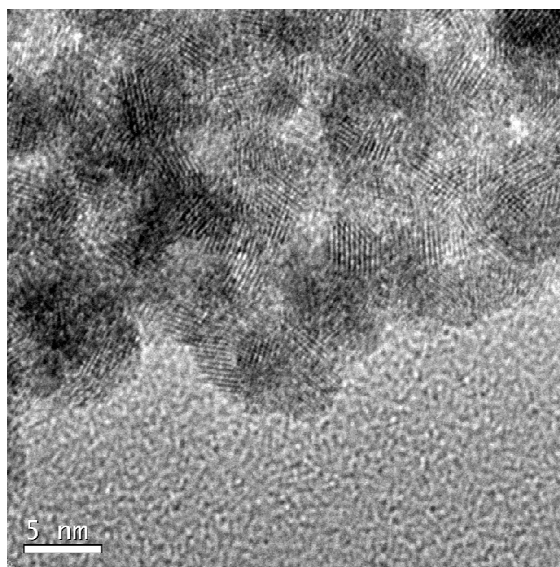


Figure 3.11 TEM image of activated STC at PTSA to β -CD weight ratio of 10

The decrease in pore volume and CO₂ adsorption capacity at PTSA to β -CD weight ratios higher than 2.5 is due to this nonporous graphite-like carbon produced from the PTSA. The information of PTSA contribution to the STC yield is vital as PTSA is a commonly used catalyst in solvothermal carbonization of biomass for the production of functional carbon materials.

The importance of the two step carbonization process, namely solvothermal carbonization and activation toward the formation of microporous carbon with better CO₂ absorption capacity was confirmed by the synthesis of carbon material by direct carbonization of β -CD at 800 °C. Thus, the prepared foam-like carbon material showed low surface area (39 m²/g), low total pore volume (0.044 cm³/g), and low CO₂ adsorption capacity (1.82 mmol/g at 25 °C) compared to the activated STC. This emphasizes the importance of intermediate solvothermal reaction for the development of microporosity. The morphology of the carbon material obtained by the direct carbonization at 800 °C of β -CD is shown in Figure 3.12.

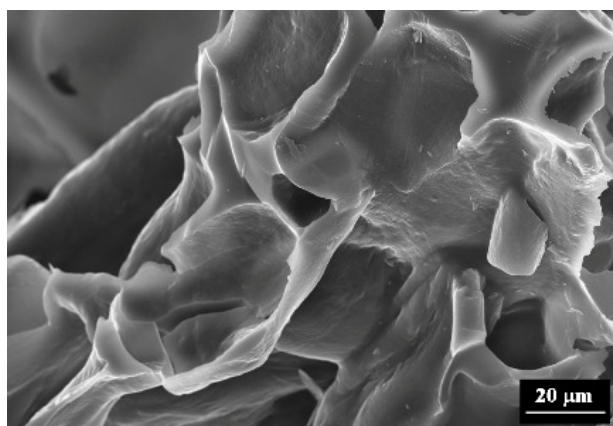


Figure 3.12 Morphology of carbon obtained by direct carbonization of β -CD at 800 °C.

3.3.7 CO₂ adsorption mechanism

To understand the CO₂ adsorption mechanism, the isotherms are simulated by Dubinin–Radushkevich (D–R) equation (Carrasco-Marín et al, 1993) . The D–R equation (Equation 3.1) is written as

$$\ln V = \ln V_o - (RT / \beta E_o)^2 [\ln (p_o / p)]^2 \quad (3.1)$$

where, V is the gas uptake when the adsorption potential is

$A = RT \ln (p_0/p)$, V_0 is the limiting micropore uptake, E_0 is the characteristic adsorption potential for a standard adsorbate and β is the affinity constant. As shown in Figure 3.13, a plot of $\ln (V)$ against $\ln^2(p/p_0)$, the adsorption data fit well with D–R equation indicating that the CO_2 adsorption on the porous carbons could be well depicted by a micropore filling mechanism.

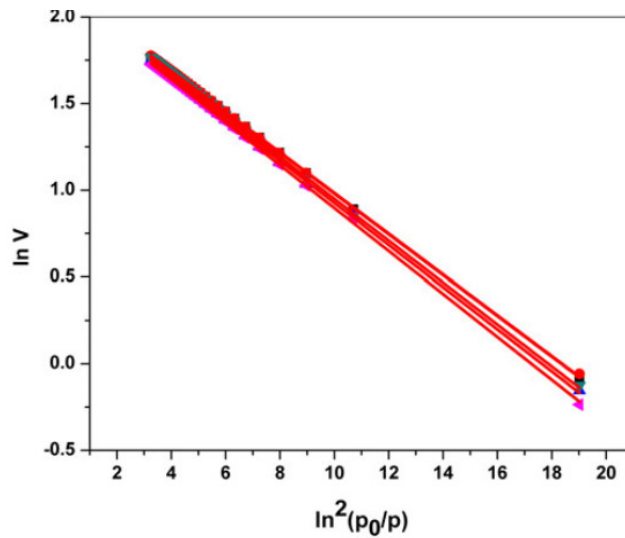


Figure 3.13 CO_2 adsorption isotherm model of activated STC fit with D-R equation

3.3.8 CO_2 adsorption from air

Capturing CO_2 directly from ambient air is commonly referred to as the direct air capture (DAC). Physisorbents such as activated carbons and zeolites are expected to have low CO_2 adsorption capacities in DAC because of their low heat of adsorption leading to shallow adsorption isotherms at very low partial pressures (Choe et al, 2009; Chue et al, 1995). The CO_2 adsorption characteristics of activated STC from dry air containing 400 ppm CO_2 were evaluated using TGA experiments. Figure 3.14 shows the weight gain of the activated STC in dry air at 25 °C as a function of time. The weight gain due to CO_2 adsorption was fast in the initial few minutes and thereafter sluggish. The sample showed a weight gain of 0.8 wt% in 30 min and 1.56% in 12 h. This

corresponds to a total CO₂ adsorption capacity of 0.35 mmol/g.

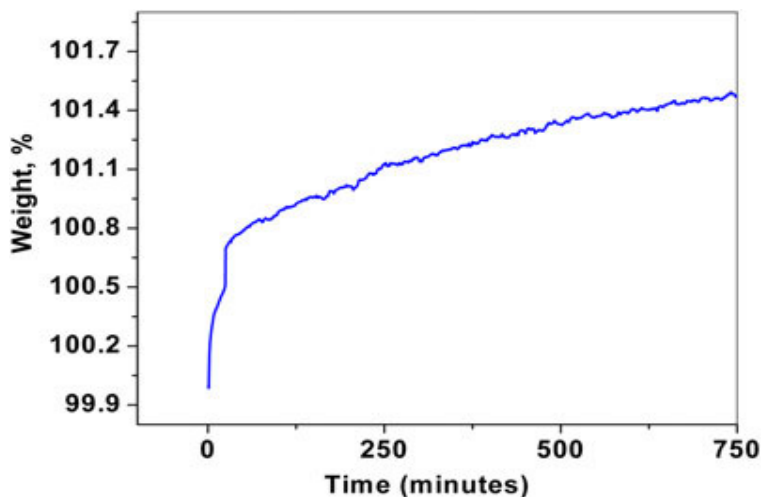


Figure 3.14 TG graph showing direct adsorption of CO₂ from air at 25 °C

The kinetics of CO₂ adsorption depends on pore size, size distribution, and presence of basic surface functional groups. In addition, adsorbent with a hierarchical pore structure containing macro, meso, and micropores facilitates adsorption as the CO₂ molecules can easily diffuse through the hierarchical pores and access the micropores. In the present case, the faster adsorption observed in the initial period is due to the filling of CO₂ molecules in the ultramicropores because of high surface potential. On the other hand, the sluggish kinetics observed after 30 min is attributed to the adsorption of CO₂ in the mesopores (Zhang et al, 2013, Wickramaratnea and Jaroniec, 2013). Lu et al. (2013) summarized the direct adsorption capacity from air of various adsorbent materials (McDonald et al, 2012; Gebald et al, 2012; Manson et al, 2011). The DAC using the activated STC is higher than for zeolites and some of the metal organic framework reported in the literature.

3.3.9 Evaluation of heat of adsorption

The adsorbent once used for CO₂ capture needs to be regenerated

either by increasing the temperature or by decreasing the pressure. Energy requirement for regeneration is one of the decisive factors for practical applications as the zeolite-based systems currently in practice face problem due to the requirement of high temperature for regeneration. Figure 3.15 is a DSC curve showing the CO₂ adsorption at 25 °C (exothermic peak) and desorption at 50 °C (endothermic peak). The activated STC once used for CO₂ adsorption could be regenerated by heating at a low temperature of 50 °C. The heat of adsorption calculated from the DSC is 32 KJ per mole of CO₂. The value of ΔH agrees well with the one reported by Chue et al (1995) implying physical adsorption.

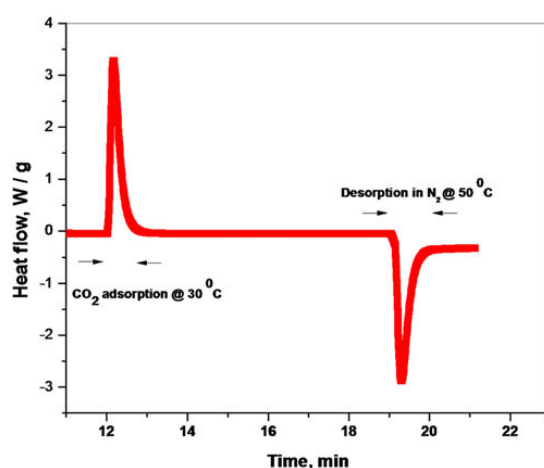


Figure 3.15 DSC graph showing CO₂adsorption at 30 °C and desorption at 50 °C.

3.3.10 Selectivity and recycle stability of STC

Recyclability and selectivity are the other two important factors for an acceptable adsorbent material. A good adsorbent should retain its adsorption capacity without any change after several adsorption–desorption cycle. In addition, the adsorbent should preferentially adsorb the adsorbate of interest in the presence of other molecules. Figure 3.16 shows the CO₂ adsorption isotherms showing the recyclability of the activated STC. The activated STC showed the same adsorption capacity when tested with pure

CO₂ gas at 25 °C for several adsorptions–desorption cycles. Figure 3.17 shows the adsorption isotherms showing the selectivity of CO₂ adsorption over N₂. The activated STC adsorbs negligible amount of N₂ gas compared to the 3.5 mmol/g CO₂ at 0 °C and 1 bar pressure, respectively.

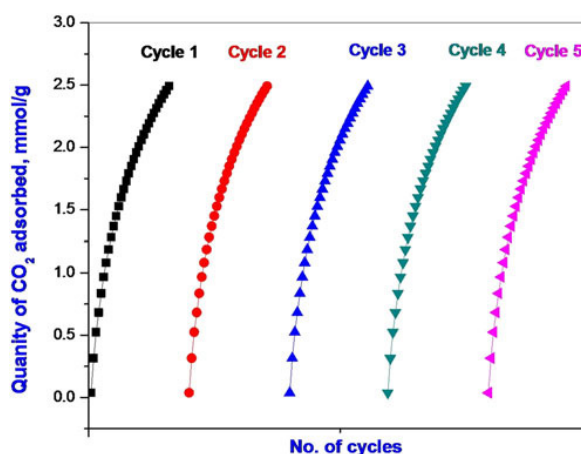


Figure 3.16 CO₂ adsorption isotherms at 25 °C showing the recyclability of activated STC.

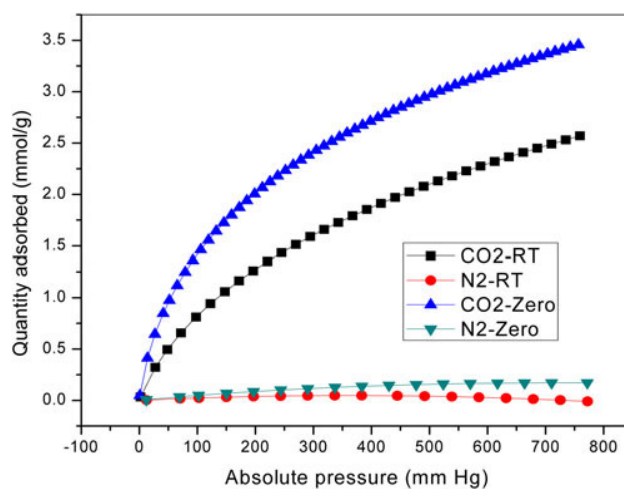


Figure 3.17 Selectivity of CO₂ adsorption over N₂ adsorption of carbon nanospheres at 25 °C and 0 °C

The selectivity of CO₂ over N₂ adsorption, calculated from the slope of the linear portion of the isotherms (Figure 3.18), as reported by Hao et al (2011) showed value of 27 at 25 °C.

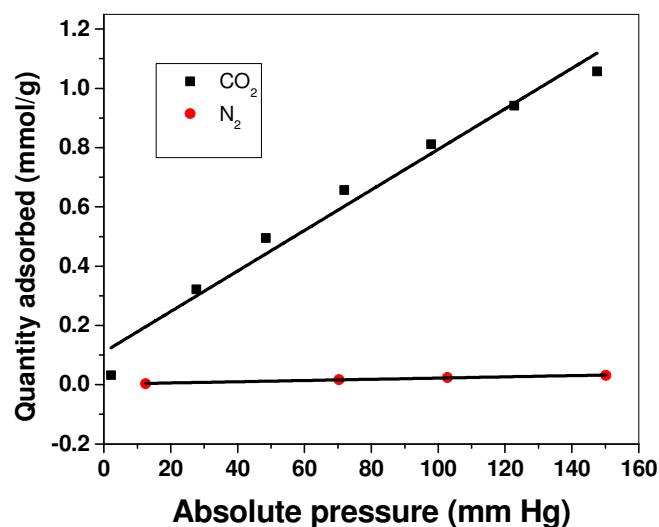


Figure 3.18 Calculation of selectivity of CO₂ adsorption over N₂ adsorption at 25 °C

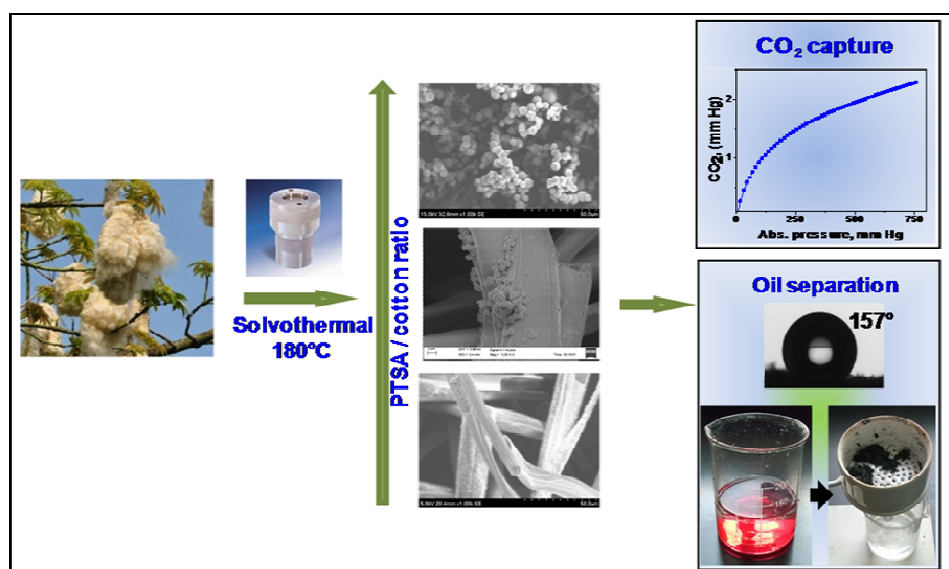
3.4 Conclusions

The effect of PTSA concentration and high-temperature activation on the textural properties and CO₂ adsorption capacity of STC obtained from β -CD has been studied. The contribution of nonporous graphite-like carbon from PTSA to the STC yield was established. The surface area, pore volume, and CO₂ adsorption capacity of the STC obtained from β -CD increased with the PTSA concentration and reached a maximum at a PTSA to β -CD weight ratio of 2.5. The activation at 800 °C increased the surface area and micropore volume due to the oxidation of carbon by 30–40 wt% oxygen present in the STC, which resulted in an increased CO₂ adsorption capacity. The high-temperature activation reduces the significance of the PTSA concentration as the CO₂ adsorption capacity of STC prepared at PTSA to β -CD weight ratios in the range of 0–2.5 shifted from a wide range of 1.04–2.44 mmol/g to a narrow range of 3.39–3.58 mmol/g after the activation. The significance of solvothermal step before high-temperature

activation for the formation of highly porous nanocarbon spheres was proved. The activated STC showed significant adsorption (0.35 mmol/g) of CO₂ from air containing 400 ppm CO₂. The CO₂ adsorption on the activated STC showed low-temperature regeneration, excellent recyclability, and good selectivity over nitrogen.

CHAPTER 4

MICROPOROUS SUPERHYDROPHOBIC CARBON FROM NATURAL COTTON FOR CO₂ AND ORGANIC SOLVENT REMOVAL



Deepthi, L. S., Narasimman, R., Rajeev, R., Prabhakaran, K. and Ninan, K. N. (2015). Solvothermal Synthesis of Microporous Superhydrophobic Carbon with Tunable Morphology from Natural Cotton for Removal of Carbon Dioxide and Organic Solvent Removal. *Journal of Materials Chemistry A*, 3: 16213–16221.

4.1 Introduction

Production of functional carbonaceous materials from biomass is getting renewed interest among the carbon researchers (Dobele et al, 2012; Hu et al, 2012). Biomass is a qualified carbon raw material for the synthesis of valuable carbon materials because of its low cost, easy access and environmental friendly nature (Xing et al, 2012; Xiaoyu et al, 2013; Titirici et al, 2007). Some examples of commonly available biomass for carbon production are sugar beet chips, pine cones, pine needles, oak leaves, orange peels, glucose, cellulose, starch, etc. Among the biomass materials that can be employed to produce carbonaceous materials, cotton is the most promising one as it is the almost pure form of cellulose available in abundance. The major constituents of cotton are cellulose (94%) with small amount of protein (1.3%) and pectin (1.2%).

Hydrothermal carbonization has been widely used to design novel carbon materials from biomass for important applications (Hu et al, 2010). Highly functionalized carbonaceous materials were produced by means of the hydrothermal carbonization of cellulose at temperatures in the 220–250 °C range by Sevilla et al (2009). However, the resultant carbon materials showed very low BET surface area of the order of 30 m²/g. Zhang et al (2013) first reported the use of carbon fiber aerogel made by the pyrolysis of raw cotton at 800 °C for 2 h at a low pressure (< 0.5 mbar) as a candidate for sorbent for oils and organic solvents from water. In 2014, Chiu et al prepared activated carbon adsorbents for solvent vapour from cotton via pyrolysis followed by ZnCl₂ activation. In the present work, we investigate the potential of natural cotton as precursor for the production of microporous carbonaceous materials with high surface area via solvothermal carbonization in o-dichlorobenzene medium. To the best of our knowledge, no one has employed cotton fibre to produce porous carbonaceous materials

by means of solvothermal carbonization. The effect of p-toluene sulfonic acid (PTSA) catalyst concentration on the textural property, morphology, CO₂ adsorption capacity and oil absorption capacity of the carbonaceous materials was evaluated.

4.2 Experimental

Raw cotton fibres were collected from cotton tree (*Bombax pentandrum* Linn-*Gossypium arboreum*) in Trivandrum, Kerala and used as such. P-toluene sulfonic acid monohydrate (PTSA) and o-dichlorobenzene were from Aldrich, India and used as received. Photograph of a cotton tree with cotton fibres is shown in Figure 4.1.



Figure 4.1 Photograph of a cotton tree with cotton fibres

4.2.1 Preparation of solvothermal carbon (STC) from cotton

The solvothermal carbonization was done using a typical Teflon-lined stainless-steel autoclave. A mixture of cotton (250 mg) and PTSA suspended in o-dichlorobenzene (10 mL) was ultrasonicated for 30 minutes. The PTSA to cotton weight ratio used was in the range of 0 to 10 (0, 0.04, 1, 2.5, 5, 7.5 and 10). The mixture was sealed in the autoclave and kept at 180 °C for 24 h. After the reaction, the autoclave was cooled down to room temperature. Black solid,

denoted as solvothermal char (STC), was filtered and washed subsequently with acetone, distilled water and ethanol. The product was dried in vacuum at 120 °C for 24 hours. The nomenclature of STCs prepared with different PTSA to cotton weight ratios are shown in Table 4.1

4.2.2 Characterization of solvothermal carbon materials (STCs)

Structure identification:

The FTIR spectra of the samples were recorded in a Perkin Elmer Spectrum GX-A FTIR spectrometer in the 4000 - 400 cm^{-1} wave number range with 16 number of scans and resolution 4 cm^{-1} .

Raman spectra were recorded using WITec alpha 300R Confocal Raman microscope (WITec GmbH, Germany) using the 532 nm line of an Nd:YAG laser as the excitation wavelength. An average of five spectra was collected with an integration time of 2 seconds/spectra to obtain a single spectrum. The spectrometer was calibrated using the 520 cm^{-1} line of Silicon prior to the analysis.

The carbon, hydrogen, nitrogen and sulfur content of STCs were determined using Perkin Elmer PE 2400 model CHNS elemental analyser. An exactly known weight (0.2 mg) of the sample was combusted in an atmosphere of pure and dry oxygen and the concentrations of individual components were measured as a function of their thermal conductivity. XPS analysis was carried out using Multilab 2000, Thermo Fisher Scientific using Al K_{α} radiation.

Textural property evaluation: The porous textural properties of STC were analyzed using the volumetric N_2 adsorption-desorption at -196 °C using a surface area analyzer (Micromeritics Tristar II, USA). The samples were degassed at 120 °C for 16 hours prior to the analysis. The specific surface area was measured from the isotherm in the relative pressure range between 0.05

and 0.2, according to the Brunauer-Emmett-Teller (BET) method. The pore size distribution was obtained from density functional theory (DFT). The micropore volume was calculated from the t-plot. The total pore volume was estimated from the amount of N₂ adsorbed at a relative pressure of 0.99.

Morphology analysis: The morphology of STC samples was analyzed using a field emission scanning electron microscope (FE-SEM JEOL Microscope JSM 6060 operating at 20 kV). Au film was deposited on the surface of the STC samples to improve conductivity.

Microstructure analysis: Microstructure of STC samples was evaluated using a transmission electron microscope (TEM, FEI, Tecnai G2 30 S-TWIN, USA) with an accelerating voltage of 300 V. The samples dispersed in acetone were drop-casted on carbon-coated copper grid and dried in vacuum at room temperature before the TEM observation.

Water contact angle measurement: The static contact angles (SCA) of water on STC surfaces was measured with Data Physics contact angle instrument OCA- 85 15EC. Samples were prepared by drop casting the STC dispersions in chloroform on glass slides followed by drying in an air oven at 100 °C. Water drops of sizes 5-10 µl were placed on the surface of the sample and contact angles were recorded by using the SCA 20 software based on Laplace-Young fitting method. The contact angle values reported are averages of four measurements made on different areas of the sample surface.

Surface analysis: Atomic force microscopy (AFM) measurements were performed on Agilent 5500 scanning probe microscope, USA. The STC sample dispersed in chloroform was drop-casted on silicon wafer and dried. The images were taken with the tapping mode.

CO₂ adsorption measurements: The CO₂ adsorption of STC was evaluated at 0 and 25 °C by volumetric gas adsorption studies using a surface area analyzer (Micromeritics Tristar II, USA). The samples were degassed overnight at 120 °C before the analysis. High pressure CO₂ adsorption measurements of the carbon samples were done on a pressure composition isotherm (PCI) measurement system (Advanced Materials Corporation, Pittsburgh, USA).

4.3 Results and Discussion

4.3.1 Structure identification of STC

The mechanism of carbonization of carbohydrates under hydrothermal and solvothermal conditions was reported by many researchers (Hu et al, 2010; Sevitta and Fuertes, 2009; Shin et al, 2008). It is generally believed that the cellulose decomposes under the solvothermal conditions to glucose anhydride which further transform to furan derivatives. The furan derivative undergoes further polymerization by intermolecular condensation and dehydration reactions to form poly furan like network containing solvothermal char (STC).

The PTSA acts as the catalyst for the intermolecular dehydration and condensation reactions. Therefore, the extent of polymerization depends on the catalyst concentration as evidenced from the increase in carbon content and decrease in oxygen concentrations in STC with an increase in PTSA concentration as shown in Table 4.1. The same trend was seen in the case of β -cyclodextrin also (Chapter 3). The oxygen to carbon atomic ratio in the STC decreases from 0.565 to 0.390 when the PTSA to cotton weight ratio increases from 0 to 10. Sevilla and Fuertes (2009) reported oxygen to carbon atomic ratios in the range of 0.239 to 0.263 in hydrochar prepared from cellulose at temperatures in the range 230 to 250 °C. The carbon enrichment in char takes place by dehydration either by $-OH$ to $-OH$ condensation or by α -elimination.

The hydroxyl condensation retains more oxygen in the char in the form of C-O-C linkages. It appears that, in PTSA catalyzed solvothermal method; –OH to –OH condensation is more favorable than the α -elimination. The presence of 0.12 to 2.2 wt% sulphur in the STC motivates us to analyze the fate of PTSA during the solvothermal reaction.

Table 4.1 Elemental composition of STC at various PTSA to cotton weight ratios

PTSA to cotton weight ratio	Nomenclature of STC	Elemental composition (wt. %)			
		C	H	O	S
0	STC-0	56.4	1.1	42.5	0
0.04	STC-0.04	58.8	1.4	39.7	0.12
1	STC-1.0	59.0	1.4	39.2	0.40
2.5	STC-2.5	59.5	1.3	36.6	2.2
5	STC-5.0	60.1	1.3	36.6	2.0
7.5	STC-7.5	60.9	1.8	35.4	1.9
10	STC-10	63.3	2.1	32.9	1.7

FTIR spectra of the cotton and STC obtained at various PTSA to cotton weight ratios are shown in Figure 4.2. The transformation of the carbohydrate to highly condensed carbon structure is evidenced from the IR spectrum as the peak at 900 cm^{-1} corresponding to the α -linkage in cotton, is absent in STC. STC contains both aromatic and aliphatic carbons as evidenced from the peaks at 1030, 1612, 1710 and 2930 cm^{-1} corresponding to the C-O stretching vibration, C=C stretching vibrations of the aromatic ring, C=O stretching vibration and stretching vibrations of aliphatic C-H, respectively. The cotton and its STC showed a broad absorption band in the region of 3000 to 3700 cm^{-1} corresponding to the –OH stretching vibrations.

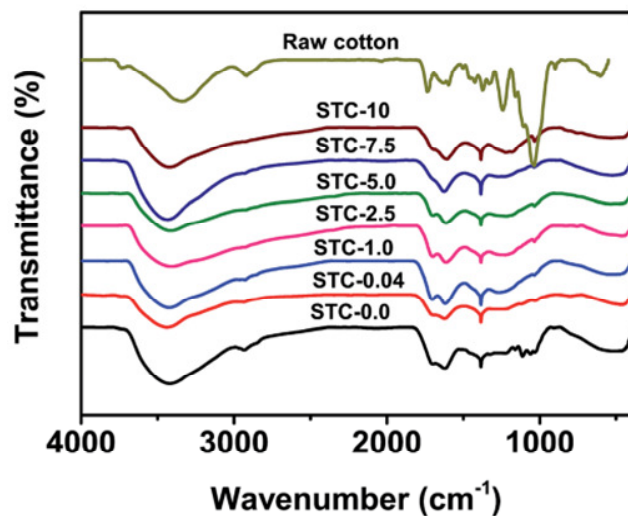


Figure 4.2 FTIR spectra of STC at various PTSA to cotton weight ratios

The aromatic and carbonyl functionality on STC is further confirmed by X-ray Photoelectron Spectroscopy (XPS) analysis. The XPS spectrum of STC-0.04 (Figure 4.3) shows C1_s peak with binding energy of 284 eV corresponding to aromatic C=C and O1_s peak with binding energy of 530 eV corresponding to C=O groups (Tien et al, 2011).

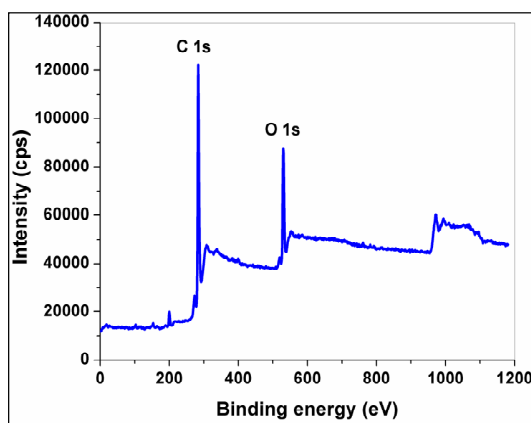


Figure 4.3 XPS spectrum of STC 0.04

Figure 4.4 shows the Raman spectra of STC prepared at various PTSA to cotton weight ratios. The Raman spectra of STC shows sharp peak at 1585

and broad peak at 1320-1350 cm^{-1} corresponding to G and D bands, respectively. The formation of condensed aromatic carbon structure by the solvothermal carbonization is further evidenced from the appearance of G-band corresponding to sp^2 carbon. The relative intensity of the G-band increased with an increase in PTSA concentration. This indicates that the concentration of condensed aromatic structures increased with an increase in PTSA concentration.

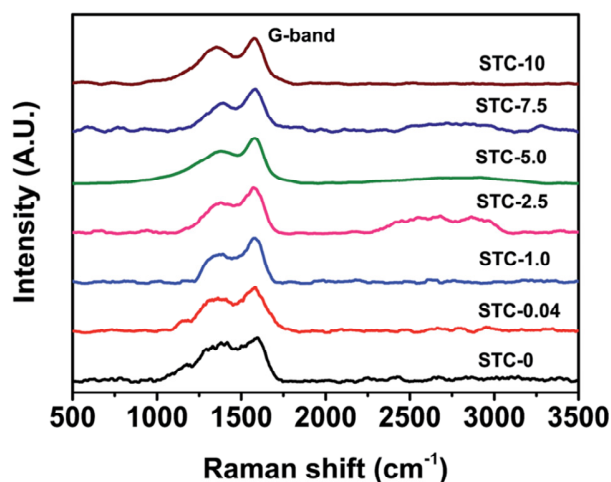


Figure 4.4 Raman spectra of STC at various PTSA to cotton weight ratios

4.3.2 Morphology analysis of STC

Figure 4.5 shows the morphology of STC prepared at various PTSA to cotton weight ratios. The hollow fibrous structure of cotton is retained in STC up to a PTSA to cotton weight ratio of 2.5. The surface of STC-0.04 is rough compared to the surface of STC-0. Well-defined particles start to appear on the surface of the fibers at a PTSA to cotton weight ratio of 2.5. It is very clearly seen in the high magnification image shown as insert in SEM photomicrograph of STC-2.5 shown in Figure 4.5. Further increase in PTSA concentration increases the concentration of the particle in STC. STC obtained at PTSA to cotton weight ratio of 5 contains agglomerated particles along with very small fraction of highly damaged fibers. On the other hand, at PTSA to cotton weight

ratio of 7.5, the fibrous morphology completely turned to particle morphology. However, the particles are very fine and highly agglomerated. Further increase in PTSA concentration results in considerable particle growth as STC prepared at PTSA to cotton weight ratio of 10 contains well defined spherical particles of size in the range of 2 to 8 μm .

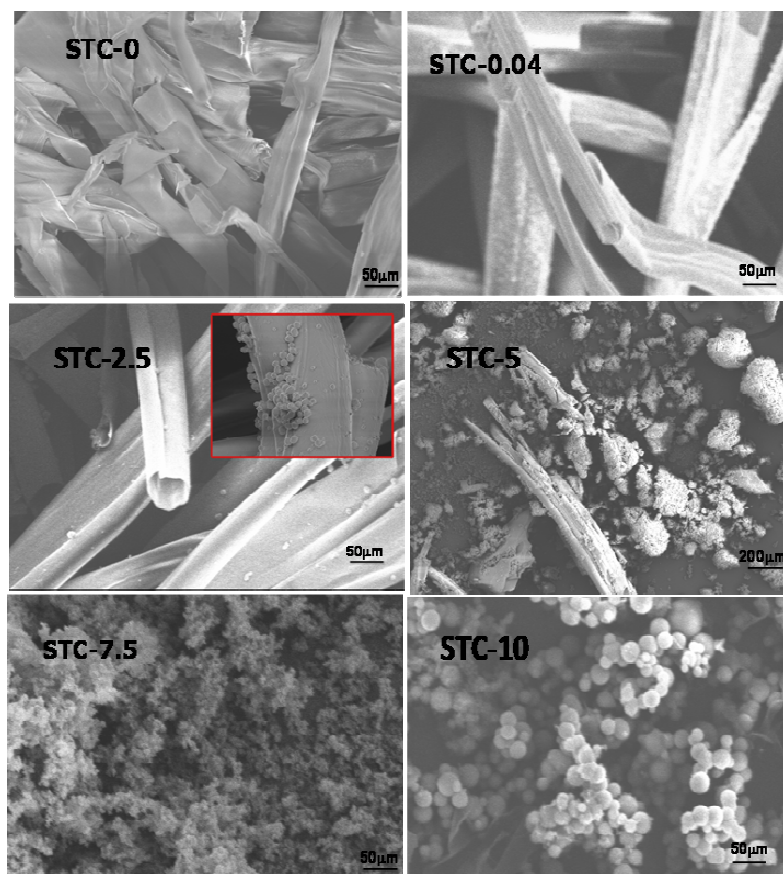


Figure 4.5 FE-SEM images of STC at various PTSA to cotton weight ratios

It appears that the condensation products of furan derivatives, which are the precursors for STC, nucleate the particle formation by either heterogeneous nucleation on the fibre surface or homogeneous nucleation in the solvent medium. As the PTSA concentration increases, more amount of cotton fiber is consumed to produce the furan derivatives which are responsible for the

growth of STC particle nuclei. This results in gradual disintegration of the fibrous morphology of the cotton. The whole cotton fibre is consumed to produce STC particles at PTSA to cotton weight ratio of 7.5. Further growth of STC particles observed at PTSA to cotton weight ratio of 10 is due to the Ostwald ripening.

4.3.3 Textural property evaluation of STC

Figure 4.6 shows the nitrogen adsorption–desorption isotherms of STC prepared at various PTSA to cotton weight ratios.

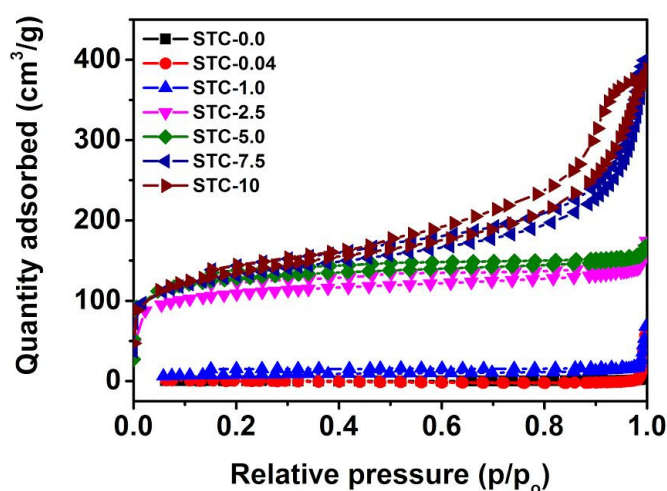


Figure 4.6 Nitrogen adsorption–desorption isotherms of STC at various PTSA to cotton weight ratios

The STC obtained at PTSA to cotton weight ratios up to 1 adsorb very small volume of nitrogen. The volume of nitrogen adsorbed increased with an increase in PTSA to cotton weight ratio up to 5 and then decreased with a further increase in PTSA to cotton weight ratio. STC showed a steep nitrogen gas uptake at the relative pressure (P/P_0) less than 0.10, a relatively slow uptake in the intermediate section, and hysteresises between adsorption and desorption branches indicating type II isotherm. This shows the presence of both micropores and mesopores in STC. The specific surface area of STC calculated using Brunauer–Emmet–Teller (BET) model for the relative pressure (P/P_0) between 0.05 and 0.20 is shown in Table 4.2 along with other textural

properties.

Table 4.2 Textural properties of STC obtained at various PTSA to cotton weight ratios

Samples	S_{BET} ($\text{m}^2.\text{g}^{-1}$)	V_{p} ($\text{cm}^3.\text{g}^{-1}$)	V_{m} ($\text{cm}^3.\text{g}^{-1}$)	Microporosity (%)
STC-0	0.7	0.03	-	-
STC-0.04	1.6	0.05	-	-
STC-1	27	0.10	-	-
STC-2.5	377	0.27	0.10	38.7
STC-5	477	0.60	0.07	11.6
STC-7.5	460	0.62	0.07	11.2
STC-10	443	0.26	0.10	37.6

Notation: V_{p} is the single point pore volume calculated from adsorption isotherm at $P/P_0 = 0.995$; S_{BET} is the BET specific surface area obtained from the adsorption data in the P/P_0 range from 0.05 to 0.2. V_{m} is the total micropore volume.

The surface area shows a moderate increase from 0.7 to 27 m^2/g when the PTSA to cotton weight ratio increased from 0 to 1. Further, increase in PTSA to cotton weight ratio to 2.5 produces a marked increase in surface area to 376 m^2/g . STC at PTSA to cotton weight ratio of 5 showed a maximum surface area of 477 m^2/g . Beyond this, the surface area decreases with an increase in PTSA to cotton weight ratio. The maximum surface area obtained in the present method is ~ 16 times higher than that of the hydrothermal char from cellulose reported by Sevilla and Fuertes (2009). The pore size distribution obtained from the nitrogen adsorption data using DFT calculations is shown in Figure 4.7.

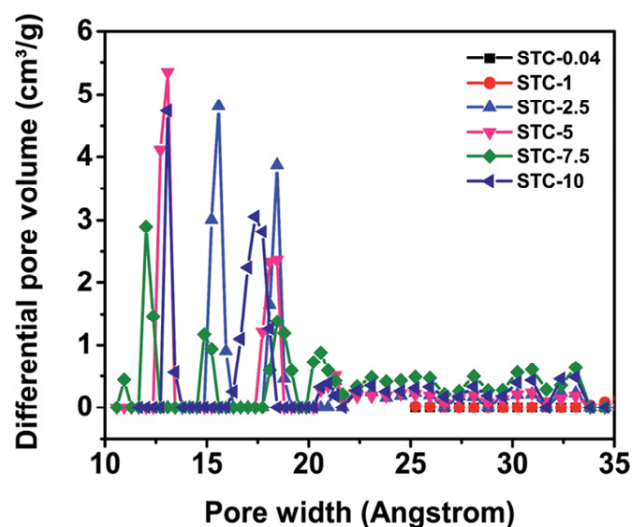


Figure 4.7 DFT pore size distribution of STC at various PTSA to cotton weight ratios

The development of microporosity is sluggish up to PTSA to cotton weight ratio up to 1. On the other hand, STC obtained at PTSA to cotton weight ratio in the range of 2.5 to 10 shows well defined peaks in the micropore size region (10 to 20 Å). STC obtained at PTSA to cotton weight ratio of 5 and 7.5 showed minor peaks in the pore size range of 20 to 35 Å corresponding to the mesopores. The total pore volume (V_p) increases from 0.10 to 0.62 cm³/g when the PTSA to cotton weight ratio increased from 1 to 7.5 (table 4.2). Further increase in the PTSA to cotton weight ratio to 10 results in a decrease of total pore volume to 0.26 cm³/g. On the other hand, STC obtained at PTSA to cotton weight ratio of 2.5 showed the highest micropore volume (V_m). The higher surface area of the STC compared to that of the hydro char reported in the literature is attributed to the formation of micropores by the self-organization of the polymer molecules produced by the condensation of furan derivatives in o-dichlorobenzene medium. These micropores retain during the subsequent dehydration, washing and drying.

The local structure of STC was investigated using high resolution transmission electron microscopy. The TEM photomicrographs of STC-0 and STC2.5 are shown in Figure 4.8. STC-2.5 showed increased

microporosity compared to the dense spherical microstructure of STC-0.

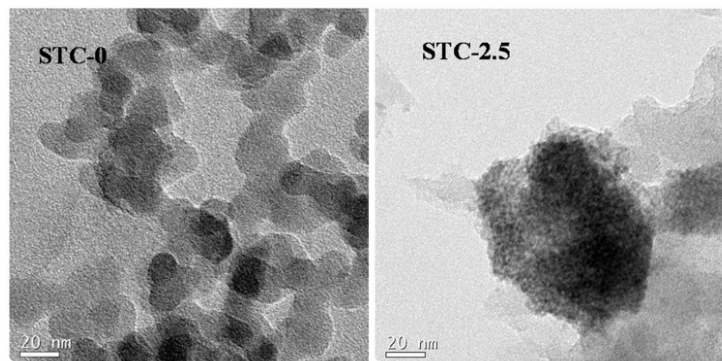


Figure 4.8 TEM images of STC-0 and STC-2.5

4.3.4 CO₂ adsorption evaluation of STC

The CO₂ adsorption isotherms of STC obtained at various PTSA to cotton weight ratios at 25 and 0 °C are shown in Figure 4.9 and Table 4.3. STC obtained without the PTSA catalyst show negligible CO₂ adsorption due to its very low surface area and unavailability of micropores. On the other hand, the CO₂ adsorption capacity of STC increased with an increase in PTSA to cotton weight ratio and reached a maximum at a PTSA to cotton weight ratio of 2.5. The maximum CO₂ adsorption capacity observed are 1.3 and 2.3 mmol/g at 25 and 0 °C, respectively. It is well known that the CO₂ adsorption capacity at ambient pressures depends on the micropore volume in the adsorbent rather than the surface area as the mechanism of adsorption is micropore filling (Zhang et al, 2013). The variation in CO₂ adsorption capacity with PTSA to cotton weight ratio is in accordance with the variation of micropore volume. STC-2.5 showed the highest micropore volume and therefore the highest CO₂ absorption capacity. The maximum CO₂ adsorption capacity obtained is higher than that of some of the carbon based adsorbents such as activated nanocarbon fibers, carbon spheres reported in the literature (Bezerra et al, 2011; Meng and Park, 2012; Hao et al, 2011).

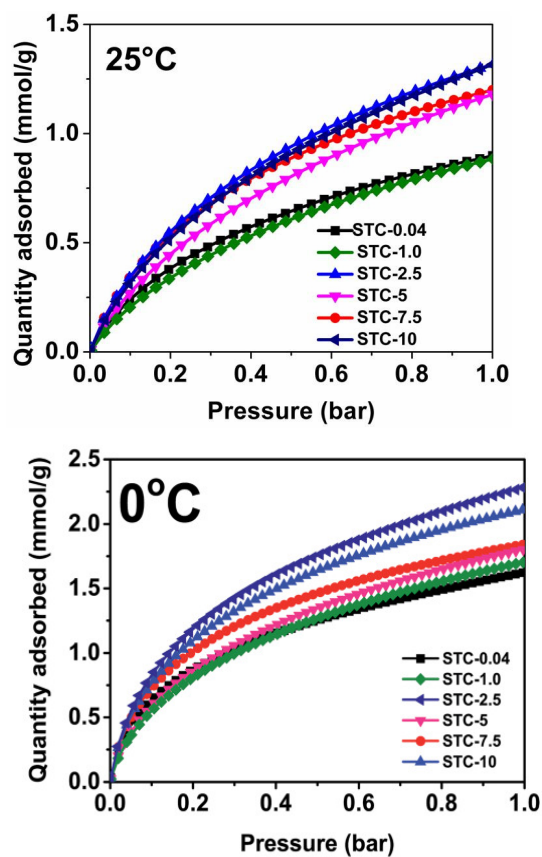


Figure 4.9 CO₂ adsorption isotherms of STC prepared at various PTSA to cotton weight ratios at 25 and 0 °C at 1 bar

Table 4.3 CO₂ adsorption capacities of STC prepared at various PTSA to cotton weight ratios

Sample	CO ₂ adsorption (mmol.g ⁻¹)	
	0 °C	25 °C
STC-0.04	1.6	0.9
STC-1.0	2.1	1.2
STC-2.5	2.3	1.3
STC-5	2.3	1.3
STC-7.5	1.7	0.88
STC-10	1.8	1.2

A comparison of the CO₂ adsorption capacity of STC-2.5 with that of other carbon adsorbents having similar textural properties reported in the literature is listed in Table 4.3.

Table 4.4 Comparison of the CO₂ adsorption performance of the STC samples and other carbons with similar pore properties

Adsorbent	Surface area, m ² /g	Total micro pore volume	Total pore volume cm ³ /g	CO ₂ absorption capacity, (1 bar, 25°C) mmol/g	References
Activated carbon	-	0.57	-	1.8	Bezerra et al (2011)
Nano carbon fibre	567	0.27	0.708	1.1	Meng and Park (2012)
Carbon sphere	390		0.17	1.4	Wickramaratne and Jaroniec, (2013)
N-doped carbon from Melamine-hcho resin	336	-	0.19	2.4	Tseng <i>et al.</i> (2015).
N-containing porous carbon	418	0.21	0.37	1.4	Zhang <i>et al</i> (2012)
Carbon from anthracite	540	-	-	1.49	Maroto-Valer <i>et al.</i> (2005)
Cotton-STC	377	0.10	0.27	1.3	Present work

Physisorbents are suitable for CO₂ capture from high pressure streams such as those relevant for pre-combustion capture in Integration Gasification Combined Cycle plants. High pressure CO₂ adsorption capacities of porous carbon materials are higher due to their large specific surface area. High pressure gas adsorption measurements for CO₂ were performed on STC using a

high pressure volumetric gas analyzer and the adsorption isotherms are given in Figure 4.10. High CO₂ uptake of 4.1 and 4.6 mmol/g at 25 °C and 20 bars pressure were exhibited by STC-2.5 and STC-5, respectively.

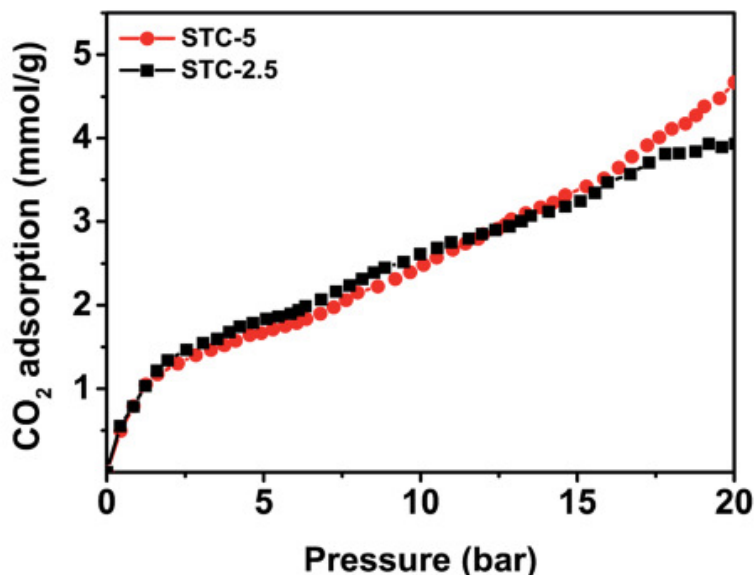


Figure 4.10 High pressure CO₂ adsorption isotherms of STC-2.5 and STC-5 measured at 25 °C

4.3.5 Evaluation of heat of adsorption

The adsorbent once used for CO₂ capture needs to be regenerated, by desorbing the adsorbed CO₂ molecules, for the efficient and repeated use of the same adsorbent. The regeneration of adsorbents is done either by increasing the temperature or by decreasing the pressure. Energy requirement for regeneration is one of the important factors for practical applications. Figure 4.11 is a DSC curve showing an exothermic peak at 25 °C corresponding to the CO₂ adsorption and an endothermic peak at 50 °C corresponding to desorption of CO₂. That is, STC once used for CO₂ adsorption could be regenerated by heating at a low temperature of 50 °C. The heat of adsorption calculated from the area under the DSC peak, weight of the loaded adsorbent sample and

amount of CO₂ adsorbed showed values nearly 22 kJ/mol implying physical adsorption.

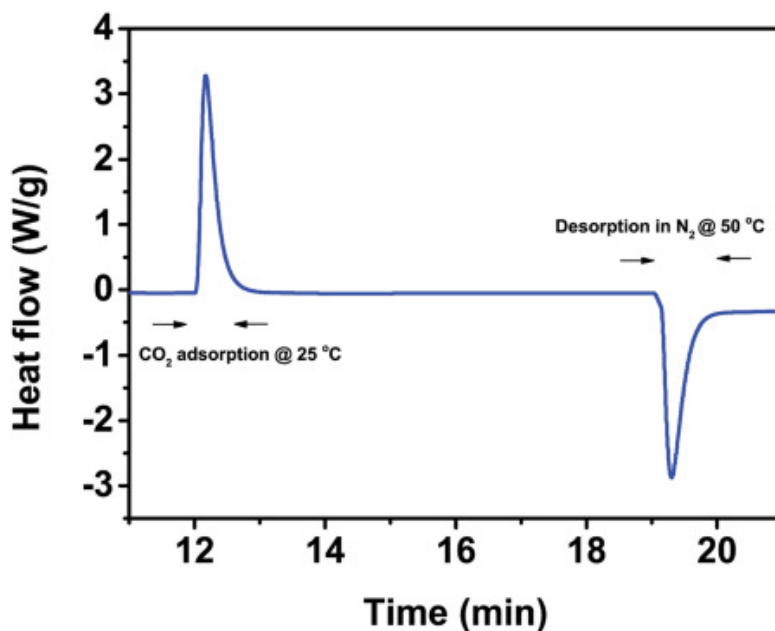


Figure 4.11 DSC graph showing CO₂ adsorption at 25 °C and desorption at 50 °C

4.3.6 Selectivity and recycle stability of STC

Recyclability is an important factor for an acceptable adsorbent material. A good adsorbent should retain its adsorption capacity without any change after several adsorption-desorption cycle. STC showed the same adsorption capacity when tested with pure CO₂ gas at 25 °C for several adsorptions-desorption cycles. The adsorption isotherms showing the recyclability of STC at PTSA to cotton weight ratio of 2.5 are shown in Figure 4.12.

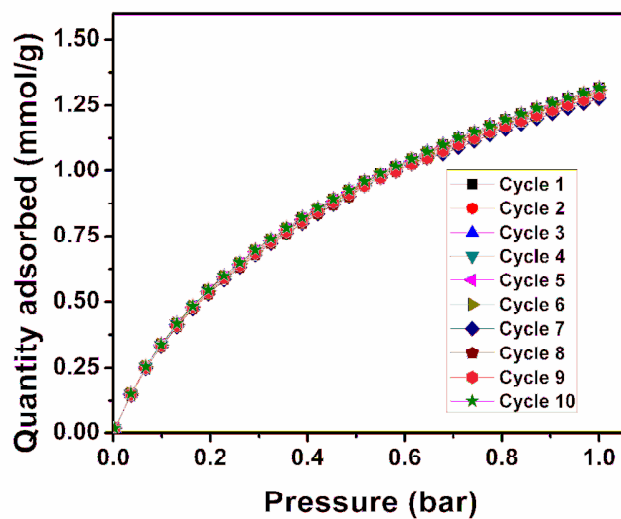


Figure 4.12 The CO₂ adsorption isotherms at 25 °C showing the recyclability

In addition to the recyclability, the adsorbent should preferentially adsorb the adsorbate of interest in presence of other molecules. The adsorption isotherms showing the selectivity of CO₂ adsorption over N₂ adsorption on STC-2.5 is shown in Figure 4.13.

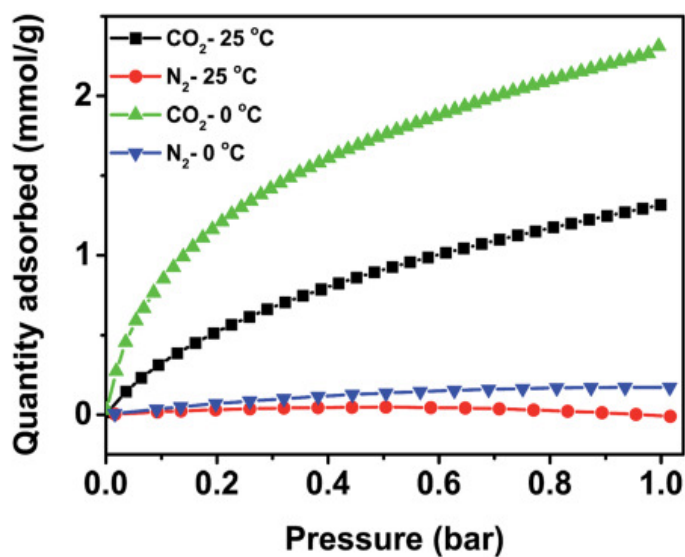


Figure 4.13 The adsorption isotherms showing selectivity of CO₂ adsorption over N₂ at 25 and 0 °C.

STC adsorb negligible amount of N₂ gas compared to the 2.28 mmol/g of CO₂ at 0 °C and 1 bar pressure. The selectivity of CO₂ over N₂ adsorption, calculated from the slope of the linear portion of the isotherms (Figure 4.14 a and 4.14 b), as reported by Hao et al (2011) showed values of 17 and 19 .05 at 25 and 0 °C, respectively.

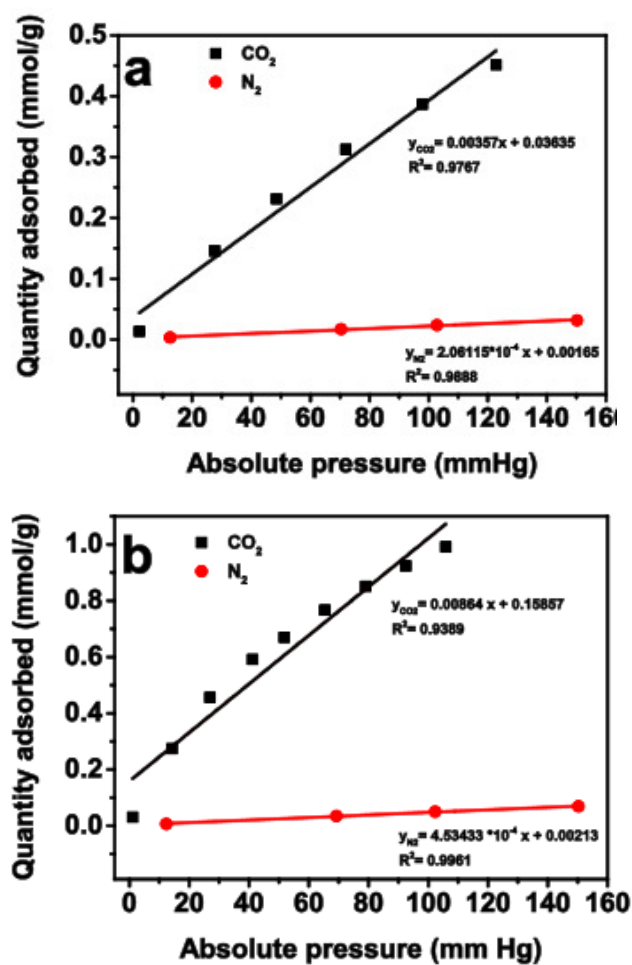


Figure 4.14 Calculation of selectivity of CO₂ adsorption over N₂ adsorption. (a) 25 °C and (b) 0 °C

4.3.7 Removal of oil and toxic pollutants from water using carbon adsorbents

Efficient techniques for the removal of highly toxic contaminants from water have attracted significant interest. The adsorption by solid adsorbents shows potential as one of the most efficient methods for the treatment and removal of contaminants in wastewater. In recent years, low-cost adsorbents, i.e., powdered activated carbons (PAC) are common adsorbents used for the removal of undesirable odor, color, and other organic and inorganic impurities from domestic and industrial waste water owing to their large surface area, micro / meso porous structure and economic viability.

Activated carbons have been successfully utilized for the removal of phenol, dyes, chlorinated solvents, perchlorate etc. from water (Auta and Hameed, 2011 and Al-Degs et al, 2008). Djilani et al. (2012) developed activated carbon from lignocellulosic coffee grounds; melon seeds and orange peels. These adsorbents worked well for the removal of organic pollutants o-nitrophenol and p-nitrotoluene from water. Activated carbon prepared from banana stalk by potassium hydroxide (KOH) and carbon dioxide (CO₂) activation was explored for its ability to remove the pesticides, 2,4-dichlorophenoxyacetic acid (2,4-D) and bentazon (Salman et al, 2011).

Oil spillage and oil contaminated industrial waste water have caused severe environmental concerns. Materials capable of separating oil–water mixtures with high absorption capacity and mechanical strength are in high demand. Carbon based absorbents have been considered to be the best candidates for this purpose as they possess high surface area, large pore volume, low density, excellent mechanical properties, good chemical stability and environmental friendliness. Carbon aerogels, graphene or carbon nanotubes coated sponges, graphene sponges, carbon coatings, activated carbon and carbon

fibers have been widely investigated for water filtration, water/oil separation and oil-spill cleanup. Wang et al (2015) fabricated carbon nanotubes reinforced superhydrophobic sponge, which exhibited significant potential as an efficient absorbent in large-scale oil–water separation applications. Li et al. (2014) reported compressible graphene aerogel with high absorption capacity up to 250 times its own weight for CCl_4 . The present study will also check the feasibility of prepared cotton derived STCs for the removal of pollutants from water.

4.3.7.1 Organic solvent removal property of STC

The most important property of an ideal sorbent material for oil spill cleanup is its hydrophobicity. The water contact angle of STC with the fibrous morphology produced at lower (0 to 2.5) PTSA to cotton weight ratios could be easily measured compared to STC with particle morphology produced at higher (5 to 10) PTSA to cotton weight ratios. Figure 4.15 shows the water contact angle of STC prepared at PTSA to cotton weight ratios in the range of 0 to 2.5.

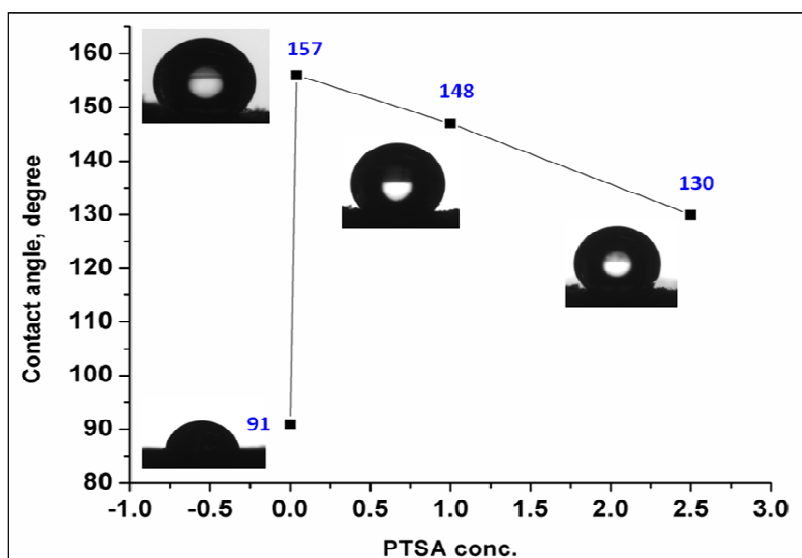


Figure 4.15 water contact angle of STC-0, STC-0.04, STC-1.0 and STC-2.5

The contact angle of STC increased from 91 to 157° when the PTSA to cotton weight ratio increased from 0 to 0.04. The deviation of individual contact angle values from the average value is within $\pm 2^\circ$. Further increase in PTSA to cotton weight ratio resulted in a decreasing trend of the water contact angle. A surface with water contact angle greater than 150° is called superhydrophobic surface. This indicates that STC-0.04 shows superhydrophobic effect. It has been reported that the superhydrophobic effect is due to the micro and nano level surface roughness produced by the micro and nano structures on the surfaces as proposed by the Cassie-Baxter models. According to this model, the liquid drop sits on the top asperities of dual scale surface structure and air is supposed to be trapped in rough structure underneath the liquid, which gives a high water contact angle (Srinivasan et al, 2008; Wang et al, 2015).

Figure 4.16 shows the AFM images of STC at various PTSA to cotton weight ratios. The AFM images of STC-0.04 showed the presence of large number of nano projections on the surface of the fibre. The population of these nano projections decreases with further increase in the PTSA to cotton weight ratio. On the other hand, STC-0 showed almost smooth topography in the AFM image.

It is clear from the AFM images that a large number of STC particles are nucleated on the fibre surface by the heterogeneous nucleation mechanism at PTSA to cotton weight ratio of 0.04. It is well known that the heterogeneous nucleation on solid surfaces takes place at low levels of super saturation of the nucleating species compared to the homogeneous nucleation in solution. It appears that at higher PTSA to cotton weight ratios, the concentrations of the nucleating species is sufficiently high for the homogeneous nucleation. i.e., At higher PTSA to cotton weight ratios, the homogeneous nucleation overtakes the heterogeneous nucleation resulted in fewer number of nano projections on the fibre surface.

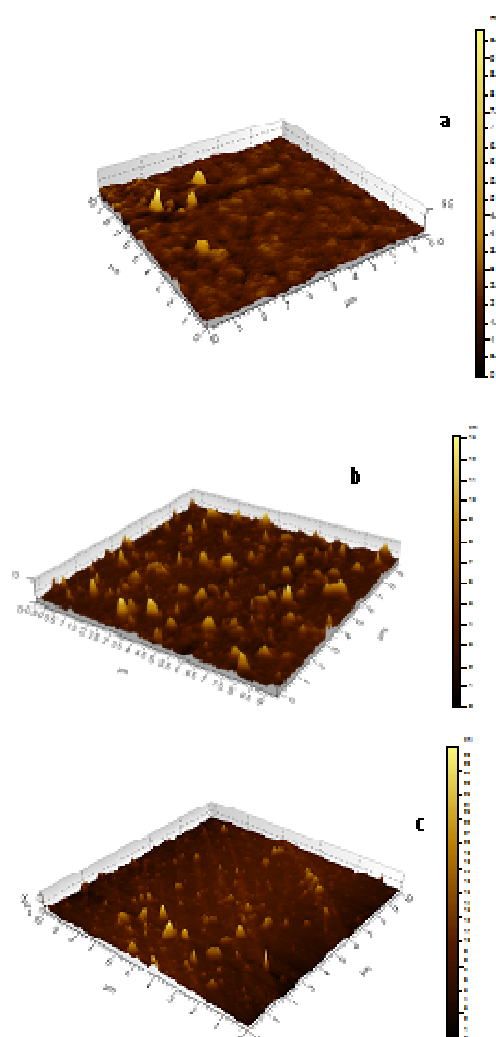


Figure 4.16 AFM images of (a) STC-0 (b) STC-0.04, and (c) STC-2.5

The decrease in contact angle at PTSA to cotton weight ratio higher than 0.04 is due to the decrease in the number of nano projections on the surface. Thus, benefited from the nano-scale structure, STC-0.04 has high nano level surface roughness. The superhydrophobic nature of STC-0.04, in spite of high oxygen content, is due to the high nano level surface roughness. Super hydrophobic effect is reported in many hydrophilic oxide materials such as ZnO, TiO₂, (Azimi et al, 2013; Feng et al, 2004) due to the

nano level surface structures. The super hydrophobic nature of STC-0.04 is further confirmed as follows: STC-0.04 was stirred with water for 1 hour and then separated by filtration. Thermogravimetric analysis of the STC-0.04 separated from water showed no weight loss up to 150°C indicating zero adsorption of water. .

In the present case, the ability of STC to separate the organic phase from water was tested as follows: A mixture containing 25 ml chloroform (stained with Sudan red 5B) and 75 ml water was stirred with 100 mg STC for 30 minutes. The mixture was then filtered through a porcelain Buchner funnel (Figure 4.17). The chloroform retained in STC was then estimated gravimetrically. The chloroform absorption ability of STC prepared at various PTSA to cotton weight ratios is shown in Table 4.5.

Table 4.5 Variation in chloroform removal efficiency of STC at various PTSA to cotton weight ratio

Sample	STC-0	STC-0.04	STC-1.0	STC-2.5	STC-5	STC-7.5	STC-10
Efficiency (g/g)	20	110	97	80	70	70	66

STC-0 absorbs 20g chloroform per gram of STC. The chloroform absorption drastically increased to 110 g/g in the case of STC-0.04. The chloroform absorption ability of STC-0.04 is comparable to the carbon fibre obtained by high temperature carbonization of cotton (Bi et al, 2013). Further increase in PTSA to cotton weight ratio resulted in decrease in the chloroform absorption capacity of STC. This trend is true with other solvents viz., heptane, toluene, dichloromethane etc. It appears that the oil absorption capacity of STC depend on its hydrophobic nature and morphology. The STC with fibrous morphology can hold more oil phase in the interfibrous space rather than the one with the particle morphology. The

maximum oil absorption capacity of STC-0.04 is due to the combination of its super hydrophobic nature and fibrous morphology.

Figure 4.17 shows separation of chloroform stained with Sudan B from water using STC-0.04. The sorbent can be regenerated and reused several times. For the regeneration, the adsorbent is first squeezed to remove the solvent and then heated in aqun oven at a temperature above the boiling point of solvent. The material can be used for the removal of oils and other immiscible organic solvents spilled in water bodies. Zhang et al first demonstrated the separation of oils from water using cotton carbonized at 800 °C (2013). However, in the present work, the maximum temperature required for the preparation of the absorbent is only 180 °C, which is really a power saving low cost method. Thus, the difficulties associated with removal of trace amount of organic solvent from water can be solved using non-toxic carbon prepared from natural cotton.

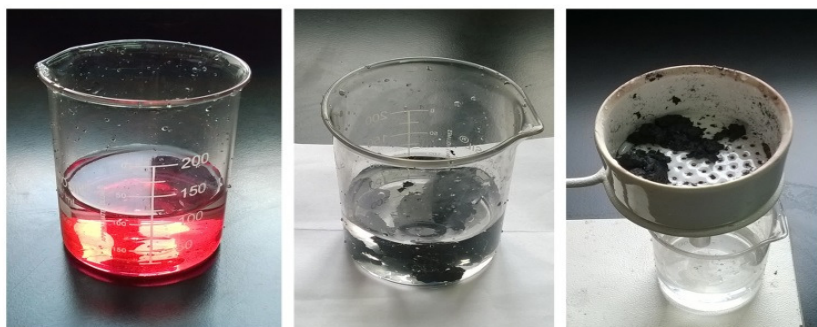


Figure 4.17 Separation of chloroform (stained with Sudan red 5B) from water using STC-0.04

Contamination of water with trace quantity of oil or organic solvent is also a major concern. Removal of this low quantity of toxic solvent is indeed a tough task when compared with that of bulk quantity. Here, trace quantity of chloroform present in water can be easily removed by STC-0.04. In a typical example, water contaminated with 0.2 ml of chloroform could be easily removed using 50 mg STC-04. Figure 4.18 demonstrates the removal of trace quantity of chloroform (stained using Sudan dye) from water, and the physical

separation of chloroform using a forceps. Thus, the difficulties associated with removal of trace amount of organic solvent from water can be solved using non-toxic carbon prepared from natural cotton.



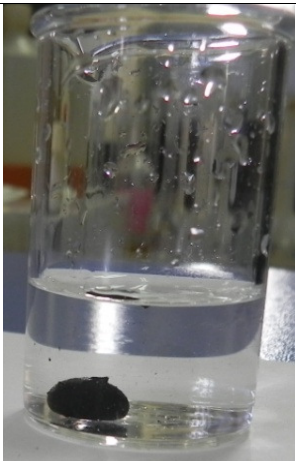

	
10 ml water + 0.2 ml chloroform	50 mg Cotton-STC-0.04
	
Cotton-STC enclose chloroform droplet	Separation of chloroform droplet using forceps.

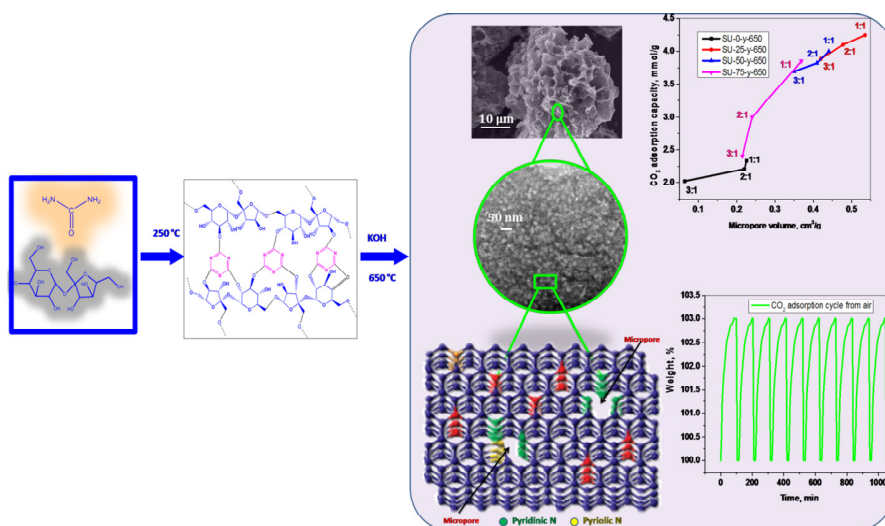
Figure 4.18 Removal of trace quantity of chloroform from water, and the physical separation of chloroform using a forceps.

4.4 Conclusions

Microporous carbonaceous materials were prepared by solvothermal carbonization of natural cotton for the first time. STC transforms from fibrous to particle morphology with an increase in concentration of PTSA. The surface area and pore volume of STC increased with PTSA concentration and reached a maximum at a PTSA to cotton weight ratio of 5. STC-2.5 showed the highest CO₂ adsorption capacity of 2.28 mmol/g at 1 bar pressure and 0 °C temperature. The CO₂ adsorption on STC showed excellent recyclability and selectivity over nitrogen gas. STC-0.04 showed superhydrophobic effect due to the nano projection on the fibre surface produced by heterogeneous nucleation of STC particles. Superhydrophobicity combined with the fibrous structure made STC-0.04 an excellent sorbent for organic solvents from solvent-water mixtures. Thus, STC obtained from cotton is an economic, efficient and safe sorbent for CO₂ and oil.

CHAPTER 5

NITROGEN ENRICHED MICROPOROUS CARBON FROM SUCROSE AND UREA FOR CO₂ REMOVAL



Deepthi, L. S., Sujith, V., Rajeev, R., Ninan, K. N. and Prabhakaran, K. (2016). Nitrogen-enriched microporous carbon derived from sucrose and urea with superior CO₂ capture performance. *Carbon*,109: 7-18.

5.1 Introduction

Many studies have proven that the CO₂ capture capacity of activated carbon (AC) sorbents can be significantly increased by introducing nitrogen (N) functional groups into their structures. N-containing functionalities increase the surface polarity and basicity of AC materials, which is beneficial for the adsorption of CO₂. N-containing carbon can be prepared directly from the carbonization of N-rich chemical precursors, polymers, ionic liquids, etc. Sevilla et al. (2011) prepared a porous carbon containing 10 wt.% nitrogen by the pyrolysis of polypyrrole at 600 °C, which showed a high CO₂ adsorption capacity of 3.9 mmol/g at 25 °C and 1 bar. Morawski et al. (2004) effectively introduced nitrogen into the framework of a commercial AC by treating porous carbon at 600–1200 °C in NH₃ atmosphere. A remarkable increase (40%) in CO₂ uptake of the AC was achieved by this treatment. In addition to the difficulty in handling gaseous ammonia, the limitation of this method is that it can incorporate only a small amount of N (<5wt%) into the carbon adsorbent. Spherical N-containing polymer and microporous carbon materials were synthesized by Yuan et al. (2012) using hexamethylenetetramine as a nitrogen source and one of the carbon precursors together with resorcinol under solvothermal conditions. At 1 bar, the equilibrium CO₂ capture capacities of the obtained microporous carbon are in the range of 2.7–4.0 mmol/g at 25 °C. Porous N-doped carbon was successfully fabricated through a facile one-pot evaporation-induced self-assembly (EISA) process of resorcinol and formaldehyde using HNO₃ as a catalyst and nitrogen source. The sample shows the highest CO₂ adsorption capacity of 4.30 mmol/g at 25 °C and 1 bar (Ma et al, 2013). Recently, Hu et al. (2015) have reported a simple and economical method to synthesize a series of N-enriched porous carbon, in which petroleum coke was used as a carbon precursor, urea as the nitrogen source, and KOH as the activating agent. The maximum CO₂ absorption capacity obtained was 4.4 mmol/g at room temperature and 1 bar. Monte et al. (2014) prepared hierarchical N-doped carbon molecular sieves from deep eutectic solvents composed of resorcinol,

hydroxypyridine, and tetraethylammonium bromide. The combination of the molecular sieve structure and nitrogen functionalization (3–9% nitrogen) resulted in a maximum CO₂ adsorption capacity of 3.7 mmol/g. A facile one-pot melt-assisted *in situ* copolymerization of resorcinol and *p*-phthalaldehyde in the presence of Pluronic F127 was developed for the synthesis of N-enriched mesoporous carbon materials (Zhang et al, 2015). The N-doped carbon material with a high surface area and N content (11 wt%) obtained by this self-pressurized solvent-free method exhibits a maximum CO₂ capture capacity of 2.73 mmol/g at 25 °C and 1 bar

However, the increase in CO₂ adsorption on N-doped carbon cannot be attributed to N-doping alone. Other factors such as micropore size distribution and the presence of ultramicropores also play an important role. Gutierrez et al. (2011) used deep eutectic solvents composed of resorcinol, 3-hydroxypyridine, and choline chloride to synthesize hierarchically structured N-doped carbon. In this study, the sample with lower N content exhibited superior CO₂ adsorption capacity because of the larger surface area associated with micropores. This result showed that the N content is not the only factor that affects CO₂ uptake in N-doped carbon.

The amount of ultramicropores also plays a very important role in promoting CO₂ adsorption. Sevilla et al. (2011) carried out a detailed analysis of the role of microporosity and N-doping in CO₂ capture of a series of N-free and N-doped microporous carbon spheres. They concluded that nitrogen functionality does not have any appreciable influence on CO₂ adsorption. Lu and coworkers (2010) prepared microporous carbon materials by polymerization of resorcinol and formaldehyde in the presence of lysine catalyst and showed that both nitrogen groups and the presence of micropores are necessary for achieving a high CO₂ capture performance. Molecular simulations were carried out by Kumar et al. (2015) to study the effect of N-doping on carbon structures of

different pore architectures for CO₂ uptake. They concluded that N-doping can only marginally improve CO₂ adsorption, and the high uptake observed in most of the reported studies might be due to the presence of ultramicropores instead of the N-doping effect or may be due to the combination of both.

Synthesis of advanced materials from naturally renewable bio-resources is of utmost importance for sustainable development. Sucrose is an economical, commercially available, and naturally renewable carbon source, and urea is a bio-molecule rich in nitrogen. However, the combination of sucrose and urea is not yet exploited for the synthesis of N-doped AC materials. This study is designed to develop an economical and simple (without hydrothermal treatment) method for the synthesis of high N-doped (6–10 wt% nitrogen) porous carbon from sucrose and urea. The N-containing polymeric materials obtained by heating sucrose and urea are activated by KOH at varying concentrations to produce the N-doped AC. The N-doped and N-free porous carbon materials thus produced were evaluated for CO₂ adsorption capacity. The effect of N-doping and microporosity of the AC materials on the CO₂ adsorption has been studied in detail.

5.2 Experimental

5.2.1 Preparation of N-containing carbon

Sucrose (AR grade) and urea (AR grade) from Merck India Pvt. Ltd were used as such. Sucrose is a disaccharide consisting of glucose and fructose connected through glycosidic linkage. The structure of sucrose is shown in Figure 5.1.

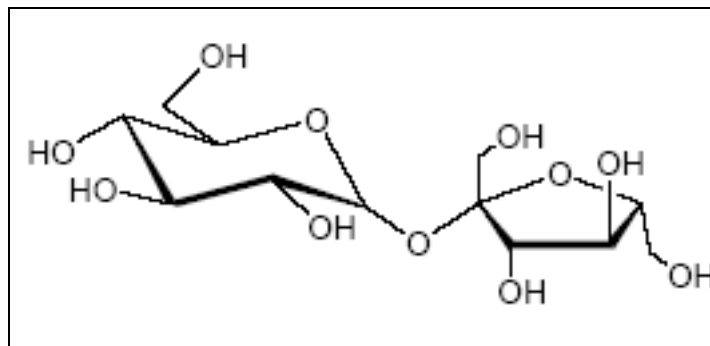


Figure 5.1 Structure of sucrose

Sucrose and urea were thoroughly mixed in various proportions using an agate and mortar. The mixture was melted in a borosilicate glass beaker at 150 °C in an air oven and stirred well with a glass rod to achieve homogeneity. The temperature of the oven was then increased to 200 °C, and this temperature was maintained until the melt becomes a brittle foamy solid polymer. The polymer was further annealed at 250 °C for 2 h for completion of the reaction and removal of volatiles. The resultant polymeric products are denoted as SU-x-250, where x represents the wt% of urea in sucrose–urea mixture. The polymeric products obtained were mixed with various amounts of KOH. Approximately 15 ml of water per 3 g of the polymer was used for proper mixing with KOH to form a paste. The paste was dried overnight at 120 °C in an air oven and heated in a platinum crucible at 650 °C for 2 h in an ultra-high pure nitrogen atmosphere in a tubular furnace. The heating rate used for activation was 2 °C/min. The same atmosphere was maintained during the cooling of the furnace. The resulting samples were washed with distilled water until KOH was completely removed. The samples were dried at 150 °C in a vacuum oven for 24 h. The carbon materials thus synthesized were designated as SU-x-y-650, where y denotes the weight ratio of KOH to SU-x-250. The composition of precursors used and nomenclature of the resulting AC are given in Table 5.1.

Table 5.1 Composition of precursors and nomenclature of the resulting AC

Sucrose (gm)	Urea (gm)	Designation of polymer	KOH to SU-x-250 ratio	Designation of N-doped AC
100	0	SU-0-250	1	SU-0-1-650
100	0		2	SU-0-2-650
100	0		3	SU-0-3-650
75	25	SU-25-250	1	SU-25-1-650
75	25		2	SU-25-2-650
75	25		3	SU-25-3-650
50	50	SU-50-250	1	SU-50-1-650
50	50		2	SU-50-2-650
50	50		3	SU-50-3-650
25	75	SU-75-250	1	SU-75-1-650
25	75		2	SU-75-2-650
25	75		3	SU-75-3-650

5.2.2 Characterization

Structure identification:

The carbon, hydrogen and nitrogen content of the prepared carbon

materials were determined using Perkin Elmer PE 2400 model CHNS elemental analyser. An exactly known weight (0.2 mg) of the sample was combusted in an atmosphere of pure and dry oxygen and the concentrations of individual components were measured as a function of their thermal conductivity. The FTIR spectra were recorded in a Perkin Elmer Spectrum GX-A FTIR spectrometer in the 4000 - 400 cm^{-1} wave number range with number of scans 16 and resolution 4 cm^{-1} . X-ray photoelectron spectroscopy (XPS) analysis was carried out with Multilab 2000 (Thermo Fisher Scientific) using Al-K α radiation.

XRD analysis: XRD analysis was carried out using Bruker D8 discover X-ray Diffraction Spectrometer, Germany with copper K α radiation. Data were digitally recorded in a continuous scan in the range of angle from 10 to 90°.

Morphology analysis: The morphology of the samples was analyzed using a field emission scanning electron microscope (FE-SEM JEOL, USA Microscope JSM 6060 operating at 20 kV). Au film was deposited on the surface of the STC samples to improve conductivity.

Microstructure analysis: Microstructure of the samples was evaluated using a transmission electron microscope (TEM, FEI, Tecnai G2 30 S-TWIN, USA) with an accelerating voltage of 300 V. The samples dispersed in acetone were drop-casted on carbon-coated copper grid and dried in vacuum at room temperature before the TEM observation.

Textural property evaluation: The porous textural properties of SU-x-y-650 were analyzed using volumetric N₂ adsorption–desorption at –196 °C using a surface area analyzer (Micromeritics Tristar II, USA). SU-x-y-650 was degassed at 300 °C for 16 h before the analysis. The specific surface area was measured from the isotherm in the relative pressure range of 0.05–0.2, according to the Brunauer–Emmett–Teller (BET) method. The pore size distribution (PSD) was

obtained from density functional theory (DFT). The Barrett–Joyner–Halenda (BJH) method was used to determine the mesopores. The micropore volume (V_m) was calculated from the t -plot. The total pore volume was estimated from the amount of N_2 adsorbed at a relative pressure of 0.99. The CO_2 adsorption capacity of SU-x-y-650 was evaluated at 0 °C and 25 °C by volumetric gas adsorption studies using the surface area analyzer. The PSD obtained by DFT calculation on CO_2 adsorption at 0 °C was analyzed for ultramicropore evaluation.

CO_2 adsorption measurements: The adsorption of CO_2 from air was studied by a gravimetric method using a thermogravimetric analyzer (PerkinElmer Pyris 1, Singapore) with the following temperature protocol. Approximately 10 mg of the adsorbent was loaded in a platinum pan of the thermogravimetric analyzer and heated at 110 °C for 10 min under an argon flow rate of 100 mL/min for desorption of adsorbed molecules. The gas flow was shifted from argon to dry air (air-dried over silica trap) containing 400 ppm of CO_2 when the sample temperature reached 25 °C. The weight gain of the sample for a period of 1 h was considered as direct CO_2 adsorption capacity.

5.3 Results and Discussion

5.3.1 Proposed reaction between sucrose and urea

The sucrose-urea mixtures form homogeneous melts on heating at temperatures nearly 150°C. These melts give brittle foamy solids on heating at 250°C for 3 hours. The urea in the melt undergoes trimerization into cyanuric acid when heated at 200°C (Chen and Isha, 1998) (Figure 5.2). The setting of the melt is due to polymerization of glucose and fructose anhydrides formed from sucrose (Figure 5.3) (Richards and Shafizadeh, 1978) and cross-linking of the resulting polymer by the cyanuric acid molecules through –OH to –OH

condensation (Figure 5.4). The foaming is due to the ammonia generated during the trimerization of urea and water vapour produced as a result of $-OH$ condensation.

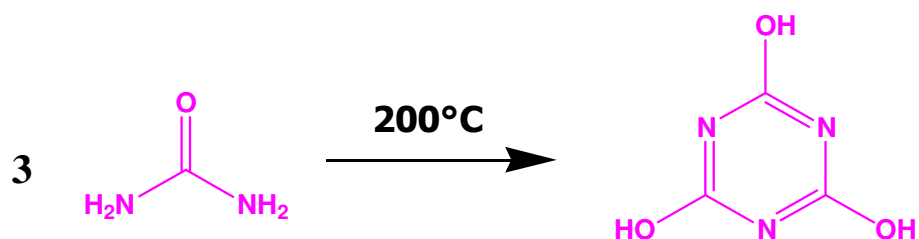


Figure 5.2 Formation of cyanuric acid by the trimerization of urea

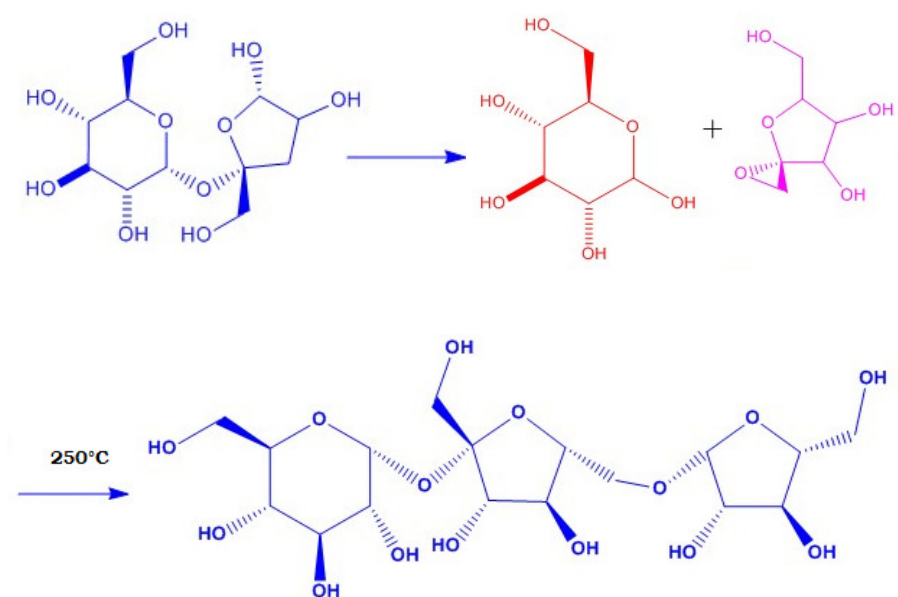


Figure 5.3 Trimerization of sucrose decomposition products

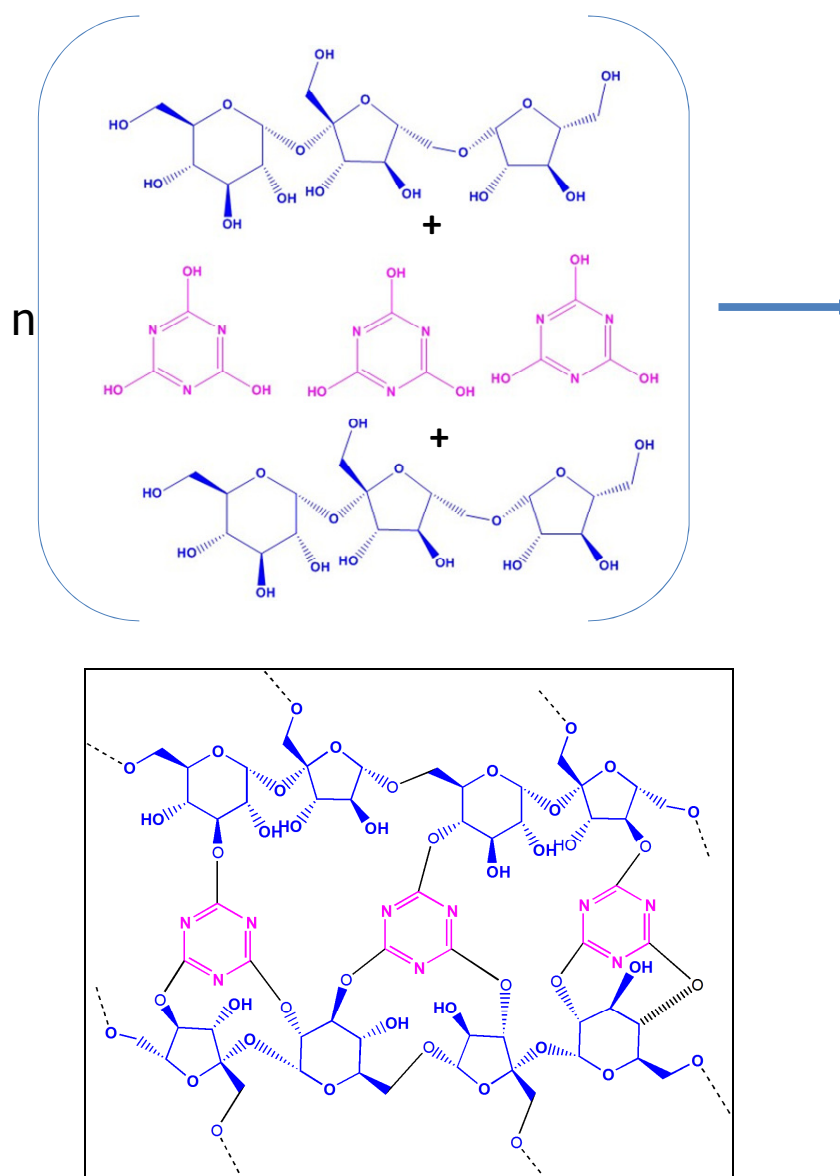


Figure 5.4 Proposed reaction and the structure of the polymeric product formed by heating sucrose and urea

5.3.2 Phase structure and morphology

XRD analysis shows the amorphous nature of the polymeric product, except SU-75-250, as shown in Figure 5.5. The sharp XRD peaks of SU-75-250

correspond to the cyanuric acid (JCPDS file No PDF 04-010-3807). It appears that in SU-25-250 and SU-50-250, the whole cyanuric acid produced from urea is incorporated in the polymeric structure, whereas in SU-75-250, the excess free cyanuric acid produces sharp peaks in the XRD spectrum because of its crystalline nature.

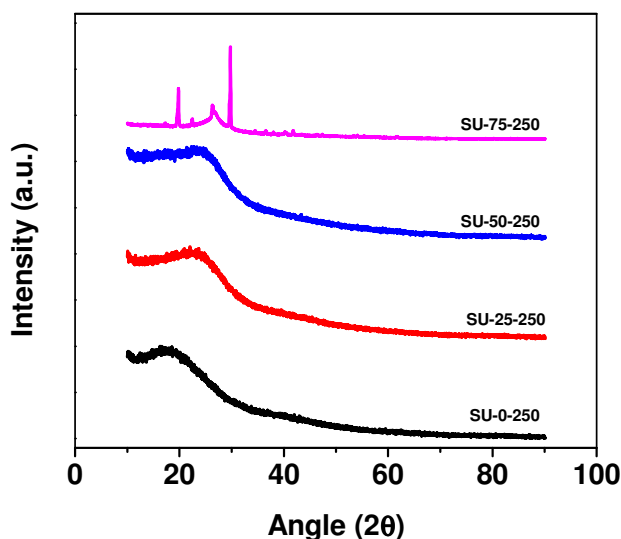


Figure 5.5 XRD pattern of SU-x-250

The IR spectrum (Figure 5.6) of SU-0-250 (polymeric product without urea) shows peaks at 776 cm^{-1} ($\text{sp}^2\text{ C-H}$ bend), 1110 cm^{-1} (-C-O stretch), 1615 cm^{-1} (alkyl C=C stretch), 1700 cm^{-1} (C=O), and 3440 cm^{-1} (-OH stretch). The C=C and C=O groups are formed by the α -elimination of water and thermal oxidation of $\text{-CH}_2\text{OH}$ in the polymeric structure produced by intermolecular condensation of glucose and fructose anhydride, respectively. SU-25-250 shows an additional peak at 1226 cm^{-1} , which can be attributed to aliphatic C-N stretching vibration. The signal at 1600 and 3426 cm^{-1} can be identified as originating from N-H in-plane deformation vibration and N-H symmetric stretching vibration and/or -OH stretching vibration, respectively. SU-50-250 has two more additional bands at 1690 cm^{-1} (C=N stretch) and 2186 cm^{-1} ($\text{C}\equiv\text{N}$). The peaks observed at frequencies in the ranges of $1535\text{--}1560\text{ cm}^{-1}$, and 784--

800 cm^{-1} in SU-75-250 are characteristic of the triazine ring (Seifer, 2002). One IR signal observed in SU-75-250 at 2830–2900 cm^{-1} was attributed to the imido group of cyanuric acid (Song et al, 2014).

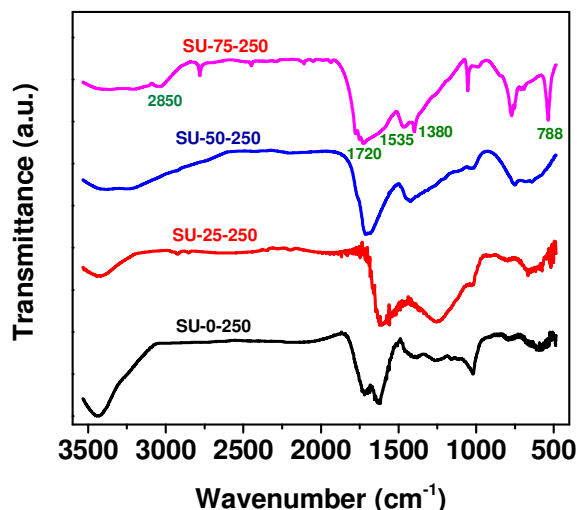


Figure 5.6 FTIR spectra of SU-x-250

The elemental analysis of the polymeric products shows an increase in the N content when the weight percentage of urea in the sucrose–urea mixture increases. The N contents of SU-25-250, SU-50-250, and SU-75-250 are 14.4, 21.2, and 28.8 wt%, respectively. The KOH activation of the polymeric product is expected to develop microporosity, retaining nitrogen in the carbon structure, which will result in increased CO_2 adsorption capacity.

The carbon materials obtained after KOH activation (SU-x-y-650) show well-developed hierarchical pore structure as evidenced from the SEM and TEM analyses. The interconnected macropores are clearly visible in the high-magnification SEM image of the AC material. In contrast, the foamy polymeric products (SU-x-250) obtained have a cellular morphology and the cell walls are dense and smooth. Figure 5.7 shows the SEM images of the polymeric product (SU-50-250) and the carbon material obtained after KOH activation. The TEM images shown in Figure 5.8 clearly indicate the presence of mesopores and

worm-like micropores in the AC materials. This hierarchical pore structure favors faster diffusion of adsorbate gases through the material and their easy access to the micropores.

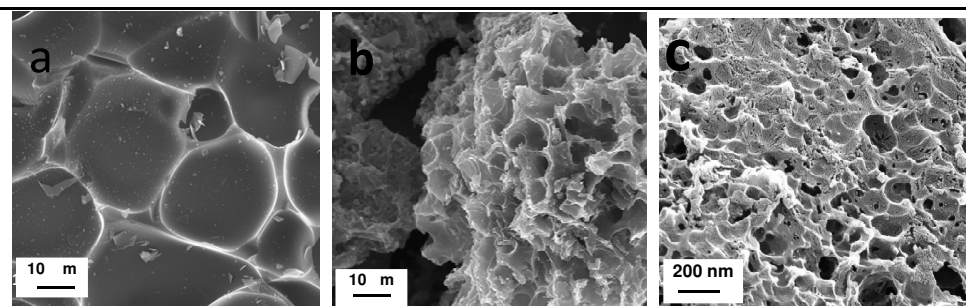


Figure 5.7 FESEM images of (a) SU-50-1-250 and (b) SU-50-1-650 at low magnification and (c) SU-50-1-650 at high magnification

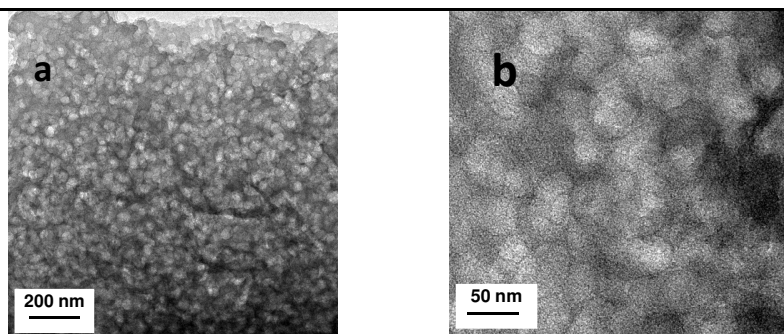


Figure 5.8 Low-magnification (a) and high-magnification (b) HR-TEM images of SU-50-1-650

Although the hierarchical pore structure is developed, KOH activation results in a decrease in N content. The N content of the prepared ACs varies from 6.0 to 10.5 wt% (Table 5.2). At a particular KOH concentration, the N content of the ACs increases with an increase in urea concentration. For example, in case of 1:1 KOH- precursor ratio, , N content increases from 7.7% (for SU-25-1-650) to 10.5% (for SU-75-1-650). At a particular weight percentage of urea, the N content of the ACs decreases with an increase in KOH concentration For example, in case of SU-50-y-650, N content decreases from 8.0% (for SU-50-1-650) to 6.1% (for SU-50-3-650). The presence of N-containing groups in the AC

is confirmed by FTIR spectroscopy. Figure 5.9 shows the FTIR spectrum of SU-x-1-650. The peak at approximately 3432 cm^{-1} is attributed to the N–H symmetric stretching vibration or –OH stretching vibration. The bands at 1644 cm^{-1} and 1282 cm^{-1} can be identified as originating from the N–H in-plane deformation vibration and C–N stretching vibration, respectively.

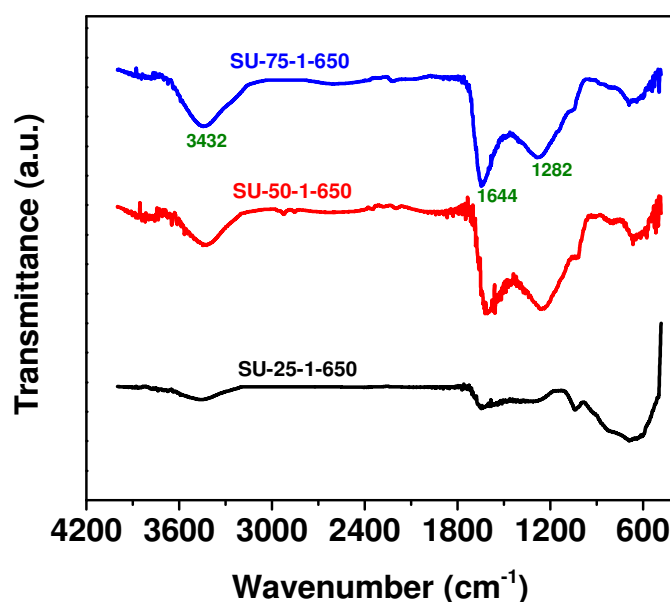


Figure 5.9 FTIR spectra of SU-x-1-650

The nature of the nitrogen moieties in SU-x-y-650 is further analyzed by XPS. Figure 5.10 shows the N 1s XPS spectrum of the representative sample, that is, SU-50-1-650. For all the samples, the XPS N 1s spectra can be deconvoluted into three peaks with binding energies centered at 398.2, 400.0, and 401.5 eV. The peak at 398.3 eV is attributed to the pyridinic-N (N-6), while the peaks at 400.0 and 401.5 eV can be attributed to pyrrolic-/pyridonic-N (N-5) and quaternary-N (N-Q), respectively. Quantitative analysis reveals that nitrogen present in the form of N-5 is more than that present in the form of N-6 and N-Q, in the order of $N-5 > N-6 > N-Q$ for all N-doped AC samples. It has been reported that the presence of nitrogen in the form of N-5 facilitates better CO_2

adsorption on AC materials than N-6 and N-Q (Pels et al, 1995; López-Salas et al, 2014). SU-50-1-650 contains 46.5% of the nitrogen in the N-5 form. This is comparable with or higher than the percentage of nitrogen in the N-5 form reported in N-doped carbons prepared from various precursors. (Chen et al, 2014; Luo et al, 2016; Yu et al, 2014)

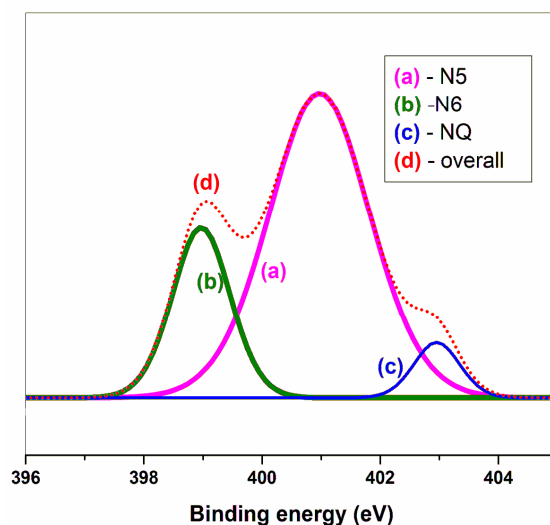


Figure 5.10 XPS spectrum of SU-50-1-650

XRD characterization of SU-x-y-650 confirms the absence of a long-range structural order for N-doped carbon. Figure 5.11 shows the XRD patterns of SU-0-1-650, SU-25-1-650, SU-50-1-650, and SU-75-1-650. Two broad diffraction peaks at around 24° and 42° are observed, corresponding to reflections from (002) and (100) & (101) planes of amorphous (turbostratic graphite) carbon. We observed a trend of slight shifting of the peak corresponding to the reflection from (002) plane to higher angles with an increase in urea concentration. This is due to the decrease in the interlayer spacing with an increase in N content of the AC (Liu et al, 2015). The interlayer spacing values calculated from the XRD data for SU-0-1-650, SU-25-1-650, SU-50-1-650, and SU-75-1-650 are 3.60, 3.50, 3.47, and 3.36 Å, respectively. It has

been reported that N-doping increases the interlayer attractive force between graphene due to the uneven distribution of charges (Canty et al, 2015). The decrease in interlayer spacing with an increase in N content is due to the increase in interlayer attractive force.

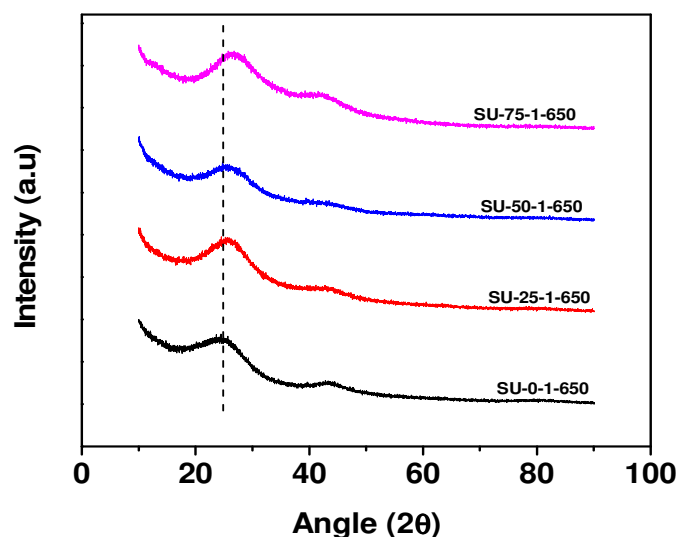


Figure 5.11 XRD pattern of SU-x-1-650

5.3.3 Textural property evaluation

The porous textures of carbon are characterized by N_2 sorption at -196°C and CO_2 sorption at 0°C . Figure 5.12 shows the N_2 adsorption/desorption isotherms of the prepared N-doped carbon. All the samples except SU-0-y-650 (without urea) exhibit type I isotherms with significant adsorption at relative pressure $P/P_0 < 0.15$. At $P/P_0 > 0.15$, the isotherm shows an almost flat sorption characteristic. The initial steep portion of the isotherm and the absence of adsorption in the P/P_0 range of 0.03–0.9 show that the porous carbon has a narrow micropore size distribution and very less mesoporosity. SU-0-3-650 shows strong hysteresis between adsorption and desorption branches, indicating a major mesoporous structure. The porous textural characterization results of the prepared carbon are given in Table 5.2.

It is evident from the results that an increase in KOH concentration is found to increase the BET surface area and total pore volume of the carbon. Carbon prepared from sucrose in the absence of urea exhibits relatively low surface area ranging from 623 to 716 m²/g and total pore volume in the range of 0.33–0.58 cm³/g. On the contrary, KOH activation of the polymer obtained by heating sucrose and urea produces N-doped carbon with high specific surface area ranging from 1745 to 2260 m²/g (for SU-25-y-650), 1413 to 2366 m²/g (for SU-50-y-650), and 634 to 1276 m²/g (for SU-75-y-650). Among the samples, SU-50-3-650 shows the highest specific surface area of 2366 m²/g. The DFT pore size distribution curves of all samples are depicted in Figure 5.12. All SU-x-y-650 samples show narrow pore size distribution (PSD) centered at approximately 10 Å. SU-25-1-650 shows the highest micropore volume and total pore volume of 0.53 cm³/g and 1.2 cm³/g, respectively.

The contribution of pyrrolic and pyridinic nitrogen to the formation of microporosity in N-doped carbon produced by the pyrolysis of MOF has been reported by Zheng et al (2014). The aggregation of graphene-like carbon with the pyrrolic and pyridinic N atoms localized at the edges generates micropores with their inner surface decorated with N atoms. They have also reported the formation of holes with length and width of 10.2 and 6 Å, respectively, in the two-dimensional graphene layers due to the presence of pyrrolic and pyridinic nitrogen. The stacking of such N-doped graphene layers in the Z-direction produces slit-like micropores. The high surface area and large micropore volume observed in SU-25-y-650 and SU-50-y-650 compared to those in SU-0-y-650 are due to the large amount of micropores formed by N-doping at the pyrrolic and pyridinic positions in addition to the micropores formed by the KOH activation. It has been reported that the reactivity of KOH with the polymer precursor decreases when the cross-linking increases (Teng and Wang, 2000). Because the cross-linking in SU-75-250 is more, its interaction with KOH is hindered, resulting in reduced porosity of SU-75-y-650.

Table 5.2 Textural properties and N content of N-doped porous carbon

Samples	S_{BET} ($\text{m}^2 \text{g}^{-1}$)	V_{p} ($\text{cm}^3 \text{g}^{-1}$)	V_{m} ($\text{cm}^3 \text{g}^{-1}$)	N content (wt%)
SU-0-1-650	624	0.34	0.22	0
SU-0-2-650	693	0.35	0.22	0
SU-0-3-650	716	0.58	0.06	0
SU-25-1-650	1745	0.90	0.53	7.7
SU-25-2-650	1995	1.1	0.48	7.5
SU-25-3-650	2260	1.1	0.42	7.4
SU-50-1-650	1413	0.73	0.44	8
SU-50-2-650	1994	0.97	0.41	6.3
SU-50-3-650	2366	1.1	0.35	6.1
SU-75-1 -650	634	0.39	0.37	10.5
SU-75-2- 650	936	0.41	0.24	8.9
SU-75-3-650	1276	0.64	0.21	6.7

V_{p} is the single-point pore volume calculated from adsorption isotherm at $P/P_0 = 0.99$; S_{BET} is the BET specific surface area obtained from the adsorption data in the P/P_0 range of 0.05–0.2; V_{m} is the total micropore volume.

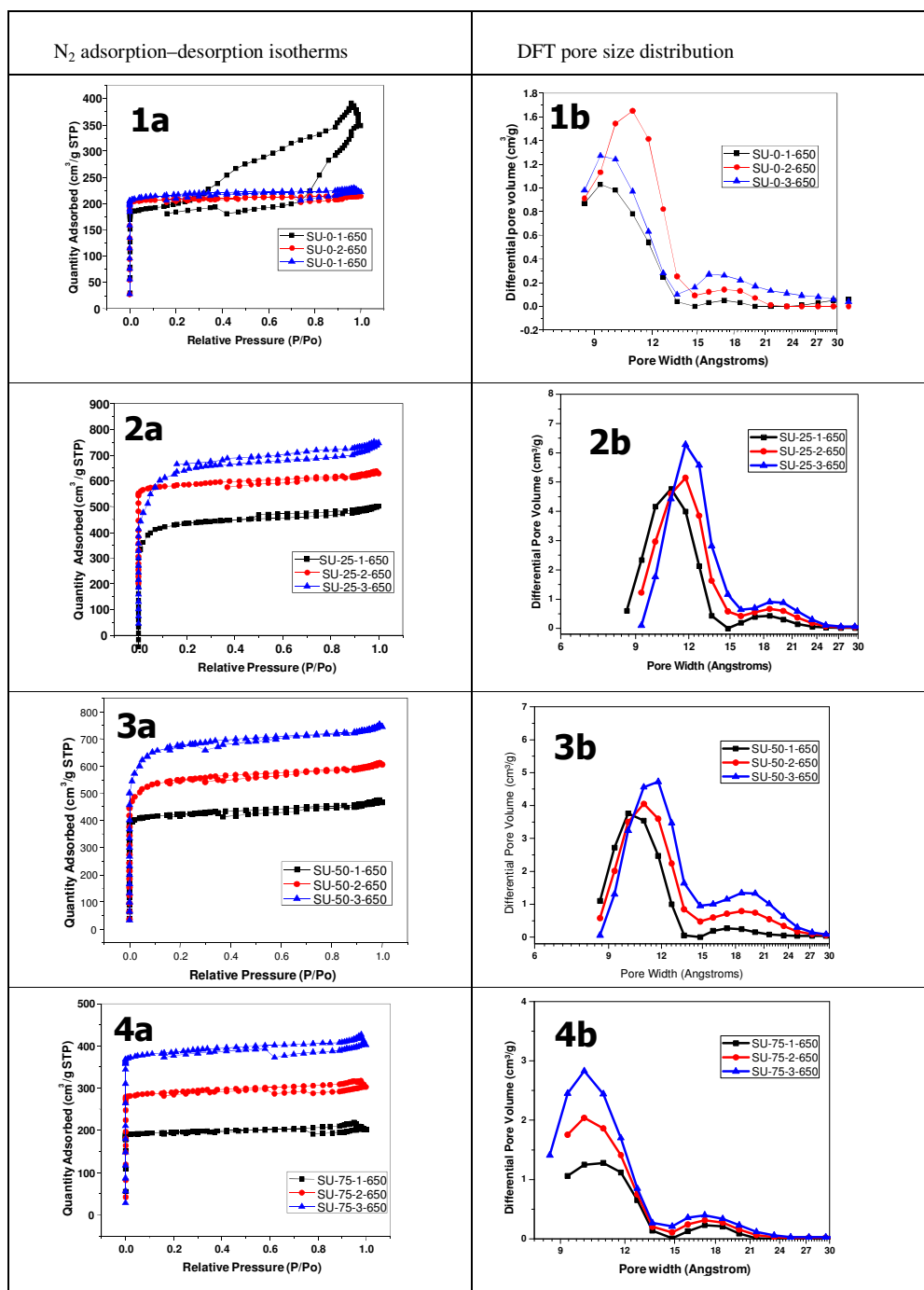


Figure 5.12 (a) N₂ adsorption–desorption isotherms and (b) DFT pore size distribution of
 (1) SU-0-y-650, (2) SU-25-y-650, (3) SU-50-y-650, and (4) SU-75-y-650

5.3.4 CO₂ adsorption evaluation

The CO₂ adsorption isotherms of the N-doped AC at 25 °C and 0 °C are shown in Figure 5.13 and Figure 5.14, respectively. Ultramicropore size distribution obtained from CO₂ adsorption at 0 °C of SU-0-y-650, SU-25-y-650, SU-50-y-650, and SU-75-y-650 are given in Figure 5.15. The CO₂ adsorption capacities of SU-x-y-650 (at 0 °C and 25 °C) and the ultramicropore volume data derived from CO₂ adsorption isotherm at 0 °C are given in Table 5.3.

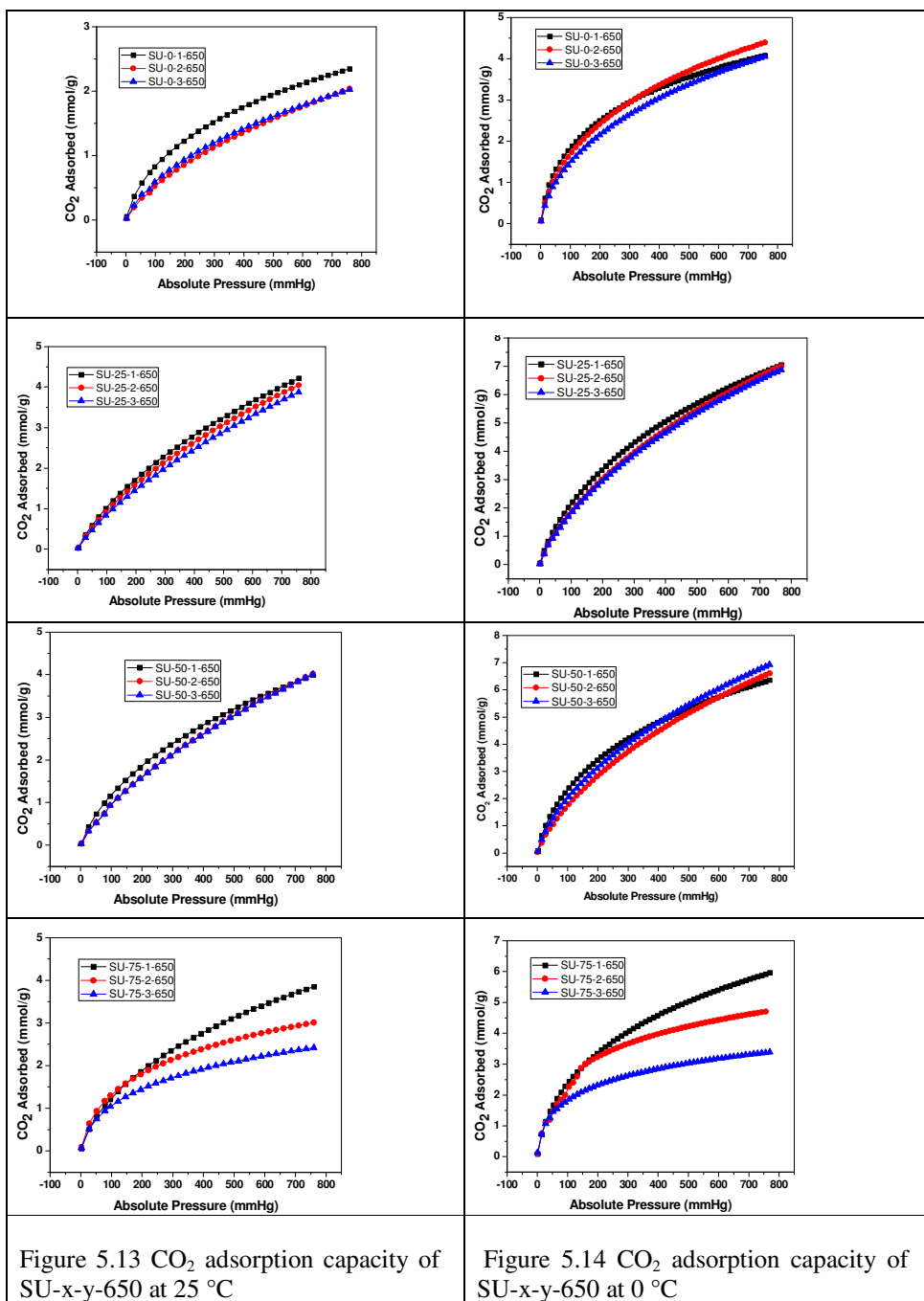
Table 5.3 CO₂ adsorption capacity and micropore volume of SU-x-y-650

<i>Samples</i>	<i>CO₂ adsorption capacity</i>		<i>Ultra micropore volume</i> <i>V₂ (cm³ g⁻¹)</i>
	<i>25 °C</i>	<i>0 °C</i>	
SU-0-1-650	2.3	4.1	0.30
SU-0-2-650	2.2	4.4	0.40
SU-0-3-650	2.0	4.1	0.42
SU-25-1-650	4.3	7.0	0.78
SU-25-2-650	4.1	7.0	0.85
SU-25-3-650	3.9	6.9	1.0
SU-50-1-650	4.0	6.3	0.56
SU-50-2-650	3.8	6.6	0.89
SU-50-3-650	3.7	6.9	1.0
SU-75-1 -650	3.8	5.9	0.20
SU-75-2- 650	3.0	4.7	0.41
SU-75-3-650	2.4	3.4	0.50

Ultramicropore analysis was carried out by CO₂ adsorption at 0 °C. All the samples show two well-defined micropore ranges, namely (I) very narrow micropores with sizes in the range of 4–7 Å and (II) micropores with sizes in the range of 7–9 Å. It may be noted that ultramicropore volume (V_2) also increases with an increasing KOH ratio, with the values ranging from 0.78 to 1.0, 0.56 to 1.0, and 0.20 to 0.50 cm³/g for SU-25-y-650, SU-50-y-650, and SU-75-y-650, respectively. The results indicate that these carbons have highly developed fine microporosity.

As reported by Lozano-Castellö et al. (2004), V_2 calculated using CO₂ adsorption at 0 °C is higher than V_m calculated using N₂ adsorption at –196 °C. This is because SU-x-y-650 contains very narrow micropores, which are not accessible at –196 °C by N₂, but are easily accessible by CO₂ at 0 °C. The ultramicropore volume obtained for SU-0-y-650 is in the range of 0.29–0.41 cm³/g. It is interesting to note that the values of V_2 obtained for SU-25-y-650 and SU-50-y-650 are much higher than that obtained for SU-0-y-650. This suggests that urea modification is an effective way to increase the porous textures of the sucrose-derived carbon, especially their fine microporosity.

SU-25-1-650 shows the highest CO₂ adsorption capacities of 4.3 and 7.0 mmol/g at 25 °C and 0 °C, respectively. This is due to the synergistic effect of the two most favorable factors of SU-25-1-650, that is, the highest microporosity (0.53 cm³/g) and high N content (7.7 wt%). SU-0-3-650 with zero nitrogen (no urea) and lowest microporosity (0.06 cm³/g) shows the lowest CO₂ adsorption capacities of 2.0 and 4.1 mmol/g at 25 °C and 0 °C, respectively.



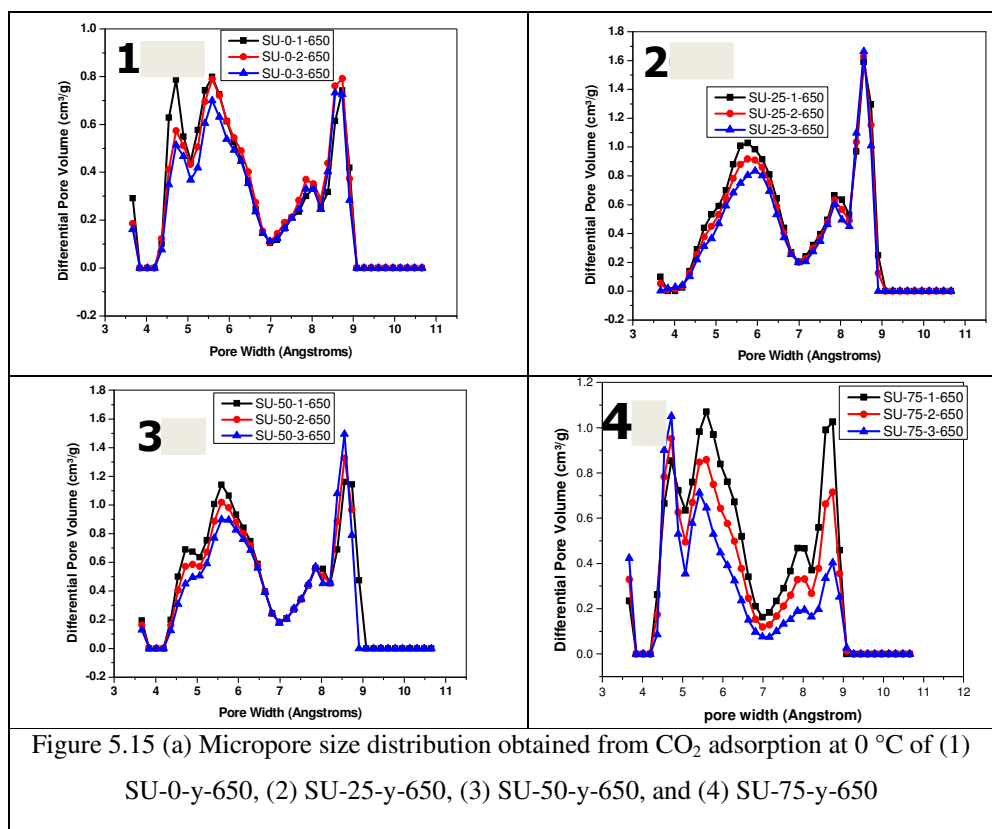


Figure 5.15 (a) Micropore size distribution obtained from CO₂ adsorption at 0 °C of (1) SU-0-y-650, (2) SU-25-y-650, (3) SU-50-y-650, and (4) SU-75-y-650

The effect of factors such as N content, micropore volume, and surface area on the CO₂ adsorption capacity of this N-doped carbon was also studied.

5.3.5 Correlation between CO₂ adsorption capacity (at 25 °C) and micropore volume

Figure 5.16 shows the correlation between CO₂ adsorption capacity of the prepared N-doped carbon and the corresponding micropore volume. Although the total pore volume increases with an increase in KOH concentration, the micropore volume shows a reverse order. As previously reported (Sevilla et al, 2012), this study also agrees with the fact that CO₂ adsorption increases with an increase in micropore volume. SU-0-3-650 with the lowest micropore volume shows the lowest CO₂ adsorption capacity, while SU-25-1-650 with the highest micropore volume shows the highest CO₂ adsorption capacity.

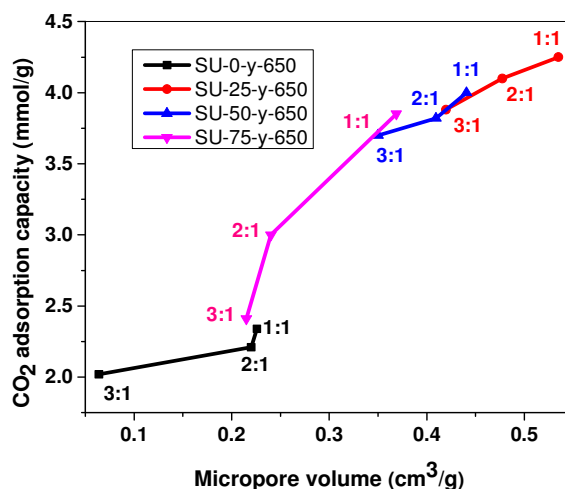


Figure 5.16 Correlation between micropore volume and CO₂ adsorption capacity. The ratios shown along with symbols indicate the ratio of KOH to SU-x-250 precursor

5.3.6 Correlation between CO₂ adsorption capacity and nitrogen content

Correlation between N content and CO₂ adsorption capacity of the prepared carbon is shown in Figure 5.17. It is evident from the CO₂ adsorption capacity values of SU-0-y-650 and SU-x-y-650 that urea modification is an effective method for increasing the CO₂ adsorption capacity of sucrose-derived AC by increasing the microporosity and N-doping. Theoretically, N-doping will improve the electron density and basicity of the carbon framework, which in turn will anchor the electron-deficient carbon of CO₂ to the micropore surface by Lewis acid–base interactions. It is evident from Figure 5.17 that within a set of N-doped AC prepared at a particular urea concentration using various amounts of KOH, the CO₂ adsorption capacity increases with an increase in N content. From this result, it can be concluded that nitrogen plays a positive role in the increase of CO₂ adsorption capacity of porous carbon. When all the prepared carbon with different pore volume / N content are compared for CO₂ adsorption, SU-75-1-650 with the highest N content shows only moderate CO₂ adsorption capacity of 3.8 mmol/g. However, it has lower textural properties of microporosity = 0.37 cm³/g and surface area = 634 m²/g, in

comparison to SU-25-1-650 (CO_2 adsorption capacity = 4.3 mmol/g) having the highest micropore volume of $0.53 \text{ cm}^3/\text{g}$ and higher surface area of $1745 \text{ m}^2/\text{g}$, but with a lower N content of 7.7 %. These results suggest that in addition to the nitrogen functional groups on the carbon surface, porous textures of the carbon also plays an important role in determining CO_2 uptake for these N-doped AC materials.

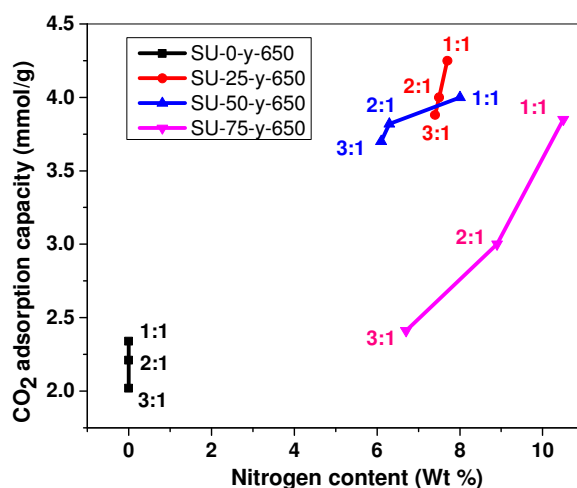


Figure 5.17 Correlation between N content and CO_2 adsorption capacity. The ratios shown along with symbols indicate the ratio of KOH to SU-x-250 precursor

5.3.7 Correlation between CO_2 adsorption capacity and surface area

Figure 5.18 shows the correlation between CO_2 adsorption capacity of the prepared N-free and N-doped AC and the corresponding surface area. The figure shows that the CO_2 adsorption capacity of the N-free and N-doped AC decreases with an increase in surface area, which is different from the expected trend. Thus, if we compare the CO_2 adsorption capacities of SU-75-1-650 (an N-doped carbon with S_{BET} of $634 \text{ m}^2/\text{g}$, V_m of $0.37 \text{ cm}^3/\text{g}$, and N-content of 10.5 wt%) and SU-0-2-650 (an N-free carbon with S_{BET} of $693 \text{ m}^2/\text{g}$, V_m of $0.22 \text{ cm}^3/\text{g}$), it can be observed that the N-doped carbon with lower surface area shows a higher CO_2 adsorption capacity (3.8 mmol/g) than the N-free carbon (2.2 mmol/g) with higher surface area. This is primarily because of the enhanced CO_2 absorption of the N-doped carbon.

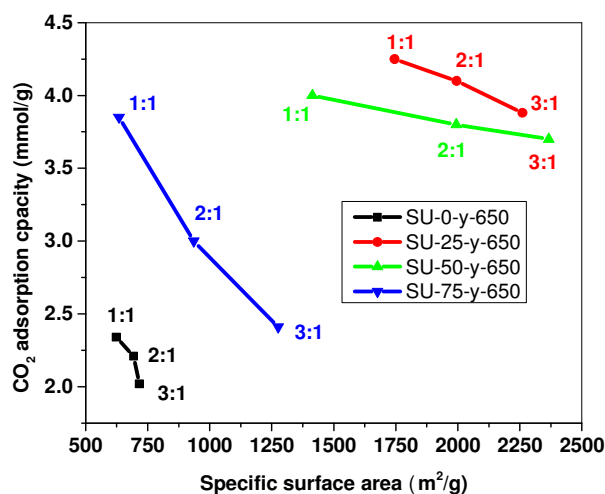
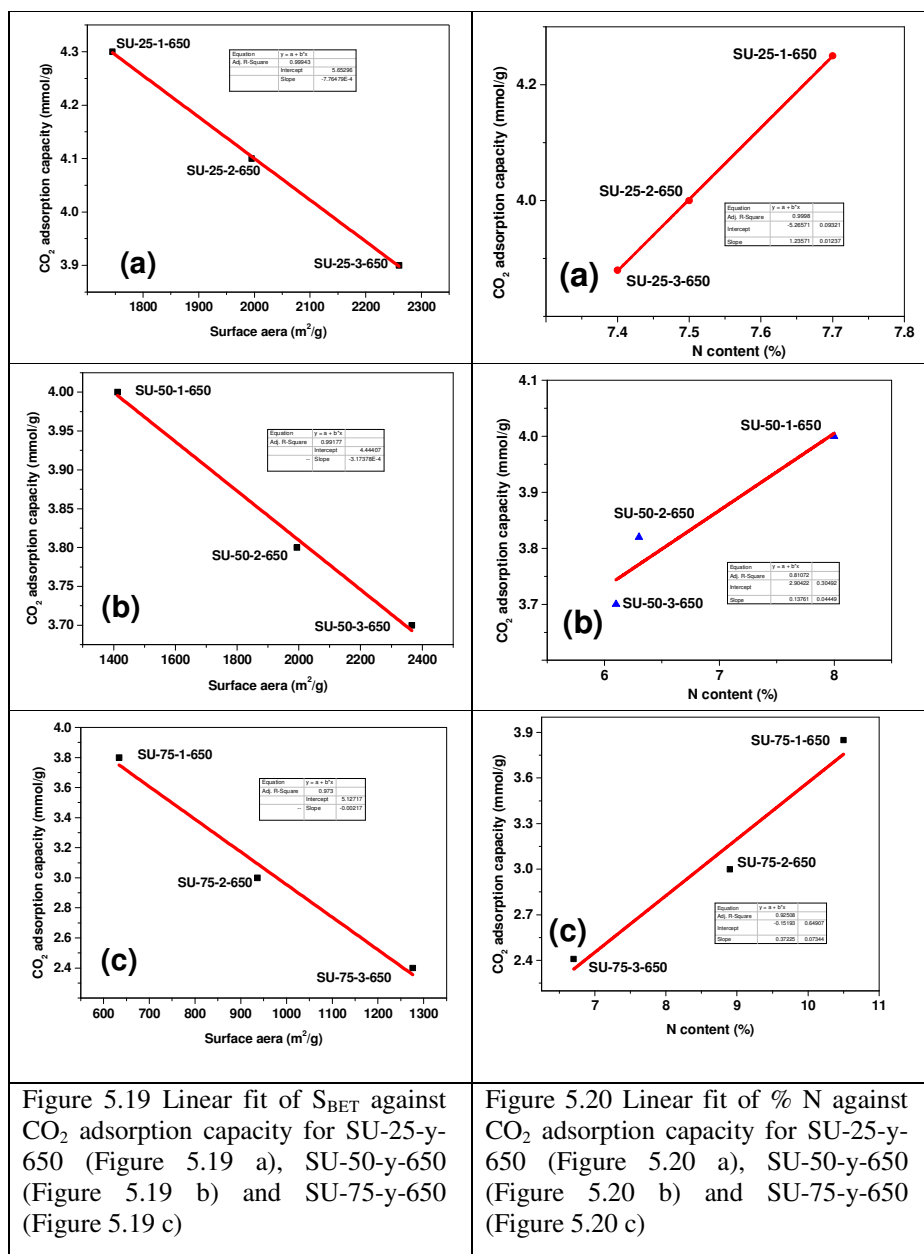


Figure 5.18 Correlation between CO₂ adsorption capacity and the corresponding surface area. The ratios shown along with symbols indicate the ratio of KOH to SU-x-250 precursor

Tables 5.2 & 5.3 show that whenever the surface area increases, the N content decreases in the case of the three N-doped porous carbon materials prepared in this study. Since CO₂ adsorption capacity depends on both N content and S_{BET} , its increase or decrease would depend on the relative role of these two properties which in the opposite direction. Thus, for SU-25-y-650, when CO₂ adsorption capacity decreases from 4.3 to 3.9 mmol/g, S_{BET} increases from 1745 to 2260 m²/g, while N content decreases from 7.7 to 7.4 %. The corresponding values for SU-50-y-650 are: CO₂ adsorption capacity = 4.0 to 3.7 mmol/g, S_{BET} = 1413 to 2366 m²/g & N content = 8.0 to 6.1 %; and for SU-75-y-650 they are: CO₂ adsorption capacity = 3.8 to 2.4 mmol/g, S_{BET} = 634 to 1276 m²/g & N content = 10.5 to 6.7%.

Though the surface area and N content are two independent properties, in order to assess the veracity of the observation of decrease in CO₂ adsorption capacity with increase in S_{BET} , it is necessary to normalize each parameter with respect to the other. The normalization is attempted by graphical interpolation of the linear fit of S_{BET} versus CO₂ adsorption capacity and N content versus CO₂ adsorption capacity of the three porous carbons from sucrose – urea mixers.

Linear fit of S_{BET} against CO_2 adsorption capacity was plotted for SU-25-y-650 (Figure 5.19 a), SU-50-y-650 (Figure 5.19 b) and SU-75-y-650 (Figure 5.19 c). Similarly, linear fit of N % against CO_2 adsorption capacity was plotted for SU-25-y-650 (Figure 5.20 a), SU-50-y-650 (Figure 5.20 b) and SU-75-y-650 (Figure 5.20 c).



For normalizing the N content with respect to S_{BET} , the amount of CO_2 adsorbed for a constant surface area of $1750 \text{ m}^2/\text{g}$ was noted from figure 5.19 (a) to (c) for the three cases of SU-x-1-650. From Figure 5.20 (a) to (c), the N content required for obtaining the CO_2 adsorption capacity so derived was computed. The normalized values of N content and the corresponding CO_2 adsorption capacity thus obtained for SU-x-1-650 are tabulated in Table 5.4.

Table 5.4 CO_2 adsorption capacity and % N normalized for a fixed surface area of $1750 \text{ m}^2/\text{g}$

Adsorbent	N (%)	CO_2 adsorption capacity (mmol/g)
SU-25-1-650	7.7 (Experimental value for S_{BET} 1750)	4.3 (Experimental value for S_{BET} 1750)
SU-50-1-650	7.1•	3.9*
SU-75-1-650	4.0•	1.3*

* Computed from linear fit plot of S_{BET} and CO_2 adsorption capacity (Figure 5.19)

• Computed from linear fit plot of % N and CO_2 adsorption capacity (Figure 5.20)

Similarly, for a fixed N content of 7.7 %, CO_2 adsorption capacity was noted from figure 5.20 (a) to (c) and from Figure 5.19 (a) to (c), S_{BET} was calculated. The results for SU-x-1-650 are tabulated in Table 5.5.

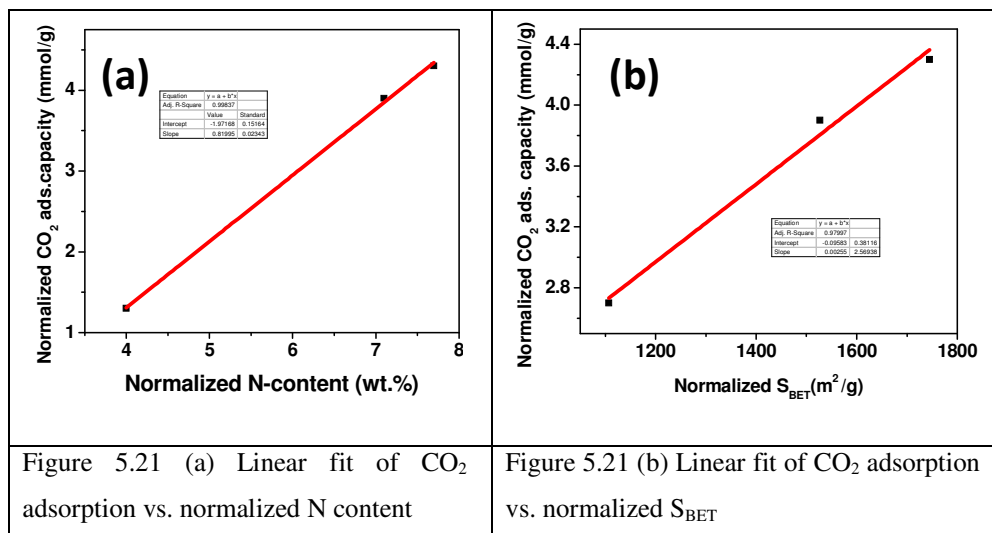
Table 5.5 CO_2 adsorption capacity and S_{BET} normalised for a fixed (7.7%) Nitrogen

	S_{BET}	CO_2 adsorption capacity (mmol/g)
SU-25-1-650	1745 (Experimental value for 7.7% N)	4.3 (Experimental value for 7.7% N)
SU-50-1-650	1527•	3.9*
SU-75-1-650	1107•	2.7*

• Computed from linear fit plot of S_{BET} and CO_2 adsorption capacity (Figure 5.19)

* Computed from linear fit plot of % N and CO_2 adsorption capacity (Figure 5.20)

The normalized results are in the expected trend of increase in the CO₂ adsorption capacity with increase in either nitrogen content (Figure 5.21 a) or surface area (Figure 5.21 b).



5.3.8 Comparison of CO₂ adsorption capacity of all adsorbents developed

Table 5.6 gives the CO₂ adsorption capacity, textural properties and % N of all the adsorbents developed in this study, which give the highest CO₂ adsorption capacity in each class [viz., aniline encapsulated β -CD, activated STC of β -CD (β -CD-STC-2.5-800), STC of cotton (Cotton-STC-2.5), carbon prepared from sucrose (SU-0-1-650) and N-doped carbon prepared from sucrose – urea mixture (SU-25-1-650)]. β -CD-aniline shows the minimum (0.70 mmol/g) and N-doped carbon prepared from sucrose-urea mixture shows the maximum (4.3 mmol/g) CO₂ adsorption capacity. The high CO₂ adsorption capacity of N-doped carbon is due to its high nitrogen content (7.7 wt.%) and micropore volume compared to the low nitrogen content (1.1 wt.%) of β -CD-aniline complex. In the case of β -CD, carbonization followed by suitable activation (which results in microporous carbon) is more advantageous than aniline encapsulation in enhancing CO₂ adsorption (CO₂ adsorption of the former is 3.7 times more than

that of the latter). Similarly, the microporous carbon prepared from sucrose – urea mixture (SU-25-1-650) has 1.9 times higher CO₂ adsorption capacity than the carbon from sucrose alone (SU-0-1-650). All the textural properties (viz., S_{BET}, V_p and V_m) of the former are higher than those of the latter and additionally it has an 7.7% N content. A combination of all these factors has resulted in SU-25-1-650 having the highest CO₂ adsorption capacity.

Table 5.6 Textural properties, % N and CO₂ adsorption capacities of all the systems

Adsorbent	S _{BET} (m ² /g)	V _p (cm ³ /g)	V _m (cm ³ /g)	N (%)	CO ₂ adsorption capacity (mmol/g)
β-CD – Aniline	-	-	-	1.1	0.70
β-CD-STC (2.5-800)	736 *(3.5 x 10 ⁻³)	0.50 (5.2)	0.25 (10.4)	-	2.6
Cotton-STC (2.5)	377 *(3.4 x 10 ⁻³)	0.27 (4.8)	0.10 (13.0)	-	1.3
Carbon from sucrose (SU-0-1-650)	624 *(3.7 x 10 ⁻³)	0.34 (6.8)	0.22 (10.5)	-	2.3
N-doped carbon from sucrose and urea (SU- 25-1-650)	1745 *(2.5 x 10 ⁻³)	0.90 (4.8)	0.53 (8.1)	7.7	4.3

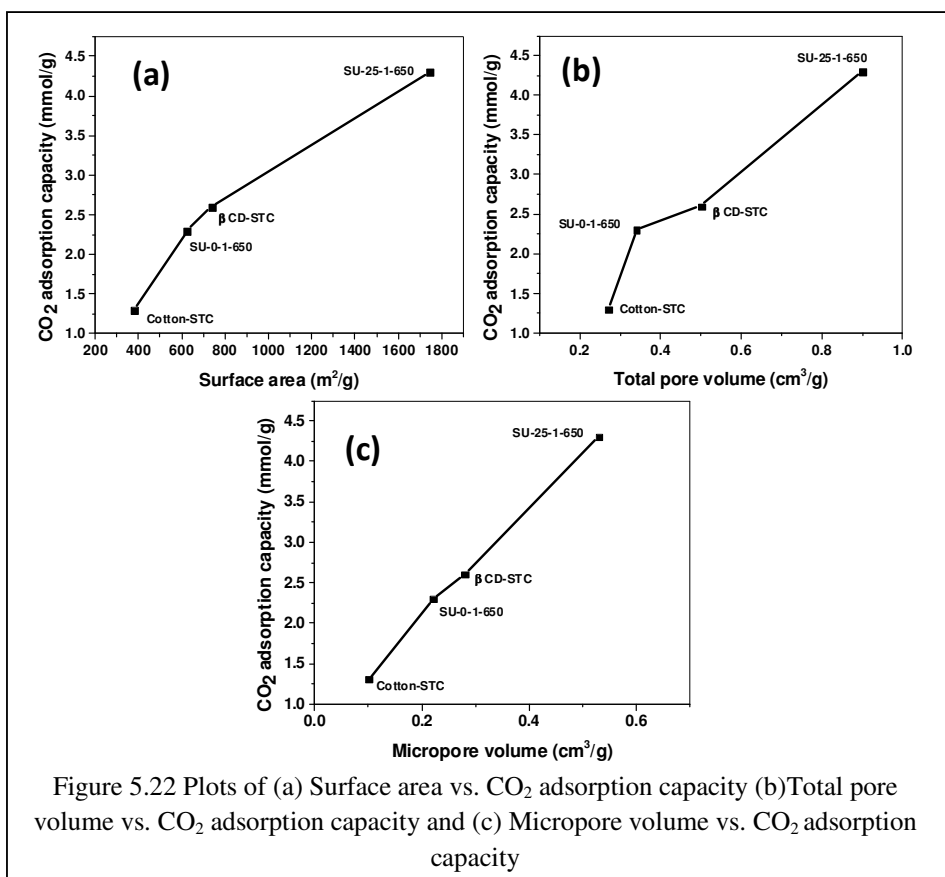
Notations: surface area (S_{BET}), total pore volume (V_p) and micropore volume (V_m)

*Values in bracket are the sensitivity of CO₂ adsorption capacity to the respective textural properties. (obtained by dividing CO₂ adsorption capacity with the value of the respective property)

Table 5.6 also shows that though CO₂ adsorption capacity of the carbon materials prepared by 4 routes is in a wide range (1.3 to 4.3 mmol/g), the differences almost disappear when normalised as sensitivity of CO₂ adsorption capacity to the respective textural property (obtained by dividing CO₂ adsorption capacity with the respective property). This clearly shows the role of the textural

properties in CO₂ adsorption capacity of the carbon materials, irrespective of their mode of preparation. It is interesting to note that the sensitivity of CO₂ adsorption of N-doped carbon from sucrose and urea (SU-25-1-650) to the three textural properties are lower than those of carbon from sucrose alone (SU-0-1-650), presumably because of the combined effect of S_{BET} + other textural properties and % N which change in opposite directions, as discussed above. However, due to the larger magnitude of the textural properties and 7.7% nitrogen content in SU-25-1-650, it has high CO₂ adsorption capacity.

Figure 5.22 (a), 5.22 (b) and 5.22 (c) are the plots of textural properties of carbon materials versus CO₂ adsorption capacity. The plots indicate that the CO₂ adsorption shows a general increasing trend with increase in all the textural properties within the range of our study, irrespective of the mode of preparation of the carbon material. Since the carbon from sucrose-urea system exhibited higher absorption of 100 % CO₂, studies were extended to CO₂ adsorption from atmospheric air using SU-25-1-650 and the results are given below:



5.3.9 CO₂ adsorption from air

Physisorbents such as AC and zeolites are expected to have low CO₂ adsorption capacity from air and low heat of adsorption, leading to shallow adsorption isotherms at very low partial pressures (Chue et al, 1995). The CO₂ adsorption characteristics of SU-25-1-650 from dry air containing approximately 400 ppm CO₂ are evaluated by TG experiments. Figure 5.23 shows the weight gain of SU-25-1-650 in dry air at 25°C as a function of time. The weight gain due to CO₂ adsorption is very fast in the initial few minutes and thereafter sluggish. The sample shows a weight gain of 2.1% in 40 min and reaches a maximum of 3.0% in 80 min. This corresponds to a total CO₂ adsorption capacity of 0.7 mmol/g. To the best of our knowledge, this is the highest reported CO₂ adsorption capacity from air by AC materials.

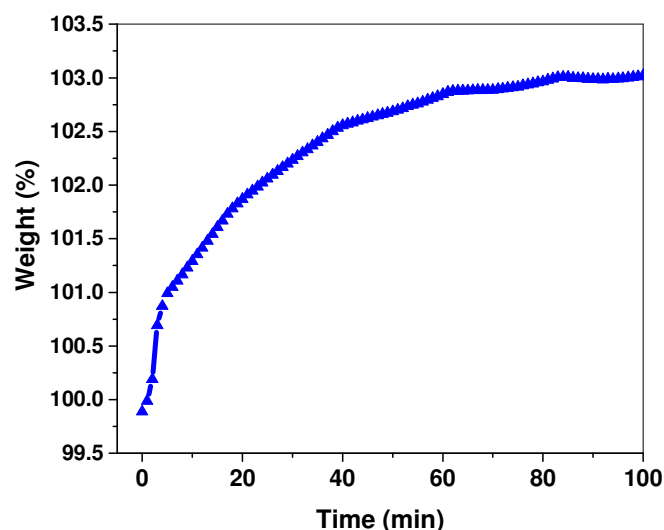


Figure 5.23 TG showing direct CO₂ capture from air at 25°C by SU-25-1-650

This CO₂ adsorption capacity is comparable with that of a number of solid amine materials (Yu et al, 2012). The adsorption half-time (time for reaching half of the adsorption capacity at saturation) and the average rate of adsorption to reach the half-maximum are used for the comparison of the reported sorbents by many researchers. Choi et al.(2011) and Abhilash et

al.(2015) compared the adsorption half-time for different adsorbents. For SU-25-1-650, the adsorption half-time of 20 min for CO₂ capture from air is better than that reported (45 minutes and more) in the case of amines on a solid support and other carbon materials. Furthermore, the rate of CO₂ capture (9 μmol/g/min) is very high and useful for practical CO₂ adsorption application from air.

5.3.10 Cyclic CO₂ adsorption capacity from air

The cyclic regeneration studies of the sorbent materials are conducted with a TG analyzer using dry ambient air. Up to 10 cycles of regeneration have been successfully shown using SU-25-1-650 without any loss in efficiency.

Figure 5.24 shows 10 consecutive regeneration cycles performed in ambient air. The recycle stability and high CO₂ adsorption capacity of this N-doped porous carbon shows that the material can be used for enhanced CO₂ removal in crew cabin of manned space vehicles, submarines, and any other closed atmosphere contaminated with CO₂. The material has additional advantages of easy bulk preparation with high yield, chemical inertness, nontoxicity, high-temperature stability, etc.

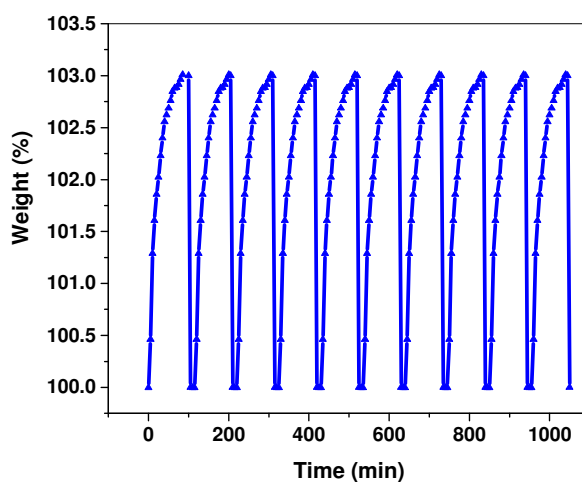


Figure 5.24 Cyclic capacity of SU-25-1-650 for direct CO₂ capture from air at 25°C

SU-x-y-650 has advantages over zeolites (Yu et al, 2012) and MOF (Hausdorf et al, 2008) materials in terms of low regeneration energy and moisture insensitiveness, respectively. It also has advantages over solid amine sorbents in terms of nontoxicity and thermal stability (Li et al, 2010).

5.3.11 Isostatic heat of adsorption (Q_{st}) evaluation

The isosteric heat of adsorption (Q_{st}) for representative N-doped carbon is calculated from the CO₂ sorption isotherms measured at 25°C and 0°C using the Clausius–Clapeyron equation (Equation 5.1):

$$Q_{st} = RT^2(\partial \ln P / \partial T)_q \quad (5.1)$$

Where P is pressure, T is temperature, q is the amount of CO₂ adsorbed, and R is the gas constant (Guo et al, 2006). Figure 5.22 shows the plot of Q_{st} versus the extent of CO₂ adsorption for SU-25-1-650. The Q_{st} for the studied carbon varies in the range of 28–34 kJ mol^{−1} at low CO₂ uptake. This value is comparable with the previously reported values for typical carbonaceous adsorbents (Bae and Snurr, 2011).

It is also found that Q_{st} decreases with an increase in CO₂ loading until a near plateau is achieved, which indicates that the binding energies of CO₂ are heterogeneous in the pores (Figure 5.24). The high initial Q_{st} values may be attributed to the strong adsorbent–adsorbate interaction between the N-containing carbon framework and CO₂ molecules, indicating that the surface chemistry of the carbon has a beneficial effect on the initial gas adsorption.

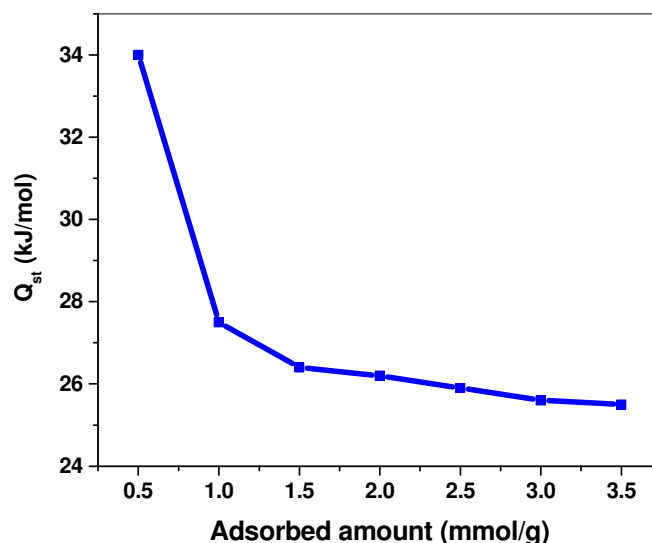


Figure 5.25 Isosteric heat of adsorption of SU-25-1-650

5.3.12 CO₂/N₂ selectivity

CO₂ has important implications for many environment-related processes, which require the separation of CO₂ from other gases (e.g., N₂) with high selectivity. The adsorption isotherms showing the selectivity of CO₂ over N₂ for SU-25-1-650 are depicted in Figure 5.26. This material adsorbs negligible amount of N₂ compared to 4.3 mmol/g of CO₂ at 25 °C and 1 bar. The selectivity of CO₂ over N₂ adsorption, calculated from the slope of the linear portion of the isotherms (Figure 5.27) as reported by Hao et al. (2011) showed the value of 39 at 25 °C. This value is comparable with the highest reported CO₂/N₂ selectivity of 46 in the category of N-doped carbon by Senker et al. (2013). For the N-free carbon SU-0-1-650, the selectivity value is 27. These results are mainly attributed to very high N-doping level in SU-25-1-650. This result proves the fact that N-doping of SU-25-1-650 is beneficial for the enhancement of CO₂/N₂ selectivity. However, further studies with CO₂-N₂ mixtures of flue gas composition are required to confirm its capability for flue gas separation.

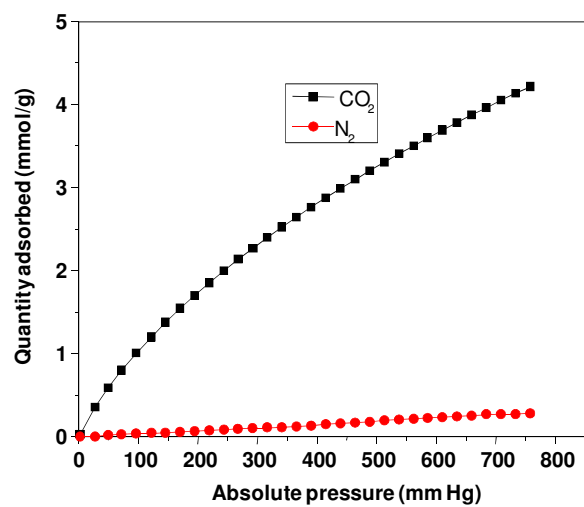


Figure 5.26 Adsorption isotherms showing the selectivity of CO₂ adsorption over N₂

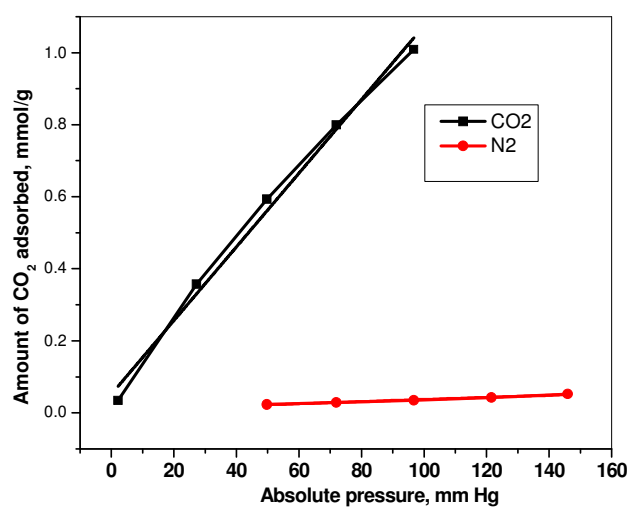


Figure 5.27 Calculation of selectivity of CO₂ adsorption over N₂ adsorption

5.4 Conclusions

Nitrogen-doped AC adsorbents having a hierarchical pore structure with high microporosity and N content were successfully synthesized with high yield by the KOH activation of the polymeric structures obtained by heating sucrose (carbon source) and urea (nitrogen source). The synergistic effect of microporosity and N-doping on CO₂ adsorption capacity of the AC is established through the investigation of the textural characteristics, N content, and CO₂ adsorption capacity of a series of N-free and N-doped AC prepared at various urea and KOH concentrations. The XPS analysis indicates the presence of pyridinic, pyrrolic, and quaternary nitrogen with the maximum amount of pyrrolic nitrogen. SU-25-1-650 with the highest microporosity of 0.50 cm³/g and a moderate N content of 7.7 wt% shows the highest CO₂ adsorption capacity of 4.3 and 7.0 mmol/g at 25 °C and 0 °C, respectively.). The synergy of textural properties and N-doping on CO₂ adsorption capacity is also evident from a comparative study of CO₂ adsorption capacity, textural properties and nitrogen content of all the four carbon materials prepared in different modes, which give the highest CO₂ adsorption capacity in each class. The CO₂ adsorption capacity (0.7 mmol/g) from air containing 400 ppm CO₂ shown by SU-25-1-650 is the highest reported for carbon-based adsorbent materials. The high direct CO₂ adsorption capacity from air, high adsorption rate, high selectivity over nitrogen, and energy-efficient and easy regeneration without the loss of adsorption capacity over large adsorption–desorption cycles make this adsorbent a suitable candidate for the removal of CO₂ from manned crew cabins in space shuttles and submarines and also a potential candidate in mitigation of global warming.

CHAPTER 6

CONCLUSIONS AND FUTURE DIRECTIONS

6.1 Conclusions

During the past few decades, much effort has been committed for the development of new CO₂ capture materials, which include liquid amines, solid sorbents etc. Liquid amines face drawbacks such as high volatility, vessel erosion and high energy consumption for regeneration. In contrast, adsorption using solid adsorbents could overcome these disadvantages and exhibits promising application for carbon capture. Porous carbons are considered as good adsorbent for CO₂ in terms of high stability, chemical inertness, low cost, low energy requirements for regeneration, and CO₂-friendly adsorption sites on the pore surface. The carbon materials prepared from various precursors show CO₂adsorption capacity in the range of 0.6-6 mmol/g at ambient temperature and 1 bar pressure. Nowadays, the foremost interest among the carbon researchers is the production of carbonaceous materials from biomass. Because of its low cost, easy availability and environmental friendship, biomass has increased demand as a raw material for CO₂ adsorbents. This thesis focuses on the development of CO₂ adsorbents from different biomass. Regenerable CO₂ capture materials were prepared using different carbohydrates as the raw materials. Three different types CO₂ capture materials were developed from biomass, viz., amine on solid support, microporous carbonaceous material, and nitrogen-doped microporous carbon. These materials were evaluated for CO₂ adsorption capacity, recycle stability, selectivity etc.

A brief review of requirement of CO₂ control and different CO₂ capture technologies is given in chapter 1. Each of the sorbents employs one of the two

possible adsorption mechanisms, either chemical adsorption or physical adsorption. Chemisorptions are driven by chemical reaction occurring at the exposed surface. The widely used chemisorbents, viz., metal oxide, metal hydroxide and amine supported solid sorbents were listed along with the CO₂ adsorption capacities achieved by each system. Physical adsorption relies on the affinity of CO₂ to the surface of a material without forming a chemical bond. The widely used physisorbents, viz., porous carbonaceous materials, zeolites, metal-organic frameworks (MOFs) etc are listed along with the CO₂ adsorption capacities achieved by each system.

Chapter 2 describes carbon dioxide adsorption on the supramolecular system of aniline encapsulated into β -cyclodextrin (β -CD) cavity. Molecular level distribution of amine on solid support is achieved. CO₂ adsorption capacity of 3.1 wt.% and high amine efficiency of 0.85 mol CO₂ / mol of nitrogen are achieved for this system at room temperature and 1 bar pressure. The mechanism of the chemisorption is through the formation of bicarbonate as confirmed by NMR and Raman spectroscopy studies. The formation of zwitterionic complex inside β -CD cavity is supported by molecular modeling studies.

Preparation of microporous carbon nanospheres from β -cyclodextrin (β -CD) by solvothermal carbonization in o-dichlorobenzene in presence of various concentrations of p-toluene sulfonic acid (PTSA) is described in chapter 3. The solvothermal carbonization was followed by high temperature activation. The highest CO₂ adsorption capacity of 2.4 mmol/g was obtained at RT and 1 bar. The contribution of non-porous graphite like carbon from the PTSA catalyst to the STC yield was established. The significance of high temperature *in situ* activation of STC towards improvement of textural properties and CO₂ adsorption capacity was established.

Chapter 4 explains the synthesis of microporous carbonaceous materials by the solvothermal carbonization of natural cotton. Morphology and surface area of solvothermal char (STC) depends on the p-toluene sulfonic acid (PTSA) concentration. STC showed maximum surface area of $477 \text{ m}^2/\text{g}$, pore volume of $0.60 \text{ cm}^3/\text{g}$ and CO_2 sorption capacity (at 25°C and 1 bar) of 1.3 mmol/g . STC-0.04 showed superhydrophobic character due to the nano projections on the fiber surface produced by heterogeneous nucleation of STC particles. STC-0.04 is an excellent sorbent for organic solvents from water-solvent mixtures.

Chapter 5 deals with the preparation of nitrogen doped activated carbon with high yield by the KOH activation of the polymeric structures obtained by heating sucrose (carbon source) and urea (N source). The effect of micro porosity and N-doping on CO_2 adsorption capacity of the activated carbon was established. Carbon with the highest micro porosity of $0.53 \text{ cm}^3/\text{g}$ and a moderate nitrogen content of 7.7 wt.% showed the highest CO_2 adsorption capacity of 4.3 mmol/g at 25 at 1 bar pressure. The CO_2 adsorption capacity of 0.7 mmol/g , from dry air containing 400 ppm CO_2 achieved was the highest reported in the category of carbonaceous materials. CO_2 adsorption capacity of all prepared carbon materials were well correlated with the microporosity.

Major findings of the work are,

- A new class of amine on solid support was realized using supramolecular guest-host system of amine encapsulated in β -cyclodextrin.
- CO_2 adsorption capacity of 0.7 mmol/g and an amine efficiency of 0.85 mol CO_2 / mol N was achieved, indicating maximum utilization of amine for CO_2 capture.

- The mechanism of CO₂ adsorption on β-CD-aniline complex was established.
- The contribution of PTSA (commonly used catalyst for solvothermal carbonization of biomass) towards solvothermal char (STC) was established for the first time.
- Microporous carbonaceous materials were developed by the solvothermal carbonization of natural cotton for the first time.
- Superhydrophobic material (solvothermal char) from cotton was realized as an efficient and safe sorbent for organic solvent removal from water
- Nitrogen doped microporous carbon materials were developed from sucrose and urea, the non-toxic precursors.
- The synergistic effect of micro porosity and N-doping on CO₂ adsorption capacity of the activated carbon was established.
- Advanced materials developed from carbohydrate exhibited CO₂ adsorption capacity ranging from 0.70 to 4.3 mmol/g at RT and 1 atmosphere pressure.
- The CO₂ adsorption capacity of 0.7 mmol/g from dry air containing 400 ppm CO₂ achieved is the highest reported in the category of carbonaceous materials, offering a great potential for CO₂ removal from air of crew cabin of manned missions and in climate engineering for mitigation of global warming.

6.2 Future Directions

Cyclodextrin based amine on solid support system has proven as a promising candidate for CO₂ removal. For demonstration of the system, simple amine, viz., aniline is immobilized in the β -CD cavity. The system achieved the maximum theoretical CO₂ adsorption capacity due to high amine efficiency. There are possibilities for further improvement in the CO₂ adsorption capacity of cyclodextrin based solid amine sorbent system, by replacing simple amine with dendrimers and amine rich polymer. Here the encapsulation of these amines can be achieved by chemically linking adamantane type of molecules to dendrimers / polymers, which best fit into the cavity of cyclodextrin. The study on the preparation of cyclodextrin – amine based CO₂ scrubber system is proposed as one of the future works.

Porous carbon prepared by the solvothermal carbonization of cotton was found as a suitable candidate for the separation of organic solvents from water. Detailed study on the separation of organic solvents / oil removal from water is required. Also, the possibility of modification of the system for improved efficiency for the removal of solvents and toxic metals from water is an area for further research.

High surface area nitrogen doped carbon was prepared from sucrose and urea for CO₂ removal application. The presence of high surface area, ultramicropore and high nitrogen content are desirable properties for the material to be utilized for electrochemical application. Study on the electrochemical properties and performance as support for cathode / anode materials for lithium ion battery and super capacitor etc. of the nitrogen doped carbon material can be done in future.

REFERENCES

1. Aaron, D. and Tsouris, C. (2005). Separation of CO₂ from flue Gas: A review. *Separation Science and Technology*, 40 (1-3): 321-348.
2. Abhilash, K. S., Deepthi, T., Sadhana, R. and Benny, K. G. (2015). Functionalized polysilsesquioxane-based hybrid silica solid amine sorbents for the regenerative removal of CO₂ from air. *ACS Applies Materials and Interfaces*, 7: 17969–17976.
3. Alabadi, A., Razzaque, S., Yang, Y., Chen, S. and Tan, B. (2015). Highly porous activated carbon materials from carbonized biomass with high CO₂ capturing capacity, *Chemical Engineering Journal*, 281 (1): 606–612.
4. Al-Degs, Y. S., Musa, I. B., Amja, H., E., Walker., G. (2008). Effect of solution pH, ionic strength, and temperature on adsorption behavior of reactive dyes on activated carbon. *Dyes and Pigments*, 77: 16-23.
5. Adeniran, B. and Mokaya, R. (2015). Low temperature synthesized carbon nanotube superstructures with superior CO₂ and hydrogen storage capacity. *Journal of Material Chemistry A*, 3: 5148-5161.
6. Amin, K., Amin, G. and Go, S. Y. (2015). High CO₂ adsorption on improved ZSM-5 zeolite porous structure modified with ethylenediamine and desorption characteristics with microwave. *Journal of Material Cycles and Waste Management*, 1-12. 10.1007/s10163-015-0436-1.
7. An, J., Geib, S. and Rosi, N. (2010). High and selective CO₂ uptake in a cobalt adeninate metalorganic framework exhibiting pyrimidine- and amino-decorated pores. *Journal of the American Chemistry Society*, 132: 38-39.
8. Auta, M. and Hameed, B. H. (2011). Preparation of waste tea activated carbon using potassium acetate as an activating agent for adsorption of Acid Blue 25 dye. *Chemical Engineering Journal*, 171: 502– 509.
9. Azimi, G., Dhiman, R., Kwon, H., Paxson, A. T. and Varanasi, K. K. (2013). Hydrophobicity of rare-earth oxide ceramics. *Nature Materials*, 12: 315-320.
10. Babarao, R. and Jiang, J. (2008). Exceptionally high CO₂ storage in covalent-organic frameworks: Atomistic simulation study. *Energy and Environmental Science*, 1: 139–143.
11. Bagreev, A. and Bandosz, T. (2004). Efficient hydrogen sulfide adsorbents obtained by pyrolysis of sewage sludge derived fertilizer modified with spent mineral oil. *Environmental Science and Technology*, 38: 345–351.

12. Bae, Y. S. and Snurr, R. Q. (2011). Development and evaluation of porous materials for carbon dioxide separation and capture. *Angewandte Chemie International Edition*, 50: 11586–11596.
13. Bai, R., Yang, M., Hu, G., Xu, L., Hu, X., Wang, S., Dai, W., Fan, M. and Li, Z. (2015). A new nanoporous nitrogen-doped highly-efficient carbonaceous CO₂ sorbent synthesized with inexpensive urea and petroleum coke. *Carbon*, 81: 465–467.
14. Babarao, R. and Jiang, J. W. (2009). Upgrade of natural gas in rho zeolite-like metal-organic framework and effect of water: a computational study, *Energy & Environmental Science*, 2: 1088-1093.
15. Balsamo, M., Budinova, T., Erto, A., Lancia, A., Petrova, B., Petrov, N. and Tsyntsarski, B. (2013). CO₂ adsorption onto synthetic activated carbon: Kinetic, thermodynamic and regeneration studies. *Separation and Purification Technology*. 116 (1): 214–221.
16. Banisheykholeslami, F., Ghoreyshi, A. A., Mohammadi, M., Pirzadeh, K. (2015). Synthesis of a carbon molecular sieve from broom corn stalk via carbon deposition of methane for the selective separation of a CO₂/CH₄ mixture. *CLEAN – Soil, Air, Water*, 43 (7): 1084-1092.
17. Bao, Z., Yu, L., Ren, Q., Lu, X. and Deng, S. (2011). Adsorption of CO₂ and CH₄ on a magnesium based Metal organic framework. *Journal of Colloid Interface Science*. 353 (2): 549-56.
18. Bender, M. L. and Komiyama, M. (1978). *Cyclodextrin Chemistry*, Springer-Verlag: New York.
19. Beruto, D., Botter, R. and Searcy, A. W. (1987). Thermodynamics of two, two-dimensional phases formed by carbon dioxide chemisorption on magnesium oxide. *Journal of Physical Chemistry*, 91 (13): 3578-3581.
20. Bezerra, D. P., Oliveira, R. S., Vieira, R. S., Cavalcante Jr., C. L. and Azevedo, D. C. S. (2011). Adsorption of CO₂ on nitrogen-enriched activated carbon and zeolite 13X. *Adsorption*, 17 (1): 235–246.
21. Bi, H., Yin, Z., Ca, X., Xie, X., Tan, C., Huang, X., Chen, B., Chen, F., Yang, Q., Bu, X., Lu, X., Sun, L. and Zhang, H. (2013). Carbon fiber aerogel made from raw cotton: a novel, efficient and recyclable sorbent for oils and organic solvents. *Advanced Materials*, 25: 5916–5921.
22. Bonenfant, D., Kharoune, M., Niquette, P., Mimeault, M. and Hausler, R. (2008). Advances in principal factors influencing carbon dioxide adsorption on zeolites, *Science and Technology of Advanced Materials*, 9 (1): 13007- 13014.

23. Boryta, D. A. and Maas A. J. (1971). Factors Influencing Rate of Carbon Dioxide Reaction with Lithium Hydroxide, *Industrial and Engineering Chemistry Process Design and Development*, 10 (4): 489-94.
24. Bourrelly, S., Llewellyn, P. L., Serre, C., Millange, F., Loiseau, T. and Ferey, G. (2005). Different adsorption behaviors of methane and carbon dioxide in the isotypic nanoporous metal terephthalates MIL-53 and MIL-47. *Journal of American Chemical Society*, 127 (39): 13519-13521.
25. Brunauer, S. (1943). *The Adsorption of Gases and Vapors. Vol. I, Physical Adsorption*. Princeton University Press: USA.
26. Brunauer, S., Emmett, P. H. and Teller, E. (1938). Adsorption of Gases in Multimolecular Layers. *Journal of American Chemical Society*, 60: 309-319.
27. Burchell, T. D., Judkins, R. R., Rogers, M. M. and Williams, A. M. (1997). A novel process and material for the separation of carbon dioxide and hydrogen sulfide gas mixtures. *Carbon*, 35 (9): 1279–1294.
28. Caplow, M. (1968). Kinetics of carbamate formation and breakdown. *Journal of American Chemical Society*, 90 (24): 6795-6803.
29. Canty, R., Gonzalez, E., MacDonald, C., Osswald, S., Zea, H., Luhrs, C. C. (2015). Reduction expansion synthesis as strategy to control nitrogen doping level and surface area in graphene. *Materials*, 8: 7048–7058.
30. Carrasco-Marin, F., Lopez-Ramon, M. V. and Moreno-Castilla, C. (1993). Applicability of the Dubinin-Radushkevich equation to carbon dioxide adsorption on activated carbons. *Langmuir*, 9 (11): 2758–2760.
31. Chaffee, A. L., Knowles, G. P., Liang, Z., Zhang, J., Xiao, P. and Webley, P. A. (2007). CO₂ capture by adsorption: materials and process development: *International Journal of Greenhouse Gas Control*, 1(1): 11–18.
32. Chaikittisilp, W., Khunsupat, R., Chen, T. T. and Jones, C. W. (2011). Poly(allylamine)–mesoporous silica composite materials for CO₂ capture from simulated flue gas or ambient air. *Industrial Engineering and Chemistry Research*, 50: 14203–14210.
33. Chandra, V., Yu, S. U., Kim, S. H., Yoon, Y. S., Kim, D. Y., Kwon, A. H., Meyyappan, M. and Kim, K. S. (2012). Highly selective CO₂ capture on N doped carbon produced by chemical activation of polypyrrole functionalized graphene sheets. *Chemical communications*, 48(5): 735–737.
34. Chen, C., Kim, J. and Ahn, W. S. (2012). Efficient carbon dioxide capture

over a nitrogen-rich carbon having a hierarchical micro-mesopore structure. *Fuel*, 95(1): 360–364.

35. Chen, J. P. and Isa, K. (1998). Thermal decomposition of urea and urea derivatives by simultaneous TG/(DTA)/MS. *Journal of Mass Spectroscopy Society of Japan*, 46: 299-303.
36. Chen, L-C., Peng, P-Y., Lin, L-F., Yang, T. C. K. and Huang, C-M. (2014). Facile preparation of nitrogen-doped activated carbon for carbon dioxide adsorption. *Aerosol and Air Quality Research*, 14: 916–927.
37. Choi, S., Drese, J. H. and Jones, C. W. (2009). Adsorbent materials for carbon dioxide capture from large anthropogenic point sources, *ChemSusChem*, 2(9): 796 – 854.
38. Chiu, K. L. and Dickon, H. L. (2014). Novel activated cotton as eco-adsorbent for solvent vapor. *Microporous and Mesoporous Materials*, 196: 122–128.
39. Choi, S., Drese, J. H., Eisenberger, P. M. and Jones, C. W. (2011). Application of amine-tethered solid sorbents for direct CO₂ capture from the ambient air, *Environmental Science and Technology*, 45: 2420-2427.
40. Chou, C-T, (2013). Carbon dioxide separation and capture for global warming mitigation. *Journal of Advancement in Engineering and Technology*, 1(1): 2348-2931.
41. Chue, K. T., Kim, J. N., Yoo, Y. J. and Cho, S. H. (1995). Comparison of activated carbon and zeolite 13X for CO₂ recovery from flue gas by pressure swing adsorption. *Industrial Engineering and Chemistry Research*, 34(2): 591–598.
42. Cinke, M., Li, J., Bauschlicher, C. W., Ricca, A. and Meyyappan, M. (2003). CO₂ adsorption in single-walled carbon nanotubes. *Chemistry Physics Letters*, 376 (5-6): 761–766.
43. Cook, A. E. (1972). Gas absorption with a first order chemical reaction and large heat effect. *Chemical Engineering Science*, 27(3): 605–613.
44. Coromina, H. M., Walsh, D. A. and Mokaya, R. (2016). Biomass-derived activated carbon with simultaneously enhanced CO₂ uptake for both pre and post combustion capture applications. *Journal of Materials Chemistry A*, 4: 280–289.
45. Cui, S., Cheng, W., Shen, X., Fan, M., Russell, A., Wuab, Z. and Yiab, X. (2011). Mesoporous amine-modified SiO₂ aerogel: a potential CO₂ sorbent. *Energy and Environmental Science*, 4: 2070–2074.

46. Cyril, S. U. and Alper, E. (2012). Reaction kinetics of carbon dioxide with 2-amino-2-hydroxymethyl-1,3-propanediol in aqueous solution obtained from the stopped flow method. *Turkish Journal of Chemistry*, 36: 427–435.
47. Dabrowski, A. (2001). Adsorption- from theory to practice. *Advances in Colloid and Interface Science*, 93: 135-224.
48. Das, A., Southon, P. D., Kepert, C. J., Harris, A. T. and D'Alessandro, D. M. (2012). Carbon dioxide adsorption by physisorption and chemisorptions interactions in piperazine-grafted Ni₂(dobdc) (dobdc = 1,4-dioxido-2,5-benzenedicarboxylate). *Dalton Transactions*, 41: 11739–11744.
49. Davis, A. R. and Oliver, B. G. J. (1972). A vibrational-spectroscopic study of the species present in the CO₂–H₂O system. *Solution Chemistry*, 1: 329–339.
50. Deanna, M. D., Smit, B. and Jeffrey, R. L. (2010) Carbon dioxide capture: prospects for new materials. *Angewandte Chemie International Edition*. 49 (35): 6058–6082.
51. Demarco, P. V. and Thakkar, A. L. (1970). Structure elucidation of benzhexol-β-cyclodextrin complex in aqueous medium by 1h nmr spectroscopic and computational methods , *Journal of Chemical Society D*, 1: 2-4.
52. Diaz, E., Munoz, E., Vega, A., and Ordonez, S. (2008). Enhancement of the CO₂ retention capacity of Y Zeolites by Na and Cs treatments: effect of adsorption temperature and water treatment. *Industrial and Engineering Chemistry Research*, 47 (2): 412-418.
53. Djilani, C., Rachida, Z., Ali, M., Marek, R., Djazia, F. and Abdelaziz, L. (2012). Elimination of organic micropollutants by adsorption on activated carbon prepared from agricultural waste. *Chemical Engineering Journal*, 189: 203– 212.
54. Dobeles, G., Dizhbite, T., Gil, M. V., Volperts, A. and Centeno, T. A. (2012). Production of nanoporous carbons from wood processing wastes and their use in supercapacitors and CO₂ capture. *Biomass Bioenergy*, 46: 145- 157.
55. Donaldson, T. L. and Nguyen, Y. N. (1980). CO₂ reaction kinetics and transport in aqueous amine membranes. *Industrial Engineering Chemistry Fundamentals*, 19 (2): 260-266.
56. Ello, A., Yapo, J. A., and Trokourey, A. (2013). N-doped carbon aerogels for carbon dioxide capture. *African Journal of Pure and Applied*

Chemistry, 7(2): 61-66.

57. Fauth, D. J., Gray, M. L., Pennline, H. W., Krutka, H. M., Sjoström, S. and Ault, A. M. (2012)/ Investigation of porous silica supported mixed-amine sorbents for post-combustion CO₂ capture. *Energy & Fuels*, 26: 2483–2496.
58. Feinle, A., Elsaesser, M. S. and Hüsing, N. (2016). Sol–gel synthesis of monolithic materials with hierarchical porosity. *Chemical Society Review*, 45: 3377-3399.
59. Feng, B., An, H. and Tan, E. (2007). Screening of CO₂ Adsorbing Materials for Zero Emission Power Generation Systems. *Energy & Fuels*, 21 (2): 426-434.
60. Feng, X., Feng, L., Jin, M., Zhai, J., Jiang, L. and Zhu, D. (2004). Reversible Super-hydrophobicity to Super-hydrophilicity Transition of Aligned ZnO Nanorod Films. *Journal of American Chemical Society*, 126: 62-63.
61. Finn, J. E. (2005). Air Quality Systems for Related Enclosed Spaces: Spacecraft Air. *The Handbook of Environmental Chemistry*, Vol. 4: 383–404.
62. Foley, H. C. (1995). Carbogenic molecular sieves: synthesis, properties and applications. *Microporous Materials*, 4 (6): 407–433.
63. Frisch, M. J. et al. (2010). Gaussian09, Rev. B.01, Gaussian, Inc., Wallingford CT.
64. Furukawa, H., Ko, N., Go, Y. B., Aratani, N., Choi, S. B., Choi, E., Yazaydin, A. O., Snurr, R. Q., O’Keeffe, M., Kim, J. and Yaghi, O. M. (2010). Ultrahigh porosity in metal-organic frameworks. *Science*, 329: 424–428.
65. Gadipelli, S., Patel, H. A., Guo, Z. (2015). An ultrahigh pore volume drives up the amine stability and cyclic CO₂ capacity of a solid amine@carbon sorbent. *Advanced Materials* 27: 4903-4909.
66. Gassensmith, J. J. Furukawa, H., Smaldone, R. A., Forgan, R. S., Botros, Y. Y., Yaghi, O. M. and Stoddart, J. F. (2011). Strong and reversible binding of carbon dioxide in a green metal–organic framework. *Journal of American Chemical Society*, 133: 15312–15315.
67. Gebald, C., Wurzbacher, J. A., Tingaut, P., Zimmermann, T. and Steinfeld, A. (2011). Amine-based nanofibrillated cellulose as adsorbent for CO₂ capture from air. *Environmental Science and Technology*, 45(20): 9101–9108.

68. Grasa, G., González, B., Alonso, M. and Abanades, J. C. (2007). Comparison of CaO-based synthetic CO₂ sorbents under realistic calcinations conditions. *Energy & Fuels*, 21(6): 3560–3562.
69. Greg, S. J. and Sing, K. S. (1982). *Adsorption, Surface area and Porosity*, Academic press, London.
70. Grigoras, M. and Conduruta, D. G. (2006). Chemical Oxidative Polymerization of β -Cyclodextrin/Aniline Inclusion Complex. *Journal of Inclusion Phenomenon and Macrocyclic Chemistry*, 54: 101–107.
71. Guais, A., Brand, G., Jacquot, L., Karrer, M., Dukan, S., Grevillot, G., Molina, T. J., Bonte, J., Regnier, M. and Schwartz, L. (2011). Toxicity of carbon dioxide: A review. *Chemical Research in Toxicology*, 24 (12): 2061–2070.
72. Guerrero, R. S., Da'na, E. and Sayari, A. (2008). One-part geopolymer mixes from geothermal silica and sodium aluminate. *Industrial Engineering and Chemistry Research*, 47: 9406–9412.
73. Guo, B., Chang, L. and Xie, K. (2006). Adsorption of carbon dioxide on activated carbon. *Journal of Natural Gas Chemistry*, 15: 223–229.
74. Gutierrez, M. C., Carriazo, D., Ania, C. O., Parra, J. B., Ferrer, M. L. and del Monte, F. (2011). Rapid synthesis of nitrogen-doped porous carbon monolith for CO₂ capture. *Energy and Environmental Science*, 4: 3535–3544.
75. Hadaruga, D. I., Hadaruga, N. G., Bandur, G. N. and Isengard, H. D. (2012). Water content of flavonoid/cyclodextrin nanoparticles: Relationship with the structural descriptors of biologically active compounds. *Food Chemistry*, 132: 1651–1659.
76. Hao, G., Li, W., Qian, D., Wang, G., Zhang, W., Zhang, T., Wang, A., Schüth, F., Bongard, H. and Lu, A. (2011). Structurally designed synthesis of mechanically stable poly(benzoxazine-co-resol)-based porous carbon monoliths and their application as high-performance CO₂ capture sorbents. *Journal of American Chemical Society*, 133: 11378–11388.
77. Hao, G. P., Li, W. C., Qian, D. and Lu, A. H. (2010). Rapid synthesis of nitrogen-doped porous carbon monolith for CO₂ capture. *Advanced Materials*, 22: 853–857.
78. Hadaruga, D. I., Hadaruga, N. G., Bandur, G. N. and Isengard, H. D. (2012). Water content of flavonoid/cyclodextrin nanoparticles: Relationship with the structural descriptors of biologically active compounds. *Food Chemistry*, 132: 1651–1659.

79. Harlick, P. J. E. and Tezel, F. H. (1998). Adsorption of carbon dioxide, methane and nitrogen: pure and binary mixture adsorption for ZSM-5 with SiO₂/Al₂O₃ ratio of 280. *Separation and Purification Technology*, 33 (2): 199-210.
80. Harlick, P. J. E. and Tezel, F. H. (2004). An experimental adsorbent screening study for CO₂ removal from N₂. *Microporous and Mesoporous Materials*, 76 (1): 71–79.
81. Hausdorf, S., Wagler, J. and Mossig, R. (2008). Synthesis and mechanism of particle- and flower-shaped ZnSe nanocrystals: Green chemical approaches toward Green Nanoproducts. *Journal of Physical Chemistry A*, 112: 7567–7576.
82. Hayashi, H., Taniuchi, J., Furuyashiki, N., Sugiyama, S., Hirano, S., Shigemoto, N. and Nonaka, T. (1998). Efficient recovery of carbon dioxide from flue gases of coal-fired power plants by cyclic fixed-bed operations over K₂CO₃-on-carbon. *Industrial and Engineering Chemistry Research*, 37(1): 185–191.
83. Hermann, W., Bosshard, P., Hung, E., Hunt, R. and Simon, A. J. (2005). An assessment of carbon capture technology and research opportunities, *Technical Assessment Report, Global Climate & Energy Project*, Stanford University, California.
84. Hicks, J. C., Drese, J. H., Fauth, D. J., Gray, M. L., Qi, G. and Jones, C. W. (2008). Designing adsorbents for CO₂ capture from flue gas: Hyperbranched aminosilicas capable of capturing CO₂ reversibly. *Journal of American Chemical Society*, 130 (10): 2902–2903.
85. Hiyoshi, N., Yogo, K. and Yashima, T. (2005) Adsorption of carbon dioxide on aminosilane-modified mesoporous silica. *Journal of the Japan Petroleum Institute*, 48(1): 29-36.
86. Ho, Y. S. (2006). Review of second-order models for adsorption systems. *Journal of Hazardous Materials*, 136: 681–689.
87. Hong, S. M., Kim, S. H. and Lee, K. B. (2013). Adsorption of carbondioxide on 3-aminopropyl-triethoxysilane modified graphite oxide. *Energy & Fuels*, 27(6): 3358–3363.
88. Hu, B., Yu, S. H., Wang, K., Liu, L. and Xu, X. (2008). Functional carbonaceous materials from hydrothermal carbonization of biomass: an effective chemical process. *Dalton Transaction*, 40: 5414–5423.
89. Hu, B. B., Wang, K., Wu, L., Yu, S. H., Antonietti, M. and Titirici, M. M. (2010). engineering carbon materials from the hydrothermal

carbonization process of biomass. *Advanced Materials*, 22: 813–828.

90. Hu, X., Radosz, M., Cychosz, K. A. and Thommes, M. (2011). CO₂-filling capacity and selectivity of carbon nanopores: synthesis, texture, and pore size distribution from quenched-solid density functional theory. *Environmental Science & Technology*, 45(16): 7068–7074.
91. Huang, L., Zhang, L., Shao, Q., Lu, L., Lu, X., Jiang, S. and Shen, W. (2007). Simulations of binary mixture adsorption of carbon dioxide and methane in carbon nanotubes: Temperature, pressure, and pore size effects. *Journal of Physical Chemistry C*, 111: 11912–11920.
92. Huesca, R., Diaz, L., and Aguilar-Armenta, G. (1999). Adsorption equilibria and kinetics of CO₂, CH₄, and N₂ in natural zeolites. *Separation and Purification Technology*, 15: 163–173.
93. Ihsanullah, H. A., Asmaly, T. A., Saleh, T., Laoui, V. K. and Gupta, M. A. (2015). Enhanced adsorption of phenols from liquids by aluminum oxide/carbon nanotubes: Comprehensive study from synthesis to surface properties. *Journal of Molecular Liquids*, 206:176-182.
94. Jaunsen, J. R. (1989). The behavior and capabilities of lithium hydroxide - carbon dioxide scrubbers in a deep sea environment, *U.S.N.A. - TSPR; 157*, United States Naval Academy, USA.
95. Jian, L., Thallapally, P. K., McGrail, P. B., Brown, D. R. and Liu, L. (2012). Progress in adsorption-based CO₂ capture by metal–organic frameworks. *Chemical Society Review*, 41(6): 2308–2322.
96. Jimenez, V., Ramirez-Lucas, A., Díaz, J. A., Sánchez, P. and Romero, A. (2012). CO₂ capture in different carbon materials. *Environmental Science and Technology*, 46(13): 7407-7414.
97. Kadirvelu, K., Kavipriya, M., Karthika, C. (2003). Utilization of various agricultural wastes for activated carbon preparation and application for the removal of dyes and metal ions from aqueous solutions. *Bioresource Technologies*, 87(1): 129–132.
98. Kamiuto, K., Abe, S. and Yasuda, M. (2002). Adsorption dynamics of carbon dioxide on a carbon molecular sieve 5A. *Applied Energy*, 72: 555–564.
99. Kenarsari, S. D., Yang, D., Jiang, G., Zhang, S., Wang, J., Russell, A. G., Weif, Q. and Fan, M. (2013). Review of recent advances in carbon dioxide separation and capture. *RSC Advances*, 3(45): 22739–22773.
100. Khalili, S., Ghoreyshi, A.A. and Jahanshahi, M. (2013). Carbon dioxide captured by multiwalled carbon nanotube and activated charcoal: a

comparative study. *Chemical Industry & Chemical Engineering Quarterly*, 19 (1): 153–164.

101. Kikkinides, E. S., Yang, R. T. and Cho, S. H. (1993). Concentration and recovery of carbon dioxide from flue gas by pressure swing adsorption. *Industrial and Engineering Chemistry Research*, 32: 2714-2720.
102. Kumar, K. V., Preuss, K., Lu, L., Guo, Z. and Titirici, M. M. (2015). Effect of nitrogen doping on the CO₂ adsorption behavior in nanoporous carbon structures: A molecular simulation study. *Journal of Physical Chemistry C*, 119: 22310-22321.
103. Langmuir, I. (1916). The constitution and fundamental properties of solids and liquids. Part I. Solids. *Journal of American Chemical Society*, 38: 2221-2295.
104. Lan, P. Q. and Wu, S.F. (2014). Synthesis of a porous nano-CaO/MgO-based CO₂ adsorbent. *Chemical Engineering & Technology*, 37: 580-586.
105. Lee, S. C., Chae, H. J., Lee, S. J., Parka, Y. H., Ryu, C. K., Yi, C. K. and Kim, J. C. (2009). Novel regenerable potassium-based dry sorbents for CO₂ capture at low temperatures. *Journal of Molecular Catalysis B*, 56: 179–184.
106. Lee, S.-Y. and Park, S.-J. (2015). A review on solid adsorbents for carbon dioxide capture. *Journal of Industrial and Engineering Chemistry*, 23: 1–11.
107. Lee, Z. H., Lee, K. T., Bhatia, S. and Mohamed, A. R. (2012). Post-combustion carbon dioxide capture: Evolution towards utilization of nanomaterials. *Renewable and Sustainable Energy Reviews*. 16(5): 2599-2609.
108. Li, B., Duan, Y., Luebke, D. and Morreale, B. (2013). Advances in CO₂ capture technology, A patent review. *Applied Energy*, 102: 1439-1447.
109. Li, D., Tian, Y., Li, L., Li, J. and Zhang, H. (2015). Production of highly microporous carbons with large CO₂ uptakes at atmospheric pressure by KOH activation of peanut shell char. *Journal of Porous Materials*, 22 (6): 1581-1588.
110. Li, D., Chen, Y., Zheng, M., Zhao, H., Zhao, Y. and Z. Sun. (2016) Hierarchically structured porous nitrogen-doped carbon for highly selective CO₂ Capture. *ACS Sustainable Chemistry & Engineering*, 4: 298–304.
111. Li, J.-R., Ma, Y., McCarthy, M. C., Sculley, J., Yu, J., Jeong, H.-K., Balbuena, P. B. and Zhou, H.-C. (2011). Carbon dioxide capture-related gas adsorption and separation in metal-organic frameworks. *Coordination*

Chemistry Review, 255:1791–1823.

112. Li, J., Meng, H., Xie, S., Zhang, B., Li, L., Ma, H., Zhang, J. and Yu, M. (2014). Ultra-light, compressible and fire-resistant graphene aerogel as a highly efficient and recyclable absorbent for organic liquids. *Journal of Materials Chemistry A*, 2: 2934-2941.
113. Li, T., Sullivan, J. E. and Rosi, N. L. (2013). Design and preparation of a core-shell metal-organic framework for selective CO₂ capture. *Journal of American Chemical Society*, 135(6): 9984–9987.
114. Li, W., Bollini, P., Didas, S. A., Choi, S., Drese, J. H. and Jones, C. W. (2010). Structural changes of silica mesocellular foam supported amine-functionalized CO₂ adsorbents upon exposure to steam. *ACS Applied Materials and Interfaces*, 2: 3363- 3372.
115. Liang, Z., Fadhel, B., Schneider, C. J. and Chaffee, A. L. (2008). Stepwise growth of melamine-based dendrimers into mesopores and their CO₂ adsorption properties. *Microporous and Mesoporous Materials*, 111: 536-543.
116. Lide, D. R. (2014). *CRC Handbook of Chemistry and Physics*, CRC Press: USA.
117. Liebl, M. R. and Senker, J. R. (2013). Microporous functionalized triazine-based polyimides with high CO₂ capture capacity. *Chemistry Materials*, 25: 970-975.
118. Liu, L., Deng, Q.-F., Hou, X.-X. and Yuan, Z.-Y. (2012). User-friendly synthesis of nitrogen-containing polymer and microporous carbon spheres for efficient CO₂ capture. *Journal of Materials Chemistry*, 31: 15540-15548.
119. Liu, W., An, H., Qin, C., Yin, J., Wang, G. and Feng, B. (2012). Performance enhancement of calcium oxide sorbents for cyclic CO₂ capture—A review. *Energy & Fuels*, 26: 2751-2767.
120. Liu, Y. and You, C. (2001). Inclusion complexation of β -cyclodextrin and 6-O- amaltosyl-and 2-O-(2-hydroxypropyl)- β -cyclodextrins with some fluorescent dyes. *Journal of Physical Organic Chemistry*, 14: 11–16.
121. Liu, Z., Zhu, Y., Sridhar, K., Yan, Z. and Zing, W. (2015). Detailed investigation of N-doped microporous carbons derived from urea furfural resin for CO₂ capture. *Journal of Porous Materials*, 22(6): 1663-1672.
122. Liu, Z., Zhu, Y., Du, Z., Xing, W., Komarneni, S. and Yan, Z. (2015). Detailed investigation of N-doped microporous carbons derived from urea

- furfural resin for CO₂ capture. *Journal of Porous Materials*, 22: 1663-1672.
123. Loganathan, S., Tikmani, M., Mishra, A. and Ghoshal, A. K. (2016). Amine tethered pore-expanded MCM-41 for CO₂ capture: Experimental, isotherm and kinetic modeling studies. *Chemical Engineering Journal*, 303: 89-99.
 124. López-Salas, N., Gutiérrez, M. C., Ania, C. O., Fierro, J. G., Ferrera, M. L. and del Monte, F. (2014) Efficient nitrogen-doping and structural control of hierarchical carbons using unconventional precursors in form of deep eutectic solvents. *Journal of Materials Chemistry A*, 2: 17387-17399.
 125. Lozano-Castelló, D., Cazorla-Amorós, D., and Linares-Solano, A. (2004). Usefulness of CO₂ adsorption at 273 K for the characterization of porous carbons. *Carbon*, 42: 1231-1236.
 126. Lu, A. H. (2014). *Porous materials for carbon dioxide capture*. Springer: London.
 127. Lu, W., Sculley, J. P., Yuan, D., Krishna, R. and Zhou, H. (2013). Carbon dioxide capture from air using amine-grafted porous polymer networks. *Journal of Physical Chemistry C*, 117(8): 4057-4061.
 128. Lu, W., Sculley, J. P., Yuan, D., Krishna, R., Wei, Z. and Zhou, H. C. (2012). Polyamine-tethered porous polymer networks for carbon dioxide capture from flue gas. *Angewandte Chemie International Edition*, 51: 7480-7484.
 129. Luo, H., Zhu, C. C., Tan, Z. C., Bao, L. W., Wang, J. J., Miao, G., Kong, L. Z. and Sun, Y. H. (2016). Preparation of N-doped activated carbon with high CO₂ capture performance from microalgae. *RSC Advances*, 6: 38724-38730.
 130. Ma, X., Cao, M. and Hu, C. (2013). Bifunctional HNO₃ catalytic synthesis of N-doped porous carbons for CO₂ capture. *Journal of Materials Chemistry A*, 1: 913-918.
 131. Ma, X., Wang, X. and Song, C. (2009). "Molecular Basket" sorbents for separation of CO₂ and H₂S from various gas streams. *Journal of American Chemical Society*, 131:5777-5783.
 132. MacDowell, N., Florin, N., Buchard, A., Hallett, J., Galindo, A., Jackson, G., Adjiman, C. S., Williams, C. K., Shah, N. and Fennell, P. (2010). *Energy and Environmental Science*, 3: 1645-1669.
 133. Mahajani, V. V. and Joshi, J. B. (1988). Kinetics of reactions between carbon dioxide and alkanolamines. *Gas Separation and Purification*, 2:

50–64.

134. Manson, J. A., Sumida, K., Herm, Z. R., Krishna, R. and Long, J. R. (2011). Evaluating metal–organic frameworks for post-combustion carbon dioxide capture via temperature swing adsorption. *Energy and Environmental Science*, 4: 3030-3040.
135. McDonald, T. M., Lee, W. R., Mason, J. A., Wiers, B. M., Hong, C. S. and Long, J. R. (2012). Capture of carbon dioxide from air and flue gas in the alkylamine-appended metal–organic framework mmen-Mg₂(dobpdc). *Journal of American Chemical Society*, 134(16): 7056-7065.
136. McDonald, T. M., Mason, J. A., Kong, X., Bloch, E. D., Dani, A. and Reimer, J. A. (2015). Cooperative insertion of CO₂ in diamine-appended metal-organic frameworks. *Nature*, 5019: 303-308.
137. Mishra, P., Edubilli, S., Mandal, B. and Gumma, S. (2014). Comprehensive study of carbon dioxide adsorption in the metal–organic frameworks M₂(dobdc) (M = Mg, Mn, Fe, Co, Ni, Cu, Zn). *Journal of Physical Chemistry C*, 5: 4969-4581.
138. Meng, L.-Y. and Park, S.-J. (2014). Superhydrophobic carbon based materials- a review of synthesis, structure, and applications. *Carbon Letters*, 15: 89-104.
139. Mochidzuki, K., Sato, N. and Sakoda, A. (2005). Production and characterization of carbonaceous adsorbents from biomass wastes by aqueous phase carbonization. *Adsorption*, 11: 669–673.
140. Mohan, D. and Singh, K. (2002). Single and multi-component adsorption of cadmium and zinc activated carbon derived from bagasse – an agricultural waste. *Water Resources*, 36: 2304–2318.
141. Narasimman, R., Sujith, V. and Prabhakaran, K. (2014). Carbon foam with microporous cell wall and strut for CO₂ capture. *RSC Advances*, 4(2): 578–582.
142. Nguyen, P. T. K., Nguyen, H. T. D, Pham, H. Q. Kim, J., Cordova, K. E. and Furukawa, H. (2015). Synthesis and selective CO₂ capture properties of a series of hexatopic linker-based metal–organic frameworks. *Inorganic Chemistry*, 54 (20): 10065–10072.
143. Norfleet, W. and Horn, W. (2013). Carbon dioxide scrubbing capabilities of two new non-powered technologies, *Report No. TR1228, Naval Submarine Medical Research Laboratory*

144. Nuckols, M. L., Purer, A. and Deason, G. A. (1985). Technical Manual-Design Guidelines for Carbon Dioxide Scrubbers, NCSC TECHMAN, 4110-1-83 (Rev A), Naval Coastal Systems Center, Florida.
145. Ochiai, B., Yokota, K., Fujii, A., Nagai, D. and Endo, T. (2008). Reversible trap-release of CO₂ by polymers bearing DBU and DBN moieties. *Macromolecules*, 41: 1229–1236.
146. Okunev, A. G., Sharonov, V. E., Gubar, A. V., Danilova, I. G., Paukshtis, E. A., Moroz, E. M., Kriger, T. A., Malakhov, V. V. and Aristov, Y. I. (2003). Sorption of carbon dioxide by the composite sorbent, potassium carbonate in porous matrix. *Russian Chemical Bulletin*, 52: 359–363.
147. Pacheco, D. M., Johnson, J. R. and Koros, W. J. (2012). Aminosilane-functionalized cellulosic polymer for increased carbon dioxide sorption. *Industrial Engineering and Chemistry Research*, 51: 503–514.
148. Parry, M. L. (2007). Climate Change 2007: Impacts, Adaptation and Vulnerability, *Fourth Assessment Report of the IPCC*, Cambridge University Press: London.
149. Patiño, J., Gutierrez, M. C., Carriazo, D., Ania, C. O., Fierro, J. L. G., Ferrer, M. L. and del Monte, F. (2014). DES assisted synthesis of hierarchical nitrogen-doped carbon molecular sieves for selective CO₂ versus N₂ adsorption. *Journal of Materials Chemistry A*, 2: 8719-8729.
150. Pels, J. R., Kapteijn, F., Moulijn, J. A., Zhu, Q. and Thomas, K. M. (1995). Evolution of nitrogen functionalities in carbonaceous materials during pyrolysis, *Carbon*, 33:1641–1653.
151. Pevida, C., Drage, T. C. and Snape, C. E. (2008). Silica-templated melamine– formaldehyde resin derived adsorbents for CO₂ capture. *Carbon*, 11(46):1464-1474.
152. Pham, T-H., Lee, B-K., Kim, J. and Lee, C-H. (2016). Enhancement of CO₂ capture by using synthesized nano-zeolite. *Journal of the Taiwan Institute of Chemical Engineers*, 64: 220-226.
153. Plaza, M. G., Pevida, C., Arias, B., Fermoso, J., Rubiera, F. and Pis, J. J. (2009). A comparison of two methods for producing CO₂ capture adsorbents. *Energy Procedia*, 1(1): 1107–1113.
154. Plaza, M. G., Gonzalez, A. S., Pevida, C., Pis, J. J. and Rubiera, F. (2012). Valorisation of spent coffee grounds as CO₂ adsorbents for postcombustion capture applications. *Applied Energy*, 99 (1): 272–279.
155. Plaza, M. G., Pevida, C., Martín, C. F., Fermoso, J., Pis, J. J. and Rubiera, F. (2010). Developing almond shell-derived activated carbons as CO₂

adsorbents. *Separation and Purification Technology*, 71(1): 102–106.

156. Prasannan, A., Truong, T. B., Hong, P., Somanathan, N., Shown, I. and Imae, T. (2011). Synthesis and characterization of “Hairy Urchin”-like polyaniline by using β -Cyclodextrin as a template. *Langmuir*, 27: 766–773.
157. Pridmore, A., Bristow, A., May, T. and Tight, M. (2003). Climate change, impacts, future scenarios and the role of transport, *Report of University of Leeds*, Institute for Transport Studies, Tyndall Centre for Climate Change Research.
158. Przepiórski, J., Skrodzewicz, M. and Morawski, A. W. (2004). High-temperature ammonia treatment of activated carbon for enhancement of CO₂ adsorption. *Applied Surface Science*, 225: 235–242.
159. Qi, G.G., Fu, L.L., Choi, B.H. and Giannelis, E.P. (2012). Efficient CO₂ sorbents based on silica foam with ultra-large mesopores. *Energy and Environmental Science*, 5: 7368–7375.
160. Rabbani, M. G. and El-Kaderi, H. M. (2012). Synthesis and Characterization of porous benzimidazole-linked polymers and their performance in small gas storage and selective uptake. *Chemistry of Materials*, 24: 1511–1517.
161. Rahimi, M., Singh, J. K., Babu, D. J., Schneider, J. and Müller-Plathe, F. (2013). Understanding carbon dioxide adsorption in carbon nanotube arrays: molecular simulation and adsorption measurements. *Journal of Physical Chemistry C*, 117: 13492–13501.
162. Ramdin, M., de Loos, T. W. and Vlugt, T. J. H. (2012). Carbon capture with ionic liquids: Overview and progress. *Energy and Environmental Science*, 5: 6668–6681.
163. Razavi, S. S., Hashemianzadeh, S. M., Karimi, H. (2011). Modeling adsorptive selectivity of carbon nanotubes for selective separation CO₂/N₂ mixtures. *Journal Molecular Modelling*, 17: 1163–1172.
164. Richards, G. N. and Shafizadeh, F. (1978). Mechanism of thermal degradation of sucrose. A preliminary study. *Australian Journal of Chemistry*, 31: 1825–1832.
165. Rekharsky, M. V. and Inoue, Y. (1998). Complexation thermodynamics of cyclodextrins. *Chemical Review*, 98: 1875–1917.
166. Roth, E. M. (1967). Selection of Space cabin atmosphere, *Space Science Review*, 6: 452–492.
167. Rodrigues, S. C., Whitley, R., and Mendes, A. (2014). Preparation and

characterization of carbon molecular sieve membranes based on resorcinol–formaldehyde resin. *Journal of Membrane Science*, 459 (1): 207–216.

168. Rutherford, S. W. and Do, D. D. (2000). Adsorption dynamics of carbon dioxide on a carbon molecular sieve 5A. *Carbon*, 38: 1339–1350.
169. Saha, D. and Deng, S. G. (2010). Adsorption equilibrium and kinetics of CO₂, CH₄, N₂O, and NH₃ on ordered mesoporous carbon. *Journal of Colloid and Interface Science*, 345(2): 402–409.
170. Saleh, M., Tiwari, J. N., Kemp, K. C., Yousuf, M. and Kim, K. S. (2013). Highly selective and stable carbon dioxide uptake in polyindole-derived microporous carbon materials. *Environmental Science Technology*, 47: 5467–5473.
171. Salman, J. M., Njoku, V. O. and Hameed, B. H. (2011) Adsorption of pesticides from aqueous solution onto banana stalk activated carbon. *Chemical Engineering Journal*, 174: 41–48.
172. Samanta, A., Shimizu, K. H., Sarkar, P. and Gupta, R. (2012). Post-Combustion CO₂ Capture Using Solid Sorbents: A Review. *Industrial Engineering and Chemistry Research*, 51: 1438–1463.
173. Samanta, A., Zhao, G., Shimizu, K. H., Sarkar, P. and Gupta, R. (2012). Post-combustion CO₂ capture using solid sorbents: a review. *Industrial and Engineering Chemistry Research*, 51: 1438–1463.
174. Samios, S., Stubos, A. K., Papadopoulos, G. K., Kanellopoulos, N. K. and Rigas, F. (2000). The structure of adsorbed CO₂ in slitlike micropores at low and high temperature and the resulting micropore size distribution based on GCMC Simulations. *Journal of Colloid and Interface Science*, 224: 272–290.
175. Satyapal, S., Filburn, T., Trela, J. and Strange, J. (2001). Performance and properties of a solid amine sorbent for carbon dioxide removal in space life support applications. *Energy & Fuels*, 15: 250–255.
176. Sayari, A., Belmabkhout, Y. and Da'na, E. (2012). CO₂ deactivation of supported amines: does the nature of amine matter? *Langmuir*, 28: 4241–4247.
177. Seema, H., Kemp, K.C., Le, N.H., Park, S.W., Chandra, V., Lee, J. W. and Kim, K.S. (2014). Highly selective CO₂ capture by S-doped microporous carbon materials. *Carbon*, 66: 320–326.
178. Seifer, G. B. (2002). Cyanuric acid and cyanurates. *Russian Journal of Coordination Chemistry*, 28: 301–324.

179. Serna-Guerrero, R., Belmabkhout, Y. and Sayari, A. (2010). Further investigations of CO₂ capture using triamine-grafted pore-expanded mesoporous silica. *Chemical Engineering Journal*, 158: 513–519.
180. Sevilla, M., Falco, C., Titirici, M. M. and Fuertes, A. B. (2012). High-performance CO₂ sorbents from algae, *RSC Advances*, 2: 12792–12797.
181. Sevilla, M., Fuertes, A. B. (2009). The production of carbon materials by hydrothermal carbonization of cellulose. *Carbon*, 47: 2281–2289.
182. Sevilla, M. and Fuertes, A. B. (2011). Sustainable porous carbons with a superior performance for CO₂ capture. *Energy & Environmental Science*, 4(5): 1765–1771.
183. Sevilla, M., Valle-Vigón, P. and Fuertes, A. B. (2011). N-doped polypyrrole-based porous carbons for CO₂ capture. *Advanced Functional Materials*, 21: 2781–2787.
184. Shimizu, S., Song, C. and Strano, M. (2011). Role of specific amine surface configurations for grafted surfaces: Implications for nanostructured CO₂ adsorbents. *Langmuir*, 27: 2861–2872.
185. Shin, Y., Li-Qiong, W., In-Tae, B., Bruce, W. A., and Gregory, J. E. (2008). Hydrothermal syntheses of colloidal carbon spheres from cyclodextrins. *Journal of Physical Chemistry C*, 112(37): 14236–14240.
186. Shengping W., Suli Y., Xinbin M. and Jinlong G. (2011). Recent advances in capture of carbon dioxide using alkali-metal-based oxides. *Energy and Environmental Science*, 10: 3805–3819.
187. Sing, B. and Vivek, P. (2016). Design of CO₂ Sorbents using Functionalized Fibrous Nanosilica (KCC-1): Insights into the effect of the silica morphology (KCC-1 vs MCM-41). *Journal of Materials Chemistry A*, 4: 7009–7019.
188. Sing, K. S. W. (1998). Adsorption methods for the characterization of porous materials. *Advances in Colloid and Interface Science*, 76–77: 3–11.
189. Sing, K. S. W., Everett, D. H., Haul, R. A. W., Moscou, L., Pierotti, R. A., Rouquerol, J. and Siemieniowska, T. (1985). Reporting physisorption data for gas/solid systems with special reference to the determination of surface area and porosity. *Journal of Pure and Applied Chemistry*, 57(4): 603–619.
190. Siriwardane, R. V., Shen, M. S., Fisher, E. P. and Poston, J. A. (2001). Adsorption of CO₂ on molecular sieves and activated carbon. *Energy & Fuels*, 15: 279–284.

191. Siriwardane, R. V., Shen, M. S., Fisher, E. P., Poston, J. A. and Shamsi, A. (2001). Adsorption and desorption of CO₂ on solid sorbents. *Journal of Energy and Environmental Research*, 1: 19-24.
192. Siriwardane, R. V., Shen, M. S. and Fisher, E. P. (2003). Adsorption of CO₂, N₂, and O₂ on Natural Zeolites. *Energy and Fuels*, 17, 571-576.
193. Son, W. J., Choi, J. S. and Ahn, W. S. (2008). Adsorptive removal of carbon dioxide using polyethyleneimine-loaded mesoporous silica materials. *Microporous and Mesoporous Materials*, 113: 31-40.
194. Srinivas, G., Krungleviciute, V., Guo, Z. X., and Yildirim, T. (2014). Exceptional CO₂ capture in a hierarchically porous carbon with simultaneous high surface area and pore volume. *Energy and Environmental Science*, 7: 335–342.
195. Srinivasan, S., Praveen, V. K., Philip, R. and Ajayaghosh, A. (2008) bioinspired superhydrophobic coatings of carbon nanotubes and linear π systems based on the “bottom-up” self-assembly approach. *Angewandte Chemie International Edition*, 47: 5750 –5754.
196. Su, F, and Lu, C. (2012). CO₂ capture from gas stream by zeolite 13X using a dual-column temperature/vacuum swing adsorption. *Energy and Environmental Science*, 5(10): 9021–9027.
197. Teng, H. and Wang, S. C. (2000). Influence of oxidation on the preparation of porous carbons from phenol-formaldehyde resins with KOH activation. *Industrial Engineering and Chemistry Research*, 39: 673-678.
198. Titirici, M. M., Antonietti, M. and Baccile, N. (2008). Hydrothermal carbon from biomass: a comparison of the local structure from poly- to monosaccharides and pentoses/hexoses. *Green Chemistry*, 10: 1204-1212.
199. Titirici, M. M., Thomas, A. and Antonietti, M. (2007). Back in the black: hydrothermal carbonization of plant material as an efficient chemical process to treat the CO₂ problem? *New Journal of Chemistry*, 31 (6): 787–789.
200. Thote, J. A., Iyer, K. S., Chatti, R., Labhsetwar, N. K., Biniwale, R. B. and Rayalu, S. S. (2010). In situ nitrogen enriched carbon for carbon dioxide capture. *Carbon*, 48(2): 396–402.
201. Tien, H. W., Huang, Y. L., Yang, S. Y., Wang, J. Y. and Ma, C. C. M. (2011). The production of graphene nanosheets decorated with silver nanoparticles for use in transparent, conductive films. *Carbon*, 49: 1550-1560.

202. Tofighy, M. A. and Mohammadi, T. (2011). Adsorption of divalent heavy metal ions from water using carbon nanotube sheets *Journal of Hazardous Materials*, 185:140–147.
203. Travis, W., Gadipelli, S. and Guo, Z. (2015). Superior CO₂ adsorption from waste coffee ground derived carbons. *RSC Advances*, 5: 29558 -29562.
204. Tseng, R-L., Wu, F-C., Juang, R-S. (2015). Adsorption of CO₂ at atmospheric pressure on activated carbons prepared from melamine-modified phenol–formaldehyde resins. *Separation and Purification Technology*, 140: 53-60.
205. Tsuda, T. and Fujiwara, T. J. (1992). Polyethyleneimine and macrocyclic polyamine silica gels acting as carbon dioxide absorbents. *Chemical Society, Chemical Communication*, 22: 1659–1661.
206. Vaidya, P. D. and Kenig, E. Y. (2007). CO₂-alkanolamine reaction kinetics: a review of recent studies. *Chemical Engineering and Technology*, 30: 1467–1474.
207. Valverde, J. M. (2013). Ca-based synthetic materials with enhanced CO₂ capture efficiency. *Journal of Materials Chemistry A*, 1:447-468.
208. Wang, H., Wang, G., Liu, Z., Dong, G., Yuan, R., Sun, L. and Zhu, Y. (2015). A novel carbon nanotubes reinforced superhydrophobic and superoleophilic polyurethane sponge for selective oil–water separation through a chemical fabrication. *Journal of Materials Chemistry A*, 3: 266-273.
209. Wade, C. R. and Dinca, M. (2012). Investigation of the synthesis, activation, and isosteric heats of CO₂ adsorption of the isostructural series of metal–organic frameworks M₃(BTC)₂ (M = Cr, Fe, Ni, Cu, Mo, Ru). *Dalton Transaction*, 41(26): 7931-7938.
210. Wang, D. X., Ma, X. L., Sentorun-Shalaby, C. and Song, C.S. (2012). Development of carbon-based “molecularbasket” sorbent for CO₂ capture. *Industrial Engineering and Chemistry Research*, 51: 3048–3057.
211. Wang, H. (2011). Nitrogen-doped graphene nanosheets with excellent lithium storage properties. *Journal of Materials Chemistry*, 21: 5430–5434.
212. Wang, J. and Liu, Q. (2014). An efficient one-step condensation and activation strategy to synthesize porous carbons with optimal micropore sizes for highly selective CO₂ adsorption. *Nanoscale*, 6: 4148-4156.
213. Wang, J., Senkovska, I., Oschatz, M., Lohe, M. R., Borchardt, L., Heerwig, A., Liu, Q. and Kaskel, S. (2013). Imine-linked polymer derived nitrogen-doped microporous carbons with excellent CO₂ capture properties. *ACS*

Applied Materials and Interfaces, 5(8): 3160-3167.

214. Wang T. C. (1981). Residence time and carbon dioxide scrubbing efficiency in life support systems, *Aviation, Space, and Environmental Medicine*, 104-108.
215. Wei, J., Zhou, D., Sun, Z., Deng, Y., Xia, Y. and Zhao, D. (2013). A Controllable Synthesis of Rich Nitrogen-Doped Ordered Mesoporous Carbon for CO₂ Capture and Supercapacitors. *Advanced Functional Materials*, 23 (18): 2322–2328.
216. Wickramarat, N. P. and Jaroniec, M. (2013). Importance of small micropores in CO₂ capture by phenolic resin-based activated carbon spheres. *Journal of Material Chemistry, A*, 1 (1): 112-116.
217. Williams, D. D. and Miller, R. R. (1969). “The Effect of Water Vapor on the LiOH-CO₂ Reaction, Part 1 - Dynamic Isothermal System” (NRL Report 6937). Washington, DC: Naval Research Laboratory.
218. Wu, S. F., Li, Q. H., Kim, J. N. and Yi, K. B. (2008). Properties of nano CaO/Al₂O₃ CO₂ sorbent. *Industrial Engineering and Chemistry Research*, 47: 180-184.
219. Xiaoyu, M., Minhua, C. and Changwen, H.(2013). Bifunctional HNO₃ catalytic synthesis of N-doped porous carbons for CO₂ capture. *Journal of Materials Chemistry A*, 1(3): 913–918.
220. Xia, Y. D., Mokaya, R., Walker, G. S. and Zhu, Y. Q. (2011). Superior CO₂ adsorption capacity on N-doped, high-surface-area, microporous carbons templated from zeolite. *Advanced Energy Materials*, 1(4): 678–683.
221. Xing, W., Liu, C., Zhou, Z., Zhang, L., Zhou, J., Zhuo, S., Yan, Z., Gao, H., Wang, G. and Qiao, S. Z. (2012). Superior CO₂ uptake of N-doped activated carbon through hydrogen-bonding interaction. *Energy and Environmental Science*, 5(6): 7323-7327.
222. Xu, X., Song, C., Andresen, J. M., Miller, B. G. and Scaroni, A. W. (2002). Novel polyethylenimine-modified mesoporous molecular sieve of MCM-41 type as high-capacity adsorbent for CO₂ capture. *Energy & Fuels*, 16: 1463 – 1469.
223. Xu, X. C., Song, C. S., Andresen, J. M., Miller, B. G. and Scaroni, A. W. (2002). Novel polyethylenimine-modified mesoporous molecular sieve of MCM-41 type as high-capacity adsorbent for CO₂ capture. *Energy & Fuels*, 16: 1463–1469.

224. Xu, X. C., Song, C. S., Miller, B. G. and Scaroni, A. W. (2005). Influence of moisture on CO₂ separation from gas mixture by a nanoporous adsorbent based on polyethylenimine-modified molecular sieve MCM-41. *Industrial Engineering and Chemistry Research*, 44(21): 8113 – 8119.
225. Yamasakim, A. (2003). An overview of CO₂ mitigation options for global warming - Emphasizing CO₂ sequestration options. *Journal of Chemical Engineering Japan*, 36:361–375.
226. Yang, F-M., Liu, Y., Chen, L., Au, C-T. and Yin, S-F. (2015). Synthesis of amine-modified solid Fe-Zr adsorbents for CO₂ adsorption. *Journal of Chemical technology and biotechnology*, 91(8): 2340-2348.
227. Yang, M., Guo, L., Hu, G., Hu, X., Xu, L., Chen, J., Dai, W. and Fan, M. (2015). Highly cost-effective nitrogen-doped porous coconut shell-based CO₂ sorbent synthesized by combining ammoxidation with KOH activation. *Environmental Science and Technology*, 49 (11): 7063–7070.
228. Yang, S. T., Kim, J. Y., Kim, J. and Ahn, W. S. (2012). CO₂ capture over amine- functionalized MCM-22, MCM-36 and ITQ-2. *Fuel*, 97: 435–442.
229. Yazaydin, A., Snurr, R., Park, T., Koh, K., Liu, J. and LeVan, M. (2009). Screening of metalorganic frameworks for carbon dioxide capture from flue gas using a combined experimental and modelling approach. *Journal of American Chemical Society*, 131:18198-18199.
230. Yu, C.-H., Huang, C.-H. and Tan, C.-S. (2012). A review of CO₂ capture by absorption and adsorption. *Aerosol and Air Quality Research*, 12: 745–769.
231. Yu, C. T. and Chen, W. C. (2014). Hydrothermal preparation of calcium-aluminum carbonate sorbent for high-temperature CO₂ capture in fixed-bed reactor. *Fuel*, 122: 179-185.
232. Yu, J. and Balbuena, P. B. (2013). Water Effects on post combustion CO₂ capture in Mg-MOF-74. *Journal of Physical Chemistry C*, 117(7): 3383-3388.
233. Yu, J., Guo, M., Muhammad, F., Wang, A., Zhang, F., Li, Q., and Zhu, Q. (2014). One-pot synthesis of highly ordered nitrogen-containing mesoporous carbon with resorcinol–urea–formaldehyde resin for CO₂ capture. *Carbon*, 69: 502 -514.
234. Yue, M. B., Sun, L. B., Cao, Y., Wang, Y., Wang, Z. J. and Zhu, J. H. (2008). Efficient CO₂ capturer derived from as-synthesized MCM-41 modified with amine. *Chemistry a European Journal*, 14: 3442- 3451.

235. Wu, Z.-Y., Li, C., Liang, H.-W., Chen, J.-F. and Yu, S.-H. (2013). Ultralight, flexible, and fire-resistant carbon nanofiber aerogels from bacterial cellulose. *Angewandte Chemie International Edition*, 52: 2925-2929.
236. Zeng, Y., Wang, K., Yao, J. and Wang, H. (2014). Hollow carbon beads fabricated by phase inversion method for efficient oil sorption. *Carbon*, 69: 25-31.
237. Zhao, B., Su, Y., Tao, W., Li, L. and Peng, Y. (2012). Post-combustion CO₂ capture by aqueous ammonia: A state-of-the-art review. *International Journal of Greenhouse Gas Control*, 9: 355–371.
238. Zhao, Y. C., Zhao, L., Li-Juan, M. and Han, B. H. (2013). One-step solvothermal carbonization to microporous carbon materials derived from cyclodextrins. *Journal of Materials Chemistry A*, 1(33): 9456–9461.
239. Zhang, Z., Wang, B., Zhu, C., Gao, P., Tang, Z., Sun, N., Wei, W. and Sun, Y. (2015). Facile one-pot synthesis of mesoporous carbon and N-doped carbon for CO₂ capture by a novel melting-assisted solvent-free method. *Journal of Materials Chemistry A*, 3: 23990-23999.
240. Zhang, Z., Zhou, J., Xing, W., Xue, Q., Yan, Z., Zhuo, S. and Qiao, S. Z. (2013). Critical role of small micropores in high CO₂ uptake. *Physical Chemistry Chemical Physics*, 15 (7): 2523-2529.
241. Zhao, Y., Hu, C., Hu, Y., Cheng, H., Shi, G. and Qu, L. (2012). A versatile, ultralight, nitrogen-doped graphene framework. *Angewandte Chemie International Edition*, 51: 11371-11375.
242. Zhou, Z., Yang, J., Zhang, Y., Chang, L., Sun, W. and Wang, J. (2007). NaA zeolite/carbon nanocomposite thin films with high permeance for CO₂/N₂ separation. *Separation and Purification Technology*, 55: 392-395.
243. Zheng, F., Yang, Y. and Chen, Q. (2014). High lithium anodic performance of highly nitrogen-doped porous carbon prepared from a metal-organic framework. *Nature Communications*, 5: 5261-5271.
244. Zheng, F., Tran, D. N., Busche, B. J., Fryxell, G. E., Addleman, R. S., Zemanian, T. S. and Aardahl, C. L. (2005). Ethylenediamine-modified SBA-15 as regenerable CO₂ sorbent. *Industrial Engineering and Chemistry Research*, 44(9): 3099-3105.
245. Zhu, X., Do-Thanh, C.-L., Murdock, C. R., Nelson, K. M., Tian, C., Brown, S., Mahurin, S. M., Jenkins, D. M., Hu, J., Zhao, B., Liu, H. and Dai, S. (2013). Efficient CO₂ capture by a 3D porous polymer derived from Tröger's base. *Macro Letters*, 2(8): 660–663.
246. Zhuo, M., Pu, F., Wang, Z. and Guan, S. (2014). Nitrogen-doped porous

carbons through KOH activation with superior performance in supercapacitors. *Carbon*, 68: 185-194.

247. Zukal, A., Dominguez, I., Mayerova, J. and Cejka, J. (2009). Functionalization of delaminated zeolite ITQ-6 for the adsorption of carbon dioxide. *Langmuir*, 25: 10314-10321.

LIST OF PUBLICATIONS BASED ON THE THESIS

Journal papers

1. Deepthi, L. S., Vijayalakshmi, K. P., Rajeev, R., Prabhakaran, K. and Ninan, K. N. (2013). Supramolecular β -cyclodextrin–aniline system: a new class of amine on solid support for carbon dioxide capture with high amine efficiency. *RSC Advances*, 3: 24041–24045.
2. Deepthi, L. S., Narasimman, R., Rajeev, R., Prabhakaran, K. and Ninan, K. N. (2015). Effect of catalyst concentration and high temperature activation on the CO₂ adsorption of carbon nanospheres prepared by solvothermal carbonization of β -cyclodextrin. *Journal of Materials Research*, 30 (11): 1761-1771.
3. Deepthi, L. S., Narasimman, R., Rajeev, R., Prabhakaran, K. and Ninan, K. N. (2015). Solvothermal Synthesis of Microporous Superhydrophobic Carbon with Tunable Morphology from Natural Cotton for Removal of Carbon Dioxide and Organic Solvent Removal. *Journal of Materials Chemistry A*, 3: 16213–16221.
4. Deepthi, L. S., Sujith, V., Rajeev, R., Ninan, K. N. and Prabhakaran, K. (2016). Nitrogen-enriched microporous carbon derived from sucrose and urea with superior CO₂ capture performance. *Carbon*, 109: 7-18.

Conference papers

1. Supra molecular β - Cyclodextrin – Aniline system for carbon dioxide removal, Conference on recent advances in material science and nanoscience, February 2013, Cochin.
2. Effect of catalyst concentration and high temperature activation on the nanoporous carbon prepared by solvothermal synthesis of cyclodextrin, Nano India-2014, February 2014, Trivandrum
3. Microporous superhydrophobic carbon from cotton for carbon dioxide and organic solvent removal applications, National Conference on Materials Science and Technology, July 2016, Trivandrum.